Check for updates

Small

NANO · MICRO small
www.small-journal.com

REVIEW

Tailoring MXene Surface Chemistry: Strategies, Mechanisms, and Functional Applications

Zhifang Liu[1] | Yipeng Cui[1] | Yilin Sun[2] | Caofeng Pan[1]

[1]Institute of Atomic Manufacturing, Beihang University, Beijing, China | [2]School of Microelectronics Science and Technology, Sun Yat-sen University, Zhuhai, China

Correspondence: Yilin Sun (sunylin7@mail.sysu.edu.cn) | Caofeng Pan (pancaofeng@buaa.edu.cn)

Received: 7 February 2026 | **Revised:** 7 May 2026 | **Accepted:** 3 June 2026

Keywords: etching | functionalization | intercalant | interlayer diffusion | MXene surface chemistry

ABSTRACT

MXenes, a burgeoning family of two-dimensional transition metal carbides, nitrides, and carbonitrides, have garnered significant attention due to their metallic conductivity, hydrophilicity, and surface-rich chemistry, offering immense potential across electrochemical energy storage, catalysis, and advanced sensing. Achieving precise control over their surface chemistry is pivotal for tailoring physicochemical properties and unlocking application-specific functionalities. This review comprehensively summarizes recent progress in MXene chemistry modulation via advanced synthesis protocols and post-synthetic modifications, with an emphasis on surface terminations and interlayer engineering. We discuss the influence of etching conditions, delamination strategies, and intercalation chemistries on the structural and electronic characteristics of MXenes. Moreover, mechanistic insights into ion intercalation and surface functional group evolution are critically analyzed to guide rational design strategies. Key challenges—including batch-to-batch variability, limited scalability, and insufficient mechanistic understanding of surface transformations—are also addressed. This review provides a forward-looking perspective on engineering MXenes with tunable interfaces for next-generation applications in energy, catalysis, and flexible electronic skin systems.

1 | Introduction

Since being firstly reported in 2011, MXene, a class of two-dimensional (2D) transition metal carbides, nitrides, and carbonitrides which exhibit exceptional electronic, optical, and mechanical properties, has created a remarkable impact in many fields, including energy storage, electronics, catalysis, and thermal management [1–11]. "MXene" derives from its precursor, the MAX phase, which consists of an early transition metal (M), a group A element (typically Al or Si), and carbon/nitrogen (X). MXenes are generally produced by selectively etching the A-layer from these precursors, leaving behind delaminated 2D nanosheets [1, 2, 4, 12, 13].

Various top-down and bottom-up MXene synthesis strategies have been developed, including water-based etching, molten salt etching, electrochemical exfoliation [14], and chemical vapor deposition (CVD) [9, 15]. These diverse techniques provide unique opportunities to tailor the structural arrangement and chemical composition of MXenes. The most commonly used strategy for MXene synthesis is the water-based method, which involves the use of hydrofluoric acid (HF) or in situ HF etching [16]. In this method, the MAX phase is immersed in a solution of HF, which selectively etches the A-element layer, generating the MXene nanosheets. The in situ HF method involves the use of a mixture of hydrochloric acid (HCl) and lithium fluoride (LiF) to generate in situ HF, which reduces the risk of handling

All rights reserved, including rights for text and data mining and training of artificial intelligence technologies or similar technologies.
© 2026 Wiley-VCH GmbH

HF. Molten salt etching is another method for MXene synthesis, which involves the use of molten salts such as lithium chloride (LiCl) or potassium chloride (KCl) to selectively etch the A-element layer [17, 18]. This method is advantageous as it allows for the synthesis of MXene with a higher degree of crystallinity and purity. The electrochemical method involves the use of an electrochemical cell to selectively etch the A-element layer, while the bottom-up method involves the assembly of MXene nanosheets from precursor molecules. The choice of method depends on the specific application requirements and the desired properties of the synthesized MXene material.

A defining feature of MXenes is their rich and heterogeneous surface chemistry. During etching, the exposed transition metal layers usually become terminated by groups such as –OH, –F, and –O [19]. The type and distribution of these surface groups are not fixed, but strongly depend on the synthesis route and post-treatment conditions. As a result, MXenes prepared by different methods often show differences in wettability, charge transfer behavior, and adsorption properties, which in turn affect their performance in energy storage, catalysis, sensing, and related applications [20–25]. Surface chemistry tailoring mainly refers to the controlled regulation of surface terminations and related interfacial features of MXenes. This includes not only adjusting the composition and coverage of surface groups, but also understanding how such changes influence electronic structure and interfacial reactivity. Rather than treating surface functionalization as a simple chemical decoration, we emphasize its central role in tuning the intrinsic properties and application behavior of MXenes. Beyond the basal plane, the confined interlayer gallery is another defining feature of 2D MXenes [26]. The deliberate introduction of specific intercalants is required not only to exfoliate the etched multilayers but also to dictate the subsequent interlayer chemical reactions and corresponding mechanisms. To date, common intercalants are primarily categorized into three types: molecular intercalants, cationic intercalants, and organic base intercalants [27]. Water molecules form complexes with different ions introduced during etching, which are difficult to completely remove after drying. Thermodynamic studies often reveal trends of specific chemical species inserting into and adapting to the interlayer spaces of MXene [28]. The summarized intercalation mechanisms cannot comprehensively encapsulate the intercalation process of MXene, as the intercalation of interlayer substances is also actually influenced by the diffusion processes of molecules/ions and water. Recently, numerous studies have begun to refocus on the intrinsic properties of MXene and have discovered many new properties such as superconductivity and terahertz shielding. Various modification approaches, such as thermal annealing, chemical functionalization, and surface modification, allow for the fine-tuning of interlayer spacing, charge exchange, and surface MXene chemistry. These modifications can not only optimize the electrochemical performance and stability of MXene for energy storage applications but also enhance the reactivity and selectivity for catalytic and sensing applications. It is believed that postsynthetic modifications of MXene have further expanded its application range.

However, the development of more mature 2D materials has shown that their practical applications often depend on how well their intrinsic properties are understood and controlled. This is particularly true for MXenes, whose surface chemistry and intercalation behavior have often been discussed in an oversimplified or ambiguous manner [29]. Although many previous reviews have summarized their synthesis and applications, the underlying physical chemistry that governs these properties remains insufficiently addressed [30]. In this review, we therefore focus on the surface and intercalation chemistry of MXenes, with particular attention to surface terminations and stoichiometry, the distinct reactivity of edges and basal planes, and the thermodynamic and kinetic factors involved in intercalation. By linking recent advances in synthesis with these underlying chemical principles, this review aims to provide a clearer framework for understanding and designing MXenes.

2 | Various Synthesis Methods of MXene

The synthesis of MXene is the first step in obtaining MXene from MAX phase, developing its properties and precise chemistry. As outlined by field pioneers, including Huang and Gogotsi, during the 2020 International MXene Conference, the development of environmentally friendly, safe, and scalable synthesis protocols remains a paramount challenge. Driven by this consensus, recent advancements in synthesis design have fundamentally reshaped MXene chemistry. A series of theories and experiments indicate the chemistry of MXene is strongly influenced by the composition and configuration of its surface terminations, with different synthesis methods directly intervening in the surface terminations of MXene, thereby affecting its practical applications [28, 29]. Researches of MXene synthesis have focused more on conventional water-based etching synthesis methods since the discovery of MXene, including direct HF etching [30], in situ HF etching [31], alkali etching [32], and electrochemical etching [33]. The main drawbacks of conventional synthesis methods are their inherent dangers, scalability issues, and challenges in achieving surface termination control [18]. Environmentally friendly chemical synthesis methods should also be considered. To mitigate these drawbacks, alternative methods have been devised, such as molten salt etching [34], directly CVD synthesizing, and directly chemically synthesizing [9]. However, due to the relative immaturity of these methods, they have not been as widely adopted as the HF etching systems [35–37]. Although many excellent reviews have been published about synthesis and applications, our focus here is more on the deviations of product structures and process characteristics of MXene in different methods, to pave the way for a detailed discussion of the surface and intercalation chemistry of MXene in the following sections.

2.1 | Direct HF Etching Method

In 2011, HF was used as an etchant to etch Al-based MAX phase precursors, resulting in the preparation of layered $Ti_3C_2T_x$ MXene [30], as illustrated in Figure 1a. This study represents the earliest research into the synthesis of MXene. Since then, HF has been widely used as an etchant in the preparation and research of MXene, especially for Al-based MAX phases [38–42]. The direct HF etching method for preparing MXene usually requires several steps [39], including HF etching treatment, centrifugation, filtration, and dispersion in deionized water. In the direct HF etching method, the temperature, concentration,

16136829, 2026, 46, Downloaded from https://onlinelibrary.wiley.com/doi/10.1002/smll.74769 by Beihang University (Buaa), Wiley Online Library on [23/09/2026]. See the Terms and Conditions (https://onlinelibrary.wiley.com/terms-and-conditions) on Wiley Online Library for rules of use; OA articles are governed by the applicable Creative Commons License

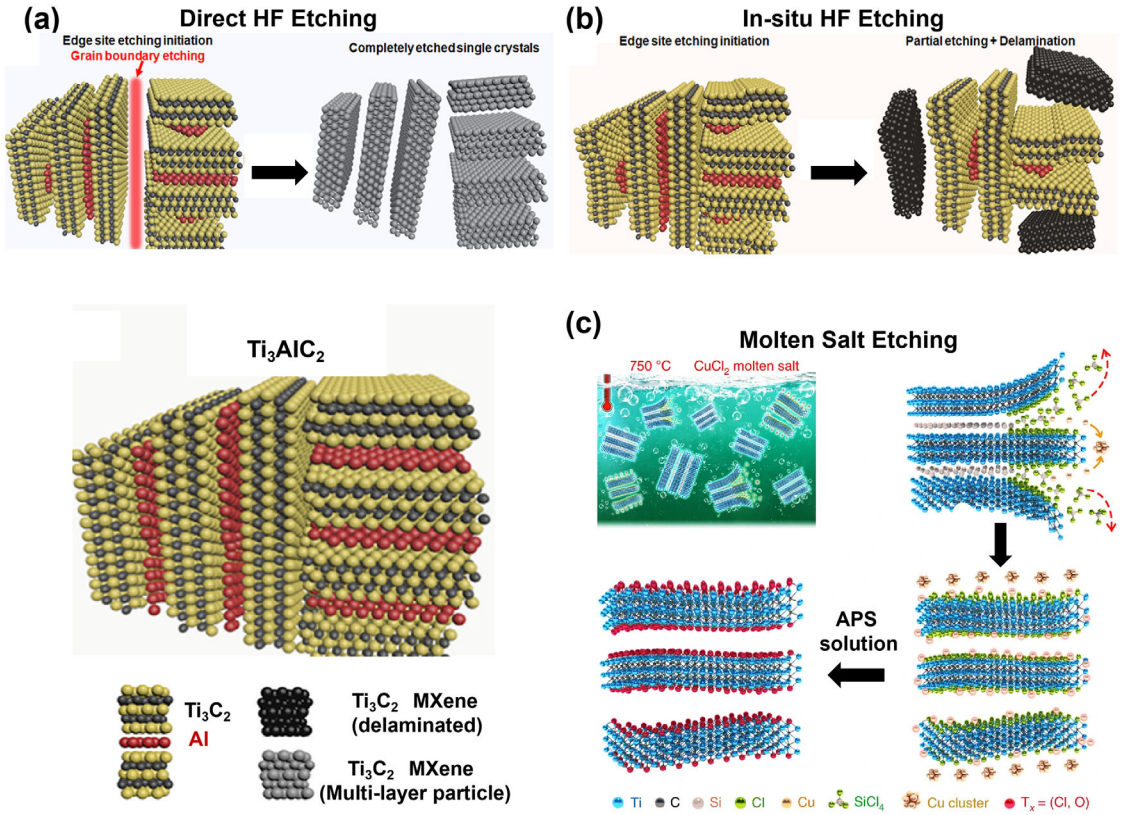

FIGURE 1 | Several methods used for etching and preparing MXene. (a, b) Schematic diagram of the Al etching mechanism for direct in situ HF (LiF/HCl)/HF solutions in polycrystal MAX particles. Reproduced with permission [43]. Copyright 2021, American Chemical Society. (c) A general Lewis acidic etching route for preparing MXene in molten salt etching method. Reproduced with permission [17]. Copyright 2020, Springer Nature.

and time of HF etching all have a significant impact on the composition and structure of the product (the properties of the MAX phase are naturally important factors but beyond the scope of this article [43, 44]). In detail, the etching process of Ti_3AlC_2 requires continuous heating, and when the reaction temperature is lower than 15 °C, the etched product will contain a large amount of Ti_3AlC_2 impurities in addition to the desired Ti_3C_2 MXene [45]. Then, the Ti vacancy concentration can be controlled by the concentration of the etchant (HF) used in the etching process. Generally speaking, with the enhancement of acidity, the vacancies in MXene increase, and it may even lead to reduced yield [38]. Interestingly, Ti vacancies are highly oxygen affinity and may become active sites for catalytic reactions [46, 47]. For example, recently by controlling the surface Ti vacancy sites of $Ti_3C_2T_x$ MXene and the redox reaction between H_2O_2 molecules, the surface defects can be transformed in situ into titanium dioxide nanoclusters anchored on amorphous carbon (TiO_x@C), which is expected to have applications in the field of chemical catalysis [46]. However, this also means that it is necessary to strictly control the concentration of the etchant to balance the etching efficiency and quality of the product. Finally, precise control of etching time and temperature can also produce layered MXene with different structures and compositions. There is a study that successfully obtained $Ti_3C_2T_x$ MXene with an accordion-like structure by etching Ti_3AlC_2 powder with a suitable concentration of HF at 50 °C for only 0.5 h [48]. It can be seen that the direct HF etching method requires strict control of etching parameters to achieve the desired etching quality. Recently, this method is gradually being standardized. By varying the HF etchant concentration, researchers produced $Ti_3C_2T_x$ samples with different surface Ti-vacancy densities and identified the vacancy level (~8 at%) that best balances catalytic activity and framework stability [49]. First-principles calculations confirm the energetic stability of Ti vacancies within 10 at%, identifying ~8 at% as the critical threshold for optimizing the hydrogen adsorption Gibbs free energy (ΔG_{H*}) toward 0 eV. This atomic-scale modulation effectively lowers catalytic activation barriers, evidenced by a significant reduction in HER overpotential from >400 to 100–150 mV. Thus, controlled etching acts as a precision tool for tuning the intrinsic activity of MXene basal planes [50, 51].

As the earliest synthetic method developed, the direct HF etching method demonstrates several basic process characteristics of water-based methods. The HF etching process reflects the coupling effect of kinetics and thermodynamics. HF is embedded and dissociated from the MAX phase edge into H and F, terminating Ti atoms, weakening Ti–Al bonds, and promoting the generation and removal of AlF_3. Low HF concentration can lead to incomplete etching, while high concentration may cause excessive etching and MXene degradation. Thermodynamically, fully F-capped MXene is most stable due to its lowest Gibbs free energy. However, in the presence of H_2O, the ΔG of different F/OH terminal configurations is very close, resulting in a random and nonuniform distribution of surface functional groups; In contrast, naked MXene ($\Delta G > 0$) is unstable and cannot spontaneously form [52]. The MXene prepared by this method is often multilayered, resembling an accordion shape.

16136829, 2026, 46, Downloaded from https://onlinelibrary.wiley.com/doi/10.1002/smll.74769 by Beihang University (Buaa), Wiley Online Library on [23/09/2026]. See the Terms and Conditions (https://onlinelibrary.wiley.com/terms-and-conditions) on Wiley Online Library for rules of use; OA articles are governed by the applicable Creative Commons License

The layers of nanosheets are tightly bound together through various interactions, including van der Waals forces and hydrogen bonds. To obtain single-layer or few-layer MXene, it is often necessary to use an intercalating agent along with ultrasound to separate the accordion-like MXene into layers. Besides, during the etching process, the adsorption of H and F atoms on Ti weakens the Ti–Al bonds, causing the release of Al atoms as AlF_3. However, at this point, the Gibbs free energy of the Ti surface is high and tends to react with chemical species in the solution, resulting in surface functional groups such as –OH, –O, and –F. Notably, while the formation of these surface terminations is thermodynamically favorable, their distribution is largely governed by kinetic factors, leading to a nonequilibrium and random arrangement of functional groups. This means that the prepared MXene surface is not bare. The distribution of surface function groups is random, as demonstrated by X-ray photoelectron spectroscopy (XPS) analysis in initial studies on MXene synthesis [39]. What's more, there are few research methods available for studying the connection process of groups on the MXene surface [53]. This is due to the corrosive etchant used in the experimental process, which can release gases and pose difficulties such as damaging the vacuum environment, obstructing visibility, and potentially damaging equipment [1]. This makes it challenging to design in situ experiments to investigate the connection process of groups with surfaces. Finally, the intrinsic toxicity and environmental hazards of HF pose significant barriers to industrial scale-up. Although mixing HF with other acids (e.g., HCl or H_2SO_4) reduces the required fluoride concentration and makes laboratory handling manageable [41, 54], these safety risks remain a critical bottleneck for mass production.

2.2 | In Situ HF Etching Method

As mentioned before, while HF can rapidly etch MAX phases to produce the MXene, this method presents several drawbacks, most significantly concerning etching quality and safety considerations. Researchers have found that the reaction of fluoride salts and acids can achieve a similar etching effect [31, 55], which can avoid the direct use of highly concentrated and highly corrosive HF in experiments. Therefore, the in situ HF etching method, which has a similar mechanism to HF, is gradually being widely used.

The in situ HF etching method was originally utilized by Ghidiu et al. [31] in 2014, in which they synthesized HF in situ using HCl and LiF to provide the necessary H and F atoms during the etching process, as shown in Figure 1b. Later on, more preparation methods for MXene using other acids and fluoride salts (such as LiF, NaF, KF, FeF_3, and NH_4F) were also developed [56, 57]. This method is similar to the majority of steps in the direct HF etching method, with the key difference being the need to mix fluoride salts and acids to produce the required HF. The influence of temperature, acid concentration, and time during etching is similar to the previously analyzed results. However, the choice of cation in the fluoride salt can significantly affect the etching effect. Studies have mixed LiF, NaF, KF, and NH_4F with HCl to etch Ti_3AlC_2 and Ti_2AlC, finding that the cation in the fluoride salt greatly influences the minimum etching time and temperature [56]. For Ti_3C_2, at the same concentration, LiF and NH_4F require 24 h of etching at 50 °C and 30 °C, respectively, while KF and NaF require 48 h of etching at 40 °C. Moreover, the cation can affect the surface structure of the etching, which is related to its intercalant and ion radius size. Fluoride salts of transition metal cations can also be used for in situ hydrofluoric acid etching [56], such as FeF_3 and HCl, but research has found that the intercalation of Fe^{3+} into the MXene layers leads to faster oxidation of MXene [58]. The types of fluoride salts are not singular, and similarly, the acid can be replaced by other acids. Research using H_2SO_4 to replace HCl and mixed with LiF for the etching of Ti_3AlC_2 [59], found that compared with $Ti_3C_2T_x$ synthesized by the conventional method (HF/LiF and HCl), the capacitance of $Ti_3C_2T_x$ got a significant improvement, attributed to the spatial and electrostatic effects brought about by the bonding of SO_4^{2-} with Ti. However, the etching of certain special MAX phases may induce the production of other impurities, such as Al_2O_3 [60].

Compared with using HF as an etchant alone, the primary characteristic of the in situ HF etching method is that it can simultaneously complete the cation intercalation step during the process [61]. Besides, In the LiF/HCl system, HF is generated in situ, leading to a lower local HF concentration and shifting the mechanism from reaction-controlled to diffusion-controlled, where F^-/HF transport into interlayers becomes rate-limiting. This results in a higher apparent activation energy (~50–70 $kJ{\cdot}mol^{-1}$) and requires moderately elevated temperatures for efficient etching. Compared to direct HF, this pathway suppresses Ti vacancy formation but promotes cation (e.g., Li^+) intercalation and yields mixed terminations with a lower –F and higher –OH fraction due to the aqueous environment. Overall, the thermodynamic driving force for Al removal remains strong, but the altered kinetics significantly influence defect density and delamination behavior. During the deionized water washing process, as the pH of the solution rises, the slightly soluble fluoride in the solution produces cations such as Li^+, which can intercalate into MXene. Some studies also suggest that this is related to the connection of Cl atoms on the surface [62]. In any case, this makes subsequent intercalation easier to carry out, even without ultrasonic assistance, the delamination process can be completed by manual shaking [63]. This is crucial for the preparation of large-area and single-layer MXene, because ultrasound can cause the MXene sheet to fracture due to cavitation. Besides, the etching process of this method is relatively mild. Mechanistic studies show that direct HF etching attacks grain boundaries, fracturing polycrystalline MAX phases into smaller microcrystals to accelerate exfoliation [40]. In contrast, in situ HF etching avoids this destructive grain boundary attack. This can reduce the generation of vacancy, but it also makes the etching process not thorough, often requiring the addition of HCl again before washing to dissolve the unreacted LiF (or other fluoride salts). In addition, the MXene prepared by this method often has a lower –F group concentration compared with the MXene directly etched out by HF [58]. In addition, since this in situ method facilitates intercalation directly within an aqueous environment, it inevitably traps water molecules within the MXene interlayers. These molecules strongly coordinate with etching residues (such as Li^+) to form robust hydration complexes, making them notoriously difficult to remove through conventional drying protocols [9, 64]. Overall, this method is currently the most practical and common etching method in MXene preparation.

16136829, 2026, 46, Downloaded from https://onlinelibrary.wiley.com/doi/10.1002/smll.74769 by Beihang University (Buaa), Wiley Online Library on [23/09/2026]. See the Terms and Conditions (https://onlinelibrary.wiley.com/terms-and-conditions) on Wiley Online Library for rules of use; OA articles are governed by the applicable Creative Commons License

2.3 | Molten Salt Etching Method

The fluorine-containing water etching system can effectively etch most of the MAX phases containing Al carbides. However, due to the influence of the water environment, some MXene with low structural stability are unstable in fluorine-containing solutions [65]. Moreover, the barrier for the transformation of nitride MXene is much higher than that of carbides [66], which makes some MAX phases insufficient to break their M–A bonds by using HF. In 2016, Urbankowski et al. [67] used molten fluorides to etch Al from the Ti_4AlN_3 phases, successfully prepared the $Ti_4N_3T_x$ MXene. Although this etching method has many drawbacks (such as the introduction of uncontrollable –OH, –O, –F groups), it proves the possibility of obtaining nitride MXene by disrupting the structure of nitride MAX phases at high temperature. In 2019, Li et al. [17] proposed a method to etch Ti_3AlC_2, Ti_2AlC, Ti_2AlN, and V_2AlC MAX phases in a mixture of $ZnCl_2$/NaCl/KCl molten salt system under nitrogen protection, as shown in Figure 1c. Compared with previous studies, it creatively prepared MXene with only –Cl surface functional groups. Inspired by this, in 2020, Li et al. [34] proposed a general route of Lewis acids etching. Unlike aqueous etching, the selectivity of these molten-salt routes is fundamentally governed by redox etching potentials. The Lewis acid cations must possess a sufficiently high reduction potential to spontaneously oxidize the "A" layers, ensuring the thermodynamic feasibility of the exfoliation while preserving the robust M–X backbone. Based on this principle, the type of etchant has expanded to Lewis acids, and the MAX phases that can be etched have also expanded from MAX phases containing Al to other MAX phases (A = Si, Zn, Ga, etc.). Even though this method needs to further remove the generated Cu particles through ammonium sulfate, the final production of functional groups only containing O and Cl is still one of its important features. This provides an important opportunity to adjust surface chemistry and performance. Kamysbayev et al. [15] used Lewis acid $CdBr_2$ to etch and prepare MXene with a surface of Br. Because halogen atoms are more likely to participate in element exchange, a series of –O, –NH, –S, –Cl, –Se, –Br, and –Te MXene were prepared, which allowed for unprecedented control over the MXene surface groups. Recently, Ding et al. [5] proposed a chemical scissors structure editing technique. By alternating the use of LAMS and metal scissors for structural editing, MAX phases and MXene can be directly exfoliated into stacked sheets in molten salt, leading to the discovery of a series of two-dimensional metal intercalated carbides. The method of obtaining different MXene by etching MAX phases with molten salt is now very mature.

In the molten salt etching method, the influence of different molten salt types on the etching of MXene is not only reflected in the etching ability and etching temperature, but also in the properties of the products. Yan et al. found in their research on fluorinated molten salt etching that after TABOH delamination, the thickness of MXene prepared with binary fluoride salt is less than that of ternary fluoride salt. In the majority of molten salt etching processes, the crucial control factor is the ratio of the molten salt. An Al-MAX/$ZnCl_2$ molar ratio of 1:1.5 can produce Zn-MAX phase, while a molar ratio of 1:6 will produce MXene [17]. Molten salt etching is highly influenced not only by the type of etching salt but also by other external conditions. Recently, Xie et al. [68] found that simultaneous microwave assistance during molten salt etching greatly shortened the etching time. The preparation of halogen functional group $Ti_3C_2T_x$ MXene only took 1 h.

A defining advantage of the molten salt etching method is its entirely water-free environment, which inherently precludes the formation of –F terminations [68, 69]. Furthermore, unlike aqueous techniques that universally yield mixed functional groups, this strategy enables highly uniform single-termination coverage. This breakthrough paves the way for sophisticated MXene engineering with precise chemical surface sensitivity [15]. However, this method is not completely perfect. A major problem to be solved is how to delaminate the MXene after etching in a nonaqueous environment [70]. Also, this method often introduces new solid impurities [17], like Cu, Zn. How to cleanly and thoroughly separate the product from the impurities is also a research direction. Overall, this is an environmentally friendly method of preparing MXene, which has great developmental prospects [71, 72]. Meanwhile the stability of single-halogen terminations in practical environments should be considered carefully. When halogen-terminated MXenes are exposed to moisture or aqueous electrolytes, ligand exchange and surface reconstruction may occur, which can gradually alter the initially prepared surface chemistry. As a result, these single-termination surfaces may be less stable in ambient or protic environments than in vacuum or nonaqueous systems. Therefore, although molten-salt synthesis provides an important way to obtain well-defined surface terminations, the preservation of these terminations during storage, device fabrication, and operation still needs further study. In this sense, such materials may be more suitable in some cases as model systems or reactive intermediates for further surface modification, rather than as permanently stable surface states in aqueous applications.

2.4 | Other Synthesis Method

In addition to the three most common etching methods for preparing MXene, there are other methods [9, 33, 69, 73]. For instance, for the etching of Al-based MAX phases, due to the amphoteric nature of Al^{3+}, F^- can be replaced by OH^-, forming the basis of an alkali etching route. Li et al. [33] proposed a NaOH-assisted hydrothermal process for etching Ti_3AlC_2 to prepare $Ti_3C_2T_x$. The results showed that in a 270 °C, 27.5 M NaOH solution, Al was selectively removed from Ti_3AlC_2, generating multilayer $Ti_3C_2T_x$ with only –OH and –O groups. The purity of products was 92 wt%. This indicates that using alkali to etch MAX phases is quite effective. The MXene prepared by this method is highly hydrophilic due to the absence of –F during the process. However, the use of alkali often introduces oxidation issues [74], and the risks associated with high concentration alkali and high temperatures limit the ability of large-scale preparation.

Electrochemical etching is also a new method for preparing MXene. Yang et al. [33] developed an efficient fluorine-free etching method based on the anodic corrosion of titanium aluminum carbide (Ti_3AlC_2) in a binary aqueous electrolyte and intercalated NH_4OH in situ after the Al was dissolved, resulting in MXene sheets ($Ti_3C_2T_x$, T_x = O, OH) up to 18.6 μm in size, with single and double layers also achieving over 90% yield. Pang et al. [73] prepared MXene (Ti_2CT_x, V_2CT_x, and Cr_2CT_x), which cannot be

16136829, 2026, 46, Downloaded from https://onlinelibrary.wiley.com/doi/10.1002/smll.74769 by Beihang University (Buaa), Wiley Online Library on [23/09/2026]. See the Terms and Conditions (https://onlinelibrary.wiley.com/terms-and-conditions) on Wiley Online Library for rules of use; OA articles are governed by the applicable Creative Commons License

prepared by conventional HF etching method, by using thermally assisted electrochemical etching. Electrochemical etching is often combined with other etching methods. Shen et al. [69] developed a molten salt-assisted electrochemical etching method to produce fluorine-free $Ti_3C_2Cl_2$. Because electrons are used as reactants, cathodic reduction and anodic etching are spatially separated, so $Ti_3C_2Cl_2$ does not contain metal impurities. Moreover, the surface groups can be in situ modified from –Cl to –O/–S, which greatly shortens the modification steps and enriches the types of surface terminations.

Beyond the conventional top-down exfoliation of MAX phases, bottom-up synthesis has emerged as a compelling alternative. Rather than etching bulk precursors, these strategies meticulously construct MXene lattices atom-by-atom or molecule-by-molecule, offering unprecedented control over intrinsic structure. Two principal bottom-up strategies have been demonstrated: The first one is solid-state direct synthesis. In this one-pot method, metal and carbon precursors react in the presence of a halide source to nucleate MXene without any HF etching. These approaches offer unparalleled control over termination chemistry and enable morphologies, such as vertical nanosheets which are difficult to achieve by etching alone [75]. The second one is CVD method, which could grow MXene films on a hot substrate by reacting vapor-phase precursors [25]. Recently, Wang et al. [9] introduced two methods for direct synthesis of MXene in their research. One method involves grinding titanium and graphite in a molar ratio of 3:1.8, mixing with 1.1 molar equivalent of $TiCl_4$, and heating at 950 °C for 2 h to directly obtain Ti_2CCl_2 MXene. However, this method may produce TiC_x impurities because the formation of MXene phases is a result of kinetic competition between Ti_2CCl_2 and TiC_x. Specifically, this phase selectivity is governed by the narrow thermodynamic window of the precursors; slight deviations in carbon activity or temperature can easily shift the growth from 2D MXenes to the more stable 3D bulk carbides [9]. Furthermore, this precise synthesis is often accompanied by a dynamic termination evolution, where kinetically favored species (like –Cl or –F) may undergo thermodynamic substitution by oxygen-based groups during subsequent processing or ambient exposure. Another method involves direct synthesis of MXene using CVD. Under an Ar atmosphere, a mixture of CH_4/N_2 and $TiCl_4$ gases is introduced, and Ti_2CCl_2 and Ti_2NCl_2 MXene are grown on the Ti surface through CVD at 950/640 °C. The obtained MXene has a more accessible surface and exposed catalytic active edges. Moreover, this MXene is grown vertically, which is of great value for certain fields (ion intercalation of supercapacitors [15], etc.). These major synthesis routes differ not only in procedure, but also in their reaction environments and phase formation mechanisms, which strongly affect structural integrity and surface terminations. Mechanistically, the overall synthesis efficiency and exfoliation quality are dictated by the transition between kinetic regimes. Initially, the process operates in a reaction-controlled regime, limited by the activation barriers of breaking metallic M–A bonds. As the interlayer opens, it shifts into a diffusion-controlled regime, where the mass transport of etchants within the confined 2D galleries becomes the rate-limiting step [7]. Direct HF etching is usually fast and effective, but the reaction is often difficult to control because of its strong acidity and high reactivity. As a result, it can easily introduce structural damage, defects, and mixed surface groups. In contrast, in situ HF etching is relatively milder because the etchant is generated gradually during the reaction. This often helps reduce excessive etching, suppress defect formation, and preserve larger flakes. Molten-salt etching differs more fundamentally from these aqueous methods because it proceeds in a high-temperature, water-free environment. Under these conditions, phase formation is more closely related to redox reactions and solid-state diffusion, rather than simple acid etching in solution. This difference also gives molten-salt methods greater potential for accessing unusual surface terminations and more uniform surface chemistry.

2.5 | Scalable Synthesis of MXene

Transitioning MXenes from milligram-scale curiosity to industrially relevant materials require etching and exfoliation processes that are safe, high-throughput, and yield uniform surface chemistry. Below we integrate recent literature demonstrations with our survey of synthesis methods to outline scalable MXene production strategies.

Building on the Lewis-acid route as shown in Section 2.3, kilogram-scale melts of $ZnCl_2$/NaCl/KCl at 400–600 °C under inert atmosphere have been shown to etch a variety of MAX phases in one step, yielding Cl-terminated MXenes with uniform single-halogen surface chemistry. Subsequent water washing removes residual salts, producing >100 g batches of $Ti_3C_2Cl_2$ with crystallinity and interlayer spacing identical to small-scale samples [17]. A stirred-tank reactor charged with Ti_3AlC_2 and LiF/HCl etchant at ~40 °C produced 50 g of $Ti_3C_2T_x$ in a single run, with the same layer spacing, conductivity, and surface –O/–F/–OH terminations as milligram-scale samples. This HF-free approach combines environmental safety with high throughput, and its single-termination control facilitates reproducible properties for energy storage and EMI-shielding applications [14].

Pumping a slurry of MAX + LiF/HCl through a heated tubular flow reactor (40–60 °C) delivers ~10 g h^{-1} of $Ti_3C_2T_x$ with consistent thickness and terminal composition, while minimizing operator exposure to HF. In a continuous foil-anode setup immersed in NH_4Cl electrolyte under applied potential, MXene sheets peel off meter-long electrode rolls, integrating etch, intercalation, and delamination in one step and eliminating batch sonication.

In a complementary roll-to-roll electrochemical configuration, a continuous metal foil coated with MAX precursor serves as the anodic electrode in an NH_4Cl bath. Upon application of a mild oxidative potential, the Al (or other A-element) is selectively dissolved, and intercalation of NH_4^+ simultaneously weakens interlayer cohesion. As the foil advances, meter-long ribbons of few-layer $Ti_3C_2T_x$ spontaneously delaminate and float off, fully integrating etching, cation insertion, and exfoliation in a single automated step [76]. This continuous process eliminates the need for time-consuming batch sonication or centrifugation, dramatically improving throughput and enabling direct collection of MXene films for downstream coating or device fabrication.

By combining molten-salt, alkali hydrothermal, continuous-flow, and electrochemical methods, researchers have demonstrated

16136829, 2026, 46, Downloaded from https://onlinelibrary.wiley.com/doi/10.1002/smll.74769 by Beihang University (Buaa), Wiley Online Library on [23/09/2026]. See the Terms and Conditions (https://onlinelibrary.wiley.com/terms-and-conditions) on Wiley Online Library for rules of use; OA articles are governed by the applicable Creative Commons License

true gram-to-kilogram MXene production without sacrificing structural or surface-chemical precision, paving the way toward commercial deployment in energy storage, catalysis, sensing, and EMI shielding [14]. The pursuit of high-quality, large-scale production is a shared goal across the 2D materials community. The field of MXene synthesis is rapidly advancing toward continuous-flow and electrochemical methods to achieve similar levels of structural and chemical precision at industrial scales. Besides, in evaluating scalable MXene synthesis, production volume alone is not sufficient. To establish a rigorous comparative framework, explicit quantitative criteria must be defined: single-layer yield, batch-to-batch reproducibility, and termination uniformity. A literature-supported comparison reveals stark differences across these routes. Traditional direct HF etching typically suffers from low single-layer yields (~30%–50%) and high defect accumulation due to the required harsh sonication. In contrast, optimized minimally intensive layer delamination protocols safely boost the yield of large, single-layer flakes [77], while continuous electrochemical exfoliation strategies have reported exceptional single/few-layer yields exceeding 90%. Regarding reproducibility, scaling up LiF/HCl etching to 50 g per batch in stirred-tank reactors has demonstrated remarkable consistency; recent studies quantify the batch-to-batch variance in macroscopic electrical conductivity to be strictly less than 5% [14]. Furthermore, molten-salt synthesis dominates the criterion of termination uniformity, overcoming the mixed-ratio variance (χ_T) of aqueous routes by yielding near 100% single-halogen coverage. These explicitly defined quantitative metrics serve as indispensable benchmarks for translating laboratory synthesis into reliable industrial production. Continuous methods may help improve yield by reducing the material loss and structural damage often caused by batch processing, and some recent electrochemical exfoliation methods have reported single-layer yields above 90% [78]. Molten-salt routes may also offer an advantage in termination uniformity, because their reaction environment is more homogeneous and can better support the formation of well-defined surface groups [79]. Therefore, scalable synthesis should be assessed not only by how much material can be produced, but also by how consistently its structure and surface chemistry can be controlled.

3 | Surface Chemistry in Synthesis Process

Although MXene was synthesized as early as 2011, the method for the systematic preparation of MXene with uniform functional groups was not mastered until 2019. The surface chemistry of MXene mainly relies on the type, quantity, and position of different surface functional groups, which have a decisive impact on the properties [80], intercalation [81], modification [81], and storage of MXene.

In the previous section, various etching methods for MXene were mainly discussed. However, our focus is on comparing the process characteristics of MXene produced by different etching methods, and a detailed introduction of surface functional groups of MXene was not provided. This section mainly introduces the surface chemistry of MXene, type, quantity, and position of surface groups to provide some assistance in gaining a more comprehensive understanding of the surface structure of MXene.

3.1 | Various Surface Structures

Different etching methods of MXene often determine the type of surface functional groups [45, 82, 83]. The etching involving HF occurs in an aqueous environment and selectively removes "A" elements during the etching process, resulting in a highly active surface. The exposed metal surface of non-terminated MXene easily reacts with surrounding substances, leading to the generation of abundant surface functional groups (–F, –OH, –O). Since XPS has a low penetration depth, it has surface sensitivity and can provide information about the chemical composition and oxidation state of elements [84, 85]. Naguib et al. [30], who first prepared MXene, as shown in Figure 2a, used XPS for characterization and found that the intensity of the Ti_3C_2 Ti-O *2p3* bond was significantly enhanced by comparing the energy spectra before and after HF treatment, which well confirmed the formation of hydroxyl and/or oxide functional groups on the MXene surface. Therefore, 'T_x' was added to its chemical symbol. Al and F peaks were also observed, with the residual aluminum content reduced to approximately 3 at% and fluorine content at around 12 at%. This is mainly attributed to the formation of the reaction by-product AlF_3. Combined with Raman spectroscopy, the weakening of the Ti-Al vibrations indicated the etching of Al atoms. The presence of -OH groups was also observed. However, when HF etching was performed, the addition of other acids (as mentioned before) was often used to reduce the concentration of the HF being used, which led to new changes in the surface functional groups of MXene. The choice of etchant significantly influences the resulting interlayer spacing. As shown in Figure 2c, samples etched exclusively with HF and subsequently washed with LiCl exhibit a $d_{(002)}$ spacing shrinkage to 12.4 Å [62], In contrast, when etching is performed using a mixture of HF and inorganic acids with larger anions, subsequent washing in a Li^+ containing solution dramatically expands the $d_{(002)}$ spacing to 16 Å. It was concluded that larger anions promoted the intercalation of water, which also meant that some anions were likely adsorbed in the interlayers, and the most likely adsorption sites were the edges of the layers [86]. This means that MXene may have –Cl or –Br surface functional groups (when HCl or HBr is used.). This also explains why the mixed acid is more likely to disperse MXene, possibly because the presence of these groups weakens the van der Waals forces and hydrogen bonds between the layers [87]. Kajiyama et al. [88] found that compared with direct etching with HF, the LiF/HCl system of Ti_2CT_x had a larger interlayer spacing (8.7 Å/7.7 Å) in their study, which was not caused by a large amount of Li embedding, as no significant amount of Li was detected by magic angle spinning nuclear magnetic resonance spectroscopy (MAS-NMR). However, XPS shows the presence of a large amount of –Cl groups on the obtained MXene surface, as illustrated in Figure 2b. Its chemical composition can be roughly expressed as $Ti_2C(OH)_{0.3}O_{0.7}F_{0.6}Cl_{0.4}$. The existence of the –Cl groups in Ti_2CT_x (LiF/HCl) is also supported by the *ab initio* calculation, the calculated d_{inter} values for "T" combinations show a continuous increase with the increase of the –Cl termination group fraction [88].

For the MXene prepared by molten salt etching method, the type of functional groups on the MXene surface seems relatively simple. Thanks to the pioneering research of Li et al. [89], MXene prepared with Lewis acid salt can achieve a single halogen

16136829, 2026, 46, Downloaded from https://onlinelibrary.wiley.com/doi/10.1002/smll.74769 by Beihang University (Buaa), Wiley Online Library on [23/09/2026]. See the Terms and Conditions (https://onlinelibrary.wiley.com/terms-and-conditions) on Wiley Online Library for rules of use; OA articles are governed by the applicable Creative Commons License

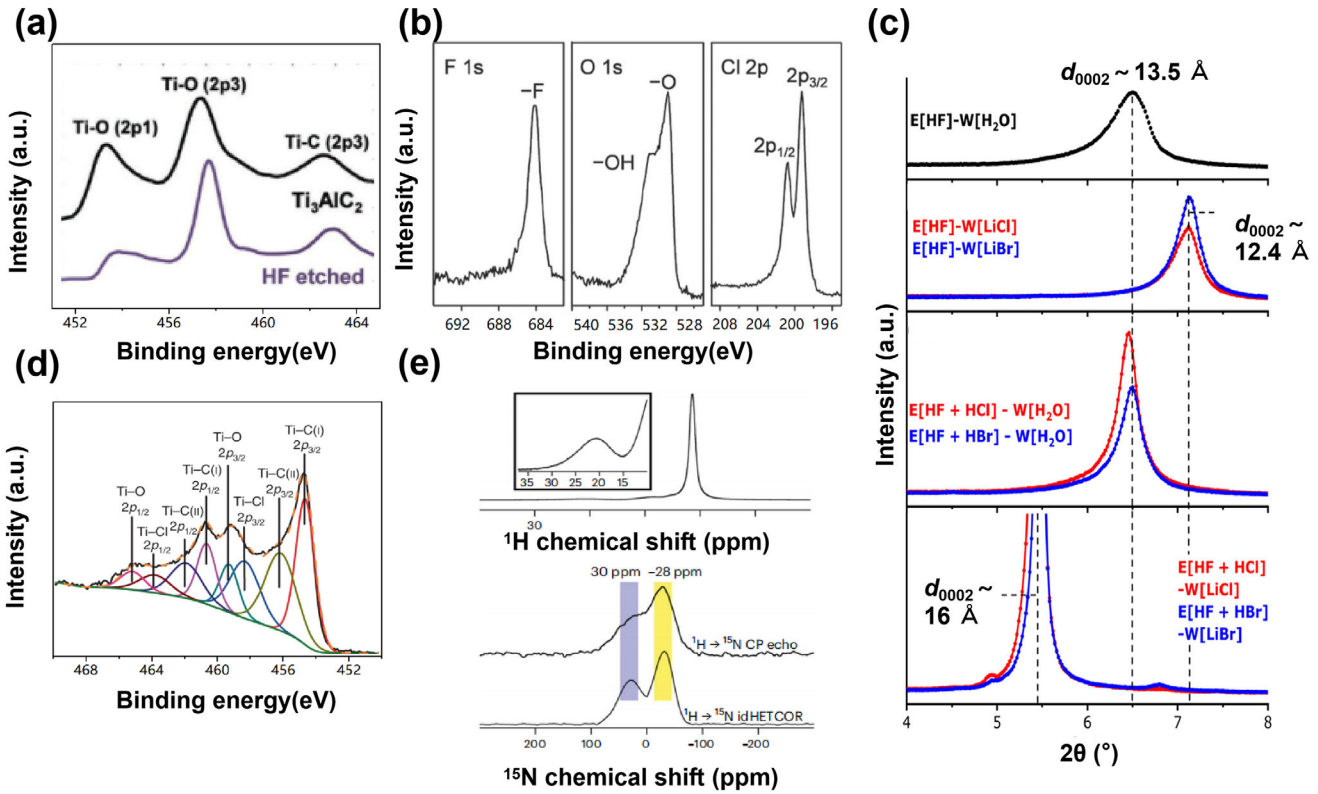

FIGURE 2 | Researches toward the type of surface groups of MXene. (a) XPS spectra of Ti_3AlC_2 before and after direct HF etching show the presence of Ti–O (–O, –OH). Reproduced with permission [30]. Copyright 2011, Wiley-VCH. (b) XPS spectra for F 1s, O 1s, and Cl 2p for Ti_2CT_x (LiF/HCl) without sputtering show the presence of –F, –O, –OH, –Cl groups. Reproduced with permission [88]. Copyright 2017, Wiley-VCH. (c) Low-angle XRD patterns of fresh, never dried $Ti_3C_2T_x$ MLs, E (etching) and then W (washing) show the influence of anions in the etching stage. Reproduced with permission [89]. Copyright 2018, American Chemical Society. (d) XPS analysis of the Ti 2p energy level from the MS-$Ti_3C_2T_x$ MXene sample, where O may have been introduced during subsequent washing processes. Reproduced with permission [89]. Copyright 2018, American Chemical Society. (e) ^{1}H spin echo, ^{1}H-^{15}N CPMAS spin echo, and ^{1}H-detected ^{15}N CPMAS spectrum of $Ti_3C_2(^{15}N\text{-dda})_{2/3}$. Reproduced with permission [90]. Copyright 2023, Springer Nature.

terminal group. Based on XPS analysis (Figure 2d), the peak at 458.1 eV is attributed to Ti–Cl ($2p_{3/2}$) bonds, and the peak at 464.1 eV is assigned to Ti–Cl ($2p_{1/2}$) bonds, confirming the presence of Ti–Cl bonds. Aside from Ti–C and Ti–Cl bonds, no other elemental bonds with titanium are observed. Furthermore, the Ti:Cl ratio determined by XPS is 2.94:2. As subsequent research progresses, the functional groups on the MXene surface have expanded to –Br [15], –S [15], –Se [15], –Te [15], –O [15], and –I [91]. Recently, Zhou et al. [90] proposed a general method to synthesize a series of organic–inorganic hybrid MXene (h-MXene) with amine and imine surface functional groups. The ^{15}N-labeled h-MXene were characterized in detail using MAS-solid-state-NMR. Through ^{1}H-^{15}N cross-polarization magic angle rotation (CPMAS) spin echo spectra, as shown in Figure 2e, significant ^{15}N NMR signals were found in the regions with chemical shifts of 30 and −28 ppm, indicating the simultaneous coordination of imine (–NR) and amine (–NHR) ligands with surface titanium atoms. Among all surface functional groups, approximately 58% exist in the form of –NR, and the remaining 42% in the form of –NHR. Through the ^{1}H-^{15}N indirect detection heteronuclear correlation (idHETCOR) experiment at inversion CP contact times of 0.4 and 8 ms, the assignment of the ^{15}N signal was further confirmed. Finally, through the ^{15}N-^{1}H heteronuclear J-resolved spin echo experiment detected by ^{1}H, it was confirmed that in -NHR, the nitrogen atom forms a covalent bond with a single hydrogen atom.

MXene prepared by the CVD method could also achieve uniform surface functional groups [9]. They can react with Ti and $TiCl_3$/$TiCl_4$ and various carbon and nitrogen sources (such as methane, graphite or nitrogen) to synthesize Ti_2CCl_2 and Ti_2NCl_2. The Ti 2p spectrum XPS of Ti_2CCl_2 shows a distinct Ti–Cl peak, indicating the formation of Cl functional groups on the surface. No Ti–C component was found in the C 1s spectrum of CVD-Ti_2NCl_2, which further confirmed the formation of pure nitride MXene.

In all synthetic methods, due to the removal of surface atom layers, the remaining uncoordinated metal atoms may possess unpaired electrons, so-called dangling bonds or defects in MXene interfaces [92–94], which could exist stably and be further modified by other organic radical functional groups. Electron paramagnetic resonance (EPR) is the most powerful tool for the structural determination and quantification of types of unpaired electrons [95–97]. Dangling bonds originate from surface vacancies (both metal and oxygen vacancies) generated during oxidative etching. These active sites significantly influence MXene's chemical reactivity, playing pivotal roles in catalysis

16136829, 2026, 46, Downloaded from https://onlinelibrary.wiley.com/doi/10.1002/smll.74769 by Beihang University (Buaa), Wiley Online Library on [23/09/2026]. See the Terms and Conditions (https://onlinelibrary.wiley.com/terms-and-conditions) on Wiley Online Library for rules of use; OA articles are governed by the applicable Creative Commons License

and sensing applications [46]. For the majority of vacancies, the Lande *g*-factor approach to 2.0023 concerning to g_e is attributed to the trapped free electrons in the vacancy site. Similar results are observed in MXene, for instance, Ti vacancies (V_{Ti}) in Ti_3C_2 MXene with $g = 2.002$, whose intensity revealed the density of V_{Ti} after different HF etching concentrations [98]. Ti vacancy could be further modified by H_2O_2 to a new coordinated environment, which is proven to be multivalence-$Ti^{\delta+}$ (δ = 0, 2, 3, and 4), resulting in a shift of *g*-factor to 2.009 [46]. Specific vacancy could also serve as the loading site of clusters, EPR intensity of V_{Ti} in $Ti_3C_2T_x$ (g = 1.941) decreased sharply after doping, suggesting the occupancy of Ti vacancy by Ru clusters [99]. O vacancies should be considered if severe oxidation was introduced, in situ forming metal oxides on the surface of MXene [100]. The spin species can be distinguished by *g*-factor, for example, 2.002 and 1.970 on M-TiO_2 evolved from MXene [101], which can be ascribed to oxygen vacancy and the accompanied Ti^{3+}. Other kinds of vacancies are also observed in MXene with different chemical compositions, unveiling the abundant defect chemistry in the design and synthesis of MXene.

Instead of relying on traditional surface functional groups, the modification of radicals on MXene presents an intriguing method for achieving chemical and physical tunability, which could be monitored by EPR. Chen et al. [102] reported the successful deposition of 4-amino-TEMPO radical on the T-$Ti_3C_2T_x$ composite film, with the emergence of triple signal lines due to the hyperfine structure of nitroxide radicals. TEMPO radicals serve as charge transfer mediators, demonstrating the improved energy storage capacity. Charge transfer in MXene induced by incorporating with surface radical dopant may also lead to the intrinsic spin polarization and diamagnetic-to-paramagnetic phase transition of MXene. The tris(4-bromophenyl)ammoniumyl hexachloroantimonate (MB) doped $Ti_3C_2T_x$ displayed an apparent EPR signal at $g = 2.0032$ with narrow linewidth of 4.26 Gauss, rather than the broader signal of MB at g = 2.0098, indicating the noncovalent interaction between MB and $Ti_3C_2T_x$ [103].

Thus, regarding the surface structure of MXene, we can give the following conclusions:

1. The surface structure of MXene includes different types of surface terminations and defect sites. The type and quantity of surface terminations are determined by the reaction environment during etching.
2. The anions of etchants will undergo substitution reactions with surface terminations during the etching process, while cations will intercalate.
3. MXene with single surface terminations can be synthesized through molten salt etching method. Surface terminations have been extended to the organic family, while surface-exposed MXene has not been reported yet.
4. Dangling bonds or defects can exist stably on the surface, and be further modified by other functional groups. Specific vacant sites can serve as loading points for clusters or be captured by radicals.

However, surface terminations are not the only factors that influence the electronic properties of MXenes. Intrinsic defects, such as metal or carbon vacancies, antisite defects, and grain boundaries, can also play an important role in charge transfer. In catalytic and optoelectronic applications, these defect sites may act as trap states or recombination centers and therefore affect carrier transport and lifetime. Their influence should not be considered separately from that of surface terminations, because the local electronic structure is often determined by both factors together. Alongside surface terminations, intrinsic defect engineering must be evaluated through a rigorous quantitative framework. To fulfill the need for specific descriptors, researchers have begun mapping exact defect densities to measurable electronic structure parameters. For instance, a recent breakthrough by Hassan et al. [104] established a quantitative correlation between precursor-derived defects and macroscopic properties. By utilizing atomic-resolution HAADF-STEM, they precisely quantified intrinsic descriptors, such as the titanium vacancy (V_{Ti}) concentration, demonstrating a controlled reduction from 3.06% down to 0.12%. Density functional theory (DFT) explicitly links these numerical descriptors to intrinsic electronic parameters: minimizing V_{Ti}, carbon vacancies (V_c), and substitutional oxygen (S_o) significantly restores both the free-electron carrier density and electron mobility. Macroscopically, this precise defect quantification translates into an exceptional electrical conductivity of 26,000 $S \cdot cm^{-1}$ and an ultralow infrared emissivity of 0.05. Therefore, defining the exact stoichiometric percentages of lattice vacancies serves as an indispensable quantitative descriptor, functioning synergistically with termination ratios to govern the ultimate electronic and thermal transport in MXenes.

3.2 | Confusing Terminal Quantity

Accurate compositional and structural characterization is essential for predicting material properties. However, deciphering the precise surface chemistry of MXenes remains fundamentally challenging, primarily due to the scarcity of analytical tools capable of definitively establishing their exact stoichiometric formulas [18]. In past studies, XPS techniques were commonly used to investigate the surface structure of MXene, but fitting the O 1s spectrum when characterizing the surface functional groups of MXene proved difficult due to the challenge of distinguishing signals from –O/–OH terminations and oxidation. Beyond these fitting challenges, the quantitative discrepancies among different characterization techniques are fundamentally rooted in the physics of the probes. Governed by the short inelastic mean free path (IMFP) of photoelectrons, XPS is restricted to an information depth of the outermost 2–10 nm. This inherent surface sensitivity inevitably biases the O/F ratio toward surface oxidation and adsorbed moisture. In contrast, volume-averaged techniques like inductively coupled plasma mass spectrometry (ICP-MS) provide a bulk representation but lack the spatial resolution to decouple surface terminations from trapped precursors or residues. As research on MXene progresses, more effective characterization methods, such as NMR and mass spectrometry, have been developed [27]. In addition, it should be noted that deviations in the processing procedures can greatly influence the accurate structural formula of MXene, as discussed previously.

Halima et al. [105] conducted a systematic study by using high-resolution XPS to identify and quantify surface groups present before and after sputter cleaning, as well as in a comparison

16136829, 2026, 46, Downloaded from https://onlinelibrary.wiley.com/doi/10.1002/smll.74769 by Beihang University (Buaa), Wiley Online Library on [23/09/2026]. See the Terms and Conditions (https://onlinelibrary.wiley.com/terms-and-conditions) on Wiley Online Library for rules of use; OA articles are governed by the applicable Creative Commons License

of newly prepared and aged multilayer cold-pressed thin sheet samples. Based on XPS peak fitting, the average and negative charge of the MXene terminals $Ti_3C_2T_x$, Ti_2CT_x, Ti_3CNT_x, Nb_2CT_x, and $Nb_4C_3T_x$ were determined to quantify the properties of the surface terminal. The obtained expressions for $Ti_3C_2T_x$ MXene are $Ti_3C_2O_{0.3}(OH)_{0.32}F_{1.2}$ and $Ti_3C_{1.8}O_{0.6}(OH)_{0.4}F_{0.8}$, with sputtering selectively removing C from the MXene lattice and reducing the concentration of F terminals. By comparing with other types of MXene, a preliminary conclusion was drawn: for Ti-based MXene, changing the number of layers "n" or "X" elements has almost no effect on the proportion of –F terminals, but these two factors will affect the ratio of –O to –OH terminals. Increasing "n" from 1 to 2 will increase the O to OH ratio, and changing 50% of the "X" elements will cause the –O to –OH ratio to decrease. For Nb-based MXene, the situation is just the opposite, changes in "n" will double the –F terminals, and the –O to –OH ratio is contrary to that of Ti-based MXene. It can be seen that it is meaningful to roughly quantify the change rules of a certain type of MXene group. These precise stoichiometric expressions should be treated as termination ratios (χ_T), a key quantitative descriptor that moves beyond empirical formulas to provide a numerical basis for predicting interfacial charge density and thermodynamic stability.

However, due to the limitations of XPS itself and the interference of surface organic matter [106–108], whether the obtained MXene expression is accurate remains to be studied. Furthermore, interpreting stoichiometry from samples subjected to traditional ion-beam sputter cleaning requires extreme caution. The preferential sputtering of lighter elements, such as terminal fluorine and lattice carbon, creates severe sputter-induced structural artifacts. Thus, depth profiling results often suffer from error propagation, where the derived stoichiometry reflects an artifact of the harsh measurement process rather than the intrinsic as-synthesized MXene chemistry. In another study on MXene composition [109], an expression of LiF/HCl MXene composition $Ti_3C_2O_{0.81}(OH)_{0.06}F_{0.77}Cl_{0.02}Li_{0.38}$ was given through ICP-MS, but the calculation method was not detailed, so it will not be discussed further.

Hope et al. [87] conducted a pioneering study of the functional groups on the surface of $Ti_3C_2T_x$ using solid-state NMR spectra. First, ^{13}C NMR verified the transformation from Ti_3AlC_2 to $Ti_3C_2T_x$ using the HF/HCl + LiCl method to prepare MXene. The decrease in the intensity of the Ti_3AlC_2 signal relative to the TiC signal and the appearance of the $Ti_3C_2T_x$ resonance peak at 412 ppm indicated the completion of the transformation. Subsequently, ^1H NMR was used to examine samples dried overnight at 200 °C, as shown in Figure 3a. Results showed signals from –OH at 18.6 and 12.5 ppm for the MXene prepared by both methods, and the peak at 6.5 ppm was due to water in the samples, indicating that vacuum drying could not completely remove interlayer water molecules in MXene. To confirm the connectivity of –OH with the sheet material, ^1H-^{13}C HETCOR NMR spectra [110] were tested, Figure 3b shows that the –OH termination at ^1H 20 ppm was clearly related to the Ti_3C_2 environment at ^{13}C 380 ppm, and other ^1H signals were not present in the spectrum, indicating environments far from the carbon layer and/or high mobility. Chemical shifts of ^1H in the system exceeded the normal ^1H chemical shifts, which might be explained from three aspects [111, 112]: Knight shifts due to metallic behavior; hyperfine (or Fermi contact) shifts due to the transfer of (unpaired) spin density from the titanium layer; and/or strong hydrogen bonds. The resonance peaks at 227 and 255 ppm in the ^{19}F NMR spectra suggested the presence of –F terminals, as shown in Figure 3c, and the formation of AlF_3 hydrate was also observed. ^1H-^{19}F HETCOR NMR indicated that the functional groups within the layers were mixed terminations, not single functional group terminations. The correlation between –F and H_2O terminals suggested the existence of interlayer water. Finally, through spin counting (comparing the signal with a known standard), the proportion of them was quantified, the mass of known impurities was corrected (EDS), assuming that each molecular formula unit had two terminals (one on each side) and the oxygen contained the remaining part to determine the fraction of oxygen terminals, the expressions of MXene prepared by the two methods were obtained: $Ti_3C_2O_{0.84}(OH)_{0.06}F_{0.25}$ (LiF/HCl), $Ti_3C_2O_{0.54}(OH)_{0.16}F_{0.8}$ (HF).

Contradictorily, early studies exhibit inconsistencies in the assignment of various peaks in the ^1H spectrum, and there is still controversy regarding the presence of water layers between MXene layers [115, 116]. Spin-echo quantitative NMR techniques have helped unveil the intercalated water inside MXene layers. Taking advantage of the fast relaxation process of water molecules, spin-echo spectra were acquired in comparison with ^1H spectra, which filtered signals assigned to water species [117]. The ^1H–^1H correlation spectroscopy revealed that surface water is not located in the vicinity of the terminal Ti–OH, suggesting that intercalated Li is present on the O-terminated surface. Despite the direct deconvolution and integration to determine the content of each species, benchmark work have reported that ^{13}C chemical shift variations can be quantitatively related to different surface compositions and a number of surface chemistry variants induced by the different etching agents [118].

Persson et al. [113] argue that there are few (or no) –OH terminations on the surface of MXene. According to their research, they performed in situ annealing of MXene prepared by HF etching on a sapphire substrate, using atomic-resolution heating in scanning transmission electron microscopy (STEM) and temperature-programmed X-ray photoelectron spectroscopy (TP-XPS). As shown in Figure 3e, the F 1s XPS spectrum contains a sharp peak at 685.3 eV, indicating the presence of an F-bearing substance coordinated to a single site. During heating, the intensity of the F 1s peak decreases to a small fraction of its original strength, indicating F desorption from the Ti_3C_2 surface at high temperatures. The O 1s XPS spectrum contains two peaks centered at 529.9 and 531.9 eV, respectively, indicating the presence of O-bearing substances in two different chemical environments on the surface. During heating, the peak at 529.9 eV significantly decreases, while a third peak gradually appears at 531.3 eV. After heat treatment at 750 °C, the latter dominates in the O 1s spectrum, and the integrated intensity of the O 1s spectrum does not change significantly during the study, indicating that no O-bearing substances desorb from the Ti_3C_2 surface. Parallel behavior is observed in the Ti 2p peaks, where the intensity is redistributed favoring the growth of the Ti $2p_{3/2}$ peak at 455.1 eV and the Ti $2p_{1/2}$ peak at 461.2 eV. In most cases, hydroxyl groups will leave during annealing [119], so hydroxides may be transformed into oxides by losing water molecules. However, –OH generally does not cause peak shifts, so

16136829, 2026, 46, Downloaded from https://onlinelibrary.wiley.com/doi/10.1002/smll.74769 by Beihang University (Buaa), Wiley Online Library on [23/09/2026]. See the Terms and Conditions (https://onlinelibrary.wiley.com/terms-and-conditions) on Wiley Online Library for rules of use; OA articles are governed by the applicable Creative Commons License

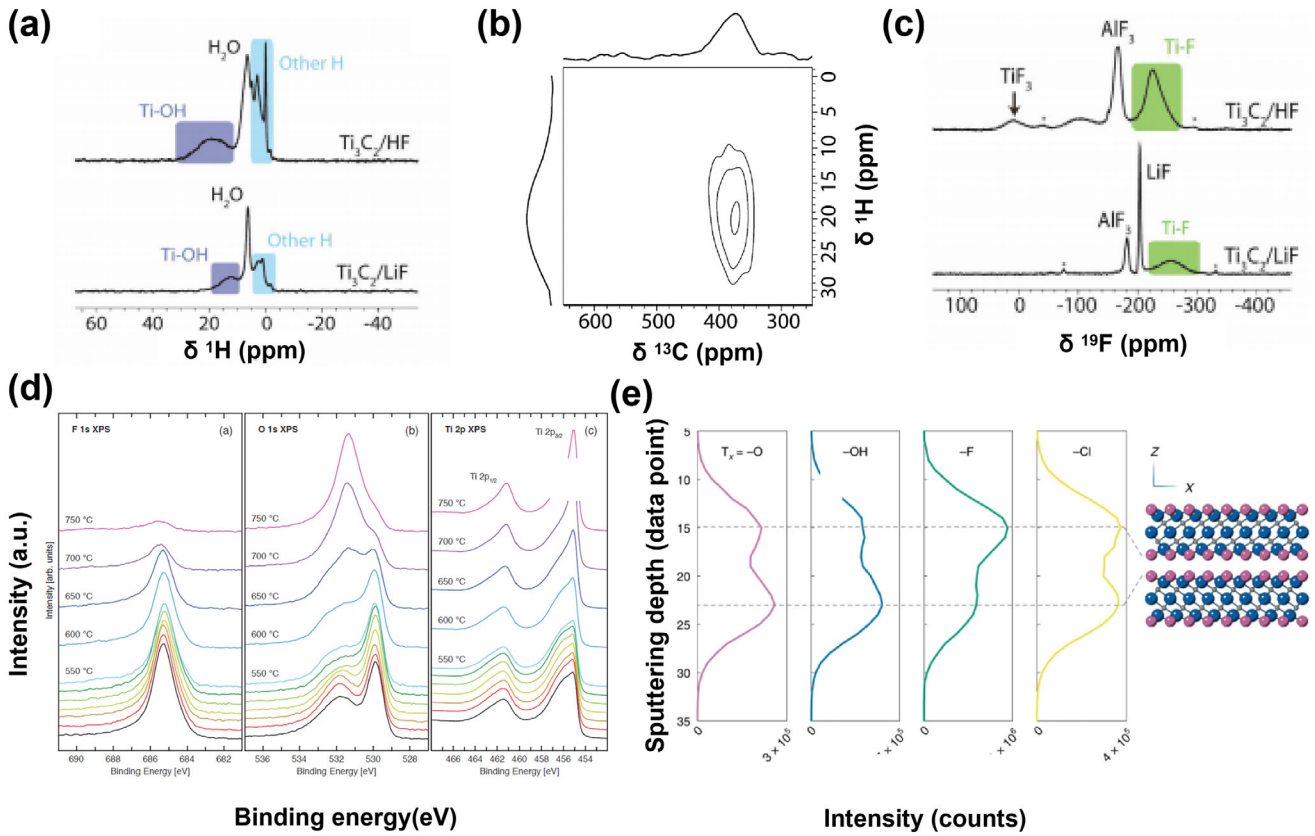

FIGURE 3 | Researches toward the quantity of surface groups of MXene. (a) ^{1}H NMR (11.7 T) spectra of HF and LiF/HCl synthesized Ti_3C_2 MXene recorded at 60 kHz MAS show the presence of –OH and interlayered H_2O. Reproduced with permission [94]. Copyright 2016, Royal Society of Chemistry. (b) ^{1}H-^{13}C HETCOR NMR (7.05 T) spectrum of HF synthesized Ti_3C_2 MXene recorded at 40 kHz MAS shows the connectivity of the –OH groups to the Ti_3C_2 sheets. (c) ^{19}F NMR (11.7 T) spectra of HF and LiF/HCl synthesized Ti_3C_2 MXene recorded at 60 kHz MAS show the presence of –F and AlF_3. (d) TP-XPS measurements revealing the temperature-dependent behavior of F 1s, O 1s, and Ti 2p conclude as few (or no) –OH terminations on the surface of MXene. Reproduced with permission [113]. Copyright 2017, IOP Publishing Ltd. (e) Depth profiles of –O, –OH, –F, and –Cl surface terminations (T) by SIMS show two peaks corresponding to two adjacent surface termination layers from the lower side of one MXene sheet and the upper side of another MXene sheet. Reproduced with permission [114]. Copyright 2022, Springer Nature.

this contradicts the observed phenomena. Therefore, they believe that the observed changes in the intensity of the O 1s peak are due to the rearrangement of surface O atoms from bridging positions to face-centered cubic (FCC) positions and that there are few or no -OH on the $Ti_3C_2T_x$ surface.

Recently, Michałowski et al. [114] proposed a new way to study the number of functional groups on the surface of MXene: ultra-low energy secondary-ion mass spectrometry (SIMS). So far, this is a pioneering study that achieves layer-by-layer sputtering of the atomic layers on the MXene surface by adjusting the incident angle of the primary Cs ion beam. When about half of the first atomic layer is sputtered, the next atomic layer is fully exposed for primary ions to interact with. This study directly detected oxygen in the sublattice of carbon, thus directly proving the existence of carbon-oxide in MXene. It was also found that the formation of such carbon-oxide phases can be avoided by using an excess of Al in the preparation of the MAX phases. For the quantity of MXene surface functional groups, the presence of oxygen, hydroxyl, fluorine, and chlorine surface terminations are monitored by measuring the signals of multi-atomic ions Ti_2O, TiOH, TiIF, and TiCl, rather than the signals of single atomic ions O, H, F, and Cl. After analyzing the composition of 150 surfaces (75 MXene layers), as shown in Figure 3f, it was concluded that the components of HF/HCl MXene produced by conventional (carbon oxides) and improved (chemically stoichiometric) MAX phases methods are $O_{0.254}(OH)_{0.456}F_{1.218}Cl_{0.072}$ and $O_{0.300}(OH)_{0.614}F_{1.016}Cl_{0.070}$, respectively. All the MXene formulas measured above are listed in Table 1.

According to the above discussion, we can get the following conclusions about MXene formula:

1. The average oxidation states of Ti and C atoms in $Ti_3C_2T_x$ are approximately +2.4 and −2.6, respectively. The net charge on the MX is positive and is neutralized by adsorbing various negative terminations.
2. Most research results indicate the presence of –OH on the surface of MXene. Although errors may occur due to surface oxides or water, it is necessary to consider –OH on MXene as surface terminations based on other properties of MXene (such as dispersibility, etc.).
3. The formula of MXene is not necessarily fixed. Newly prepared MXene surfaces are predominantly occupied by –F terminations, followed by = O, and subsequent oxidation

16136829, 2026, 46, Downloaded from https://onlinelibrary.wiley.com/doi/10.1002/smll.74769 by Beihang University (Buaa), Wiley Online Library on [23/09/2026]. See the Terms and Conditions (https://onlinelibrary.wiley.com/terms-and-conditions) on Wiley Online Library for rules of use; OA articles are governed by the applicable Creative Commons License

TABLE 1 | MXene formula extracted from analysis by different quantitative methods.

Method	Formula	Refs.	Detection nature
XPS	$Ti_3C_2O_{0.3}(OH)_{0.32}F_{1.2}$ $Ti_3C_{1.8}O_{0.6}(OH)_{0.4}F_{0.8}$ (sputtered)	[105]	Surface-sensitive (~5 nm); biased by oxidation
ICP-MS	$Ti_3C_2O_{0.81}(OH)_{0.06}F_{0.77}Cl_{0.02}$	[109]	Bulk-averaged; cannot resolve location
NMR	$Ti_3C_2O_{0.84}(OH)_{0.06}F_{0.25}$ (LiF/HCl) $Ti_3C_2O_{0.54}(OH)_{0.16}F_{0.8}$ (HF)	[87]	Local environment-sensitive; distinguishes –OH/H_2O
TP-XPS	$Ti_3C_2O_xF_y$ (original)	[113]	/
SI-MS	$Ti_3(C\text{-}O)_2O_{0.254}(OH)_{0.456}F_{1.218}Cl_{0.072}$ (carbon oxides) $Ti_3C_2O_{0.300}(OH)_{0.614}F_{1.016}Cl_{0.070}$ (chemically stoichiometric)	[114]	/

processes result in gradual changes in surface terminations, including adsorption of H_2O.

4. Characterization methods and sample treatments can affect the measurement results of the MXene formula. For example, cleaning sputtering of samples selectively reduces C in the lattice and decreases the F content.
5. The structure of the MX skeleton not only impacts the C–O component of the MXene formula. MX with stoichiometric ratios have more = O and –OH terminations and fewer –F terminations, which is related to overall binding energy and electronic structure.

In sum, due to the complexity of the surface groups of MXene, the phenomenon of interlayer water, and the limitations of past characterization methods [120], relying on a single technique often yields conflicting stoichiometric formulas. Future quantitative studies should use solid-state NMR to fundamentally decouple structural –OH from intercalated H_2O, employ ultra-low energy SIMS to map the precise layer-by-layer terminal distribution without harsh sputter damage, and utilize XPS primarily for comparative surface screening coupled with established correction factors. Fortunately, we now have other methods such as Lewis acid etching to prepare MXene with controllable surface groups, but when we study its application in water environments [121–123], the exchange between terminal groups is still an unavoidable problem. By unifying these advanced characterization tools and analytical frameworks, researchers can move beyond empirical approximations toward precise stoichiometric design and a deeper understanding of MXene chemistry [26, 124].

3.3 | Regular Terminal Location

Thermal annealing studies have demonstrated that surface oxygen atoms can spontaneously migrate to different crystallographic sites at elevated temperatures. This dynamic behavior underscores the critical need to rigorously investigate the precise spatial positioning of functional groups on the MXene basal plane. Theoretically, the distribution of different types of surface groups on the MXene surface is random [125]. For the surface groups of $Ti_3C_2T_x$ MXene, there are mainly four types of crystal sites that can exist [126–128], as shown in Figure 4a. When surface groups are placed directly above the middle layer Ti atoms, they occupy the FCC sites of the top and bottom Ti layers, called FCC configuration; when the surface groups are placed directly above the surface Ti atoms, it is called TOP configuration; when the surface groups are directly above C atoms, i.e., they occupy the hexagonal close-packed (HCP) sites relative to the surface Ti atoms, called HCP configuration; when the surface groups occupy positions between Ti atoms not defined by FCC or HCP, it is called Bridge configuration. For MXene with surface groups such as –OH, –O, –F, –Cl, many DFT calculation studies have been conducted. As shown in Figure 4b, Tang et al. [126] calculated three configurations of –OH, –F on MXene surface: in configuration A, the groups occupy FCC positions, in configuration B, the groups occupy HGP positions, in configuration C, it is a mixture of A and B. The results found that –OH and –F are more likely to occupy configuration A. Michael et al. [129] calculated the process of the groups gradually occupying the surface, as shown in Figure 4c, and found that after all FCC sites are saturated, the E_b of all –OH, –O, –F increases sharply, indicating that when all FCC sites are occupied and HCP sites are empty, the surface energy of the system is minimized. TEM research also shows that most groups occupy FCC positions. As shown in Figure 4d, Lu et al. [130] used HAADF-STEM to characterize the MXene prepared with Lewis acid melt with Cl surface groups, and found that Cl tends to occupy the FCC sites in MXene crystals. However, these DFT results should be interpreted with caution, because they usually describe idealized structures under simplified conditions. In real MXene systems, the distribution of surface terminations can also be affected by solvent molecules, intercalated species, thermal fluctuations, and local structural disorder. As a result, the most favorable sites predicted in vacuum may not always correspond to the actual terminal arrangement under experimental conditions. In addition, while theoretical models often assume ordered surfaces, PDF studies suggest that local heterogeneity and disorder are common in real samples. Therefore, terminal positioning is better understood as environment-dependent and locally variable, rather than as a fixed structural feature.

To move beyond a purely descriptive discussion of surface groups such as O, F, OH, and Cl, a mechanistic understanding is needed. First, the bare MXene surface is unstable because the exposed metal atoms are under-coordinated. As a result, adsorption of surface groups is energetically favorable and helps lower the surface energy. Calculations generally show that O binds more strongly than F and OH, which is consistent with its stronger interaction with the surface metal atoms. Second, the preferred

16136829, 2026, 46, Downloaded from https://onlinelibrary.wiley.com/doi/10.1002/smll.74769 by Beihang University (Buaa), Wiley Online Library on [23/09/2026]. See the Terms and Conditions (https://onlinelibrary.wiley.com/terms-and-conditions) on Wiley Online Library for rules of use; OA articles are governed by the applicable Creative Commons License

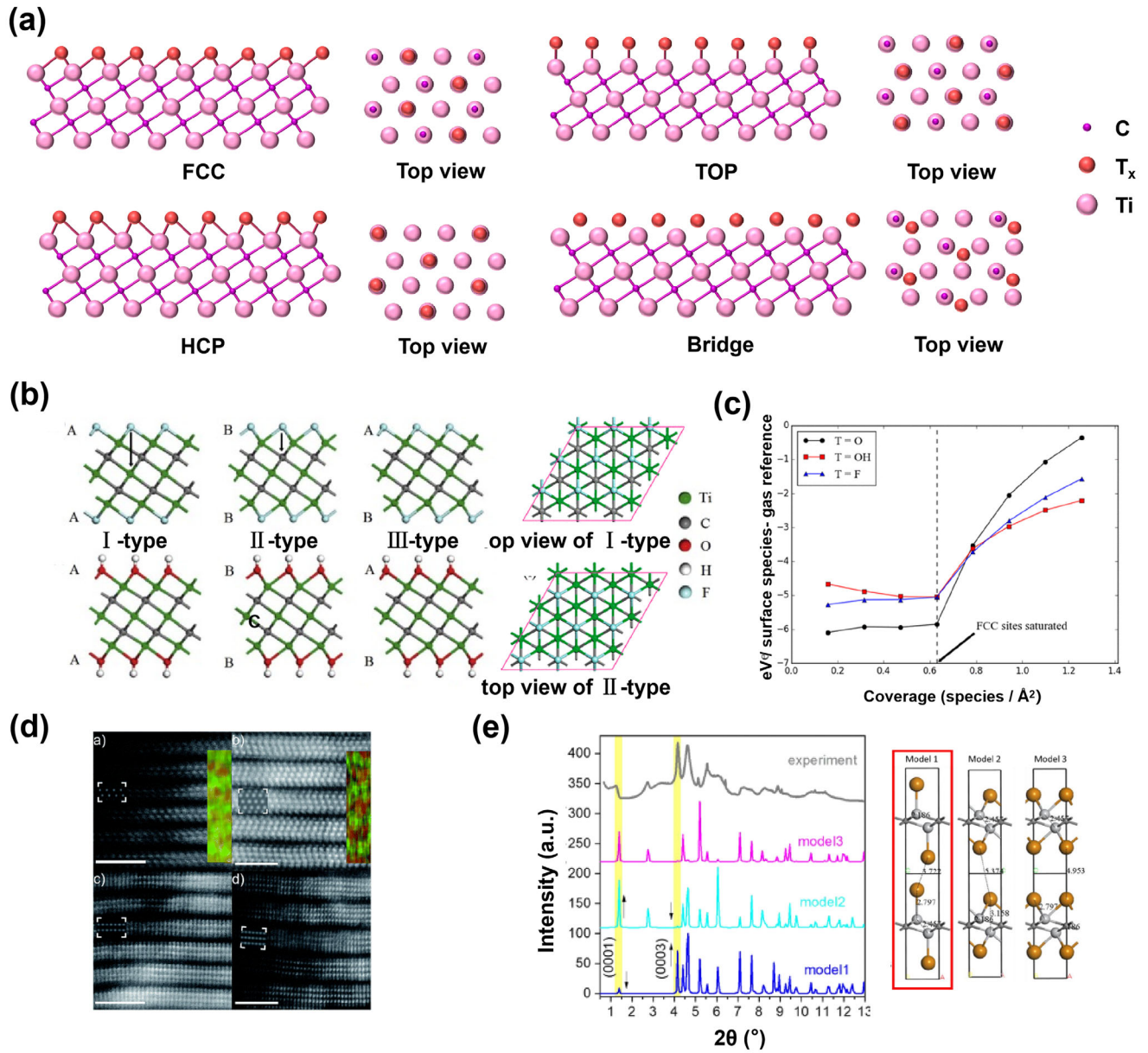

FIGURE 4 | Researches toward the position of surface groups of MXene. (a) Four sites occupied by MXene surface groups. (b) Optimized geometries of the free-standing Ti_3C_2 monolayer and its fluorinated and hydroxylated structural forms. Reproduced with permission [126]. Copyright 2012, American Chemical Society. (c) Binding energy vs coverage for –O, –OH, and –F on a Ti_2C surface by DFT shows all species exactly saturate the FCC sites. Reproduced with permission [129]. Copyright 2016, American Chemical Society. (d) Atomically resolved cross-sectional HAADF-STEM images for Ti_2CCl_2 and $Ti_3C_2Cl_2$. Reproduced with permission [130]. Copyright 2019, Royal Society of Chemistry. (e) Comparison between simulated and experimental XRD patterns for Ti_2CTe MXene, model 1 is the only model out of three that has (0003) peak dominating among (000l) family peaks. Reproduced with permission [15]. Copyright 2020, The American Association for the Advancement of Science.

adsorption site depends on both bonding strength and steric effects. For small groups such as O, F, and OH, hollow sites are usually more favorable than top sites because they allow stronger and more stable bonding with the surface atoms. For larger halogen groups such as Cl, steric effects become more important, so the site preference can be weaker and local distortion may occur. Third, the location and identity of surface terminations can strongly influence both stability and electronic behavior. Different terminations change the local charge distribution and therefore affect properties such as work function and conductivity. In addition, well anchored terminations can help stabilize the surface, whereas defect regions or less stable local configurations are often more prone to degradation or exchange reactions.

For some special cases, such as Ti_2CTe MXene, Kamysbayev et al. [15] compared the actual XRD results with the simulated XRD results of three different models, as shown in Figure 4e, and found that the XRD pattern generated at the top sites of adjacent Ti atoms is the only one in the three models where the (0003) peak dominates in the (000l) series of peaks, which may be due to Te having a larger volume. In addition, in some special cases, functional groups may also occupy other positions, or even not

16136829, 2026, 46, Downloaded from https://onlinelibrary.wiley.com/doi/10.1002/smll.74769 by Beihang University (Buaa), Wiley Online Library on [23/09/2026]. See the Terms and Conditions (https://onlinelibrary.wiley.com/terms-and-conditions) on Wiley Online Library for rules of use; OA articles are governed by the applicable Creative Commons License

be on the surface [62, 81]. In a word, some conclusions could be drawn as:

1. Smaller terminals tend to occupy FCC sites of MXene, while larger terminals may have more complex structures.
2. The occupied sites depend on the total energy of the system, the position of the terminal changes with the change of system temperature.

3.4 | Ionizable Surface and Edge

While the majority of MXene surface chemistry studies concentrate on the basal plane—where functional groups critically govern macroscopic properties—the structural dynamics and reactivity of the edge sites remain profoundly underexplored. The studies of two-dimensional materials such as graphene oxide show that the ionization process of the surface and edge structure has a pivotal influence on the dispersion and stability of two-dimensional materials in solvents [131]. This also affects intercalation chemistry, which will be discussed in detail later.

In terms of structure, the exposed Ti_3C_2 is theoretically positively charged because there are three Ti atoms with +2.4 charges and only two C atoms with −2.4 charges [105]. In the process of etching and intercalating, the surface charge is neutralized by different functional groups. The surface of MXene prepared in water system will inevitably carry –OH. When MXene nanosheets are placed in neutral water, the deprotonation of some hydroxyl groups will lead to negative charge on the sheets, which leads to negative *zeta* potential of MXene.

Compared with the surface, the edge appears narrow and cannot be completely neutralized by functional groups. This results in exposed and positively charged regions at the edge. A direct proof is provided by Natu et al., who mixed a suspension of charged Au NPs with $Ti_3C_2T_x$flakes and dried the mixture [132]. As shown in Figure 5a, TEM analysis showed that positively charged Au particles were uniformly dispersed on the surface of MXene, while negatively charged Au particles aggregated at the edge of MXene. This difference suggests that the chemical behavior of edges and basal planes is not the same. In MXenes, oxidation is often initiated at the edges, but this should be understood as a kinetic process rather than a fixed structural fact. Because the edge atoms are less coordinated and less effectively protected by surface terminations, they are generally more reactive than the basal plane. As a result, oxygen or water can react more easily at these sites, and the local oxidation process may gradually propagate inward during aging. The extent of this edge-dominated reactivity can also depend on the chemical environment, including pH and electrochemical conditions, which may change the relative rates of edge reconstruction and surface reaction. From this perspective, edge chemistry is closely related not only to initial surface reactivity, but also to the long-term stability of MXenes during storage and operation. The exposed edge, as opposed to surface covered by functional groups, is more prone to oxidation. Mechanistically, this degradation is governed by specific kinetic barriers [133]. Quantifying these degradation kinetics provides a rigorous physical basis for targeted protection. For example, the subsequent study following Natu et al. [86] used negatively charged polyanionic salts for edge capping, which experimentally suppresses the oxidation rate constant by orders of magnitude, resulting in excellent antioxidative properties, as shown in Figure 5b.

The difference in edge and surface charge of MXene can affect its ionization mechanism at different pH levels, thereby affecting its dispersion in water and other liquids [132], as shown in Figure 5c,e. In a neutral water environment, ionization process of $Ti_3C_2T_x$ (T = OH, O, F) is:

$$(Ti_3C_2)_n(OH)_x(O^-)_yF_z + aH_2O \Leftrightarrow (Ti_3C_2)_n(OH)_{x-a}(O^-)_{y+a}F_z + aH_3O^+ \quad (1)$$

Deprotonation of hydroxyl groups leads to a decrease in the –OH groups and an increase in the –O groups. The dissociated protons combine with water, resulting in a *zeta* potential of approximately −53 mV. At this point, MXene exhibits good dispersibility and can form stable colloidal solution.

Adding acidic (such as HCl) lowers the pH, resulting in an increase in H^+ concentration and shifting the chemical equilibrium to the left. It is worth noting that generally, the larger the ionic radius, the lower the likelihood of edge adsorption. Lawrence et al. conducted bond energy calculations on kaolinite and found that OH^- preferentially adsorb to the clay edge rather than Cl^- [134]. In addition, it has been discovered that the anion exchange capacity was much lower compared with the cation exchange capacity [135]. Therefore, it can be inferred that under low pH conditions, MXene edge still have a significant amount of exposed sites, which is influenced by the electronegativity [136] and hydration radius [137]. In acidic aqueous environments (such as HCl), the ionization process of $Ti_3C_2T_x$ (T = OH, O, F) can be described as:

$$(T_3C_2)_n(OH)_x(O^-)_yF_z + aH^+ \Leftrightarrow (T_3C_2)_n(OH)_{x+a}(O^-)_{y-a}F_z \quad (2)$$

Adding alkaline (such as NaOH) increases the pH, resulting in a higher degree of hydroxyl ionization on the surface. Theoretically, the *zeta* potential would continue to decrease, but the results of *zeta* potential titration experiments show that the change in *zeta* potential is not significant, which may be due to the adsorption of cations (Na^+) on the surface. Natu et al. found that in alkaline systems, MXene can undergo dehalogenation reactions, where cations (Na^+) may induce the detachment of –OH, resulting in –O– terminals and water molecules [81], as shown in Figure 5d. The deprotonated terminals compensate with cations, further weakening the interlayer forces. In addition, in a high pH environment, hydroxyl groups may neutralize the positive edges. With the presence of other cations, the –F terminal groups on the MXene surface can also undergo base exchange reactions with Na^+, leading to a reduction in the number of –F groups [138, 139]. Taking all these factors into consideration, in alkaline aqueous environments (such as NaOH), the ionization process of $Ti_3C_2T_x$ (T = OH, O, F) could be described as:

$$(T_3C_2)_n(OH)_x(O^-)_yF_z + aNa^+ + bOH^- \Leftrightarrow (T_3C_2)_n(OH)_{x-b}(ONa)_cF_{z-(a-c)} + (a-c)\,NaF + bH_2O \quad (3)$$

16136829, 2026, 46, Downloaded from https://onlinelibrary.wiley.com/doi/10.1002/smll.74769 by Beihang University (Buaa), Wiley Online Library on [23/09/2026]. See the Terms and Conditions (https://onlinelibrary.wiley.com/terms-and-conditions) on Wiley Online Library for rules of use; OA articles are governed by the applicable Creative Commons License

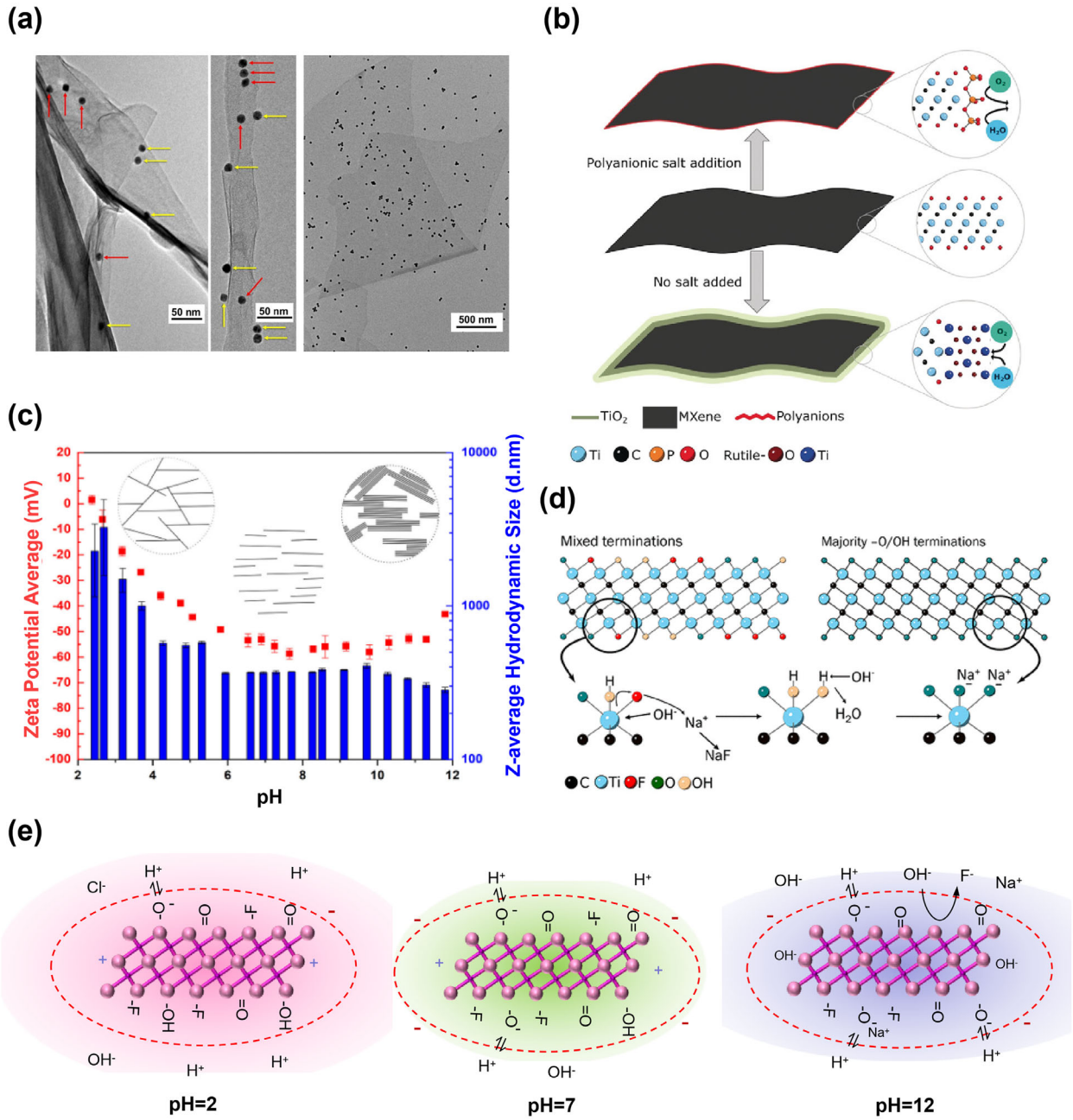

FIGURE 5 | Researches toward the ionizable surface and edge of MXene. (a) Typical TEM images of $Ti_3C_2T_z$ flakes decorated by Au nanoparticles. Reproduced with permission [132]. Copyright 2018, American Chemical Society. (b) Edge capping of MXene sheets by polyanions. Reproduced with permission [86]. Copyright 2019, Wiley-VCH. (c) Zeta potential (left *y*-axis) and average hydrodynamic size (right *y*-axis) vs pH. Insets show probable aggregate structures formed at low pH (left) and high pH (right), whereas complete deflocculation is represented by the middle inset [132]. (d) Schematic diagram showing possible defluorination and consequent Na-ion intercalation reactions during NaOH treatment of HF-MX ML powders. Reproduced with permission [81]. Copyright 2022, American Chemical Society. (e) Effect of the difference in edge and surface charge of MXene on the ionization mechanism at different pH levels.

Ionizable edge and surface can affect the dispersibility of MXene at different pH levels, as well as its dispersibility in neutral electrolyte salts [132]. The colloidal theory proposed by Derjaguin et al. suggests that the addition of electrolytes can result in the formation of a double layer [140], and increasing the ion strength of the electrolyte can lead to a decrease in thickness, reducing the repulsive forces between particles and eventually causing aggregation due to van der Waals forces. This phenomenon has been observed in many experiments. In sum, we could get following precise conclusions about MXene surface and edge:

1. MXene is negatively charged on the surface and positively charged at the edge. The causes of charging are ionization of the hydroxyl groups and incomplete coordination.
2. Acidic environment can inhibit the ionization of the surface, while there are still a large number of exposure sites at

16136829, 2026, 46, Downloaded from https://onlinelibrary.wiley.com/doi/10.1002/smll.74769 by Beihang University (Buaa), Wiley Online Library on [23/09/2026]. See the Terms and Conditions (https://onlinelibrary.wiley.com/terms-and-conditions) on Wiley Online Library for rules of use; OA articles are governed by the applicable Creative Commons License

the edge, which is affected by the electronegativity of the adsorptive anions and the hydration radius.

3. Alkaline environment can promote the dehalogenation of the surface, while partial surface terminals will exchange with anions.
4. High concentration of ions in acidic, alkaline and neutral salts will form electrolyte layer around the surface, which reduces the dispersion of MXene.

Ionizable surface and edge are of great value in studying the precise chemistry of MXene. Understanding the surface state and dispersibility of MXene helps in selectively functionalizing different surfaces [86], altering properties, particularly to achieve good transportability and stability, which is crucial for the production and application. Considering the specific requirements of piezoelectric sensors, chemical regulation through surface functionalization of MXenes significantly enhances their piezoelectric effect, thereby improving the sensitivity of the sensors [141, 142].

Although no universal method exists that can precisely control every type and proportion of surface termination on all MXenes, several strategies developed in recent years have demonstrated both high tunability and broad applicability. One can add functionalizing agents (e.g., amines, organic acids, ligand molecules) directly into the etching solution so that etching and intercalating occur simultaneously. For example, incorporating quaternary ammonium salts into an HF-free etch yields $Ti_3C_2T_x$ MXene rich in $-NR_4^+$ groups [143–145] with a controlled –O/–OH ratio. This approach has been validated on multiple Ti- and V-based MXenes, and can also be used to suppress or enhance –F content. Moreover, by annealing the as-etched MXene under different atmospheres (Ar [146], NH_3 [147], H_2 [148], etc.) and temperatures, one can reversibly convert among –O, –OH, and –F terminations. By applying a controlled potential to the MXene electrode [16] and by varying post-etch washing and soaking treatments, one could also tune the surface terminations; however, these approaches generally offer lower precision.

3.5 | Correlation Between Surface Chemistry and Material Performance

Surface chemistry is fundamentally linked to the macroscopic performance of MXenes by directly dictating interfacial reactions and charge transfer. Empirically, this manifests as distinct performance variations across applications: in energy storage, O-rich surfaces enhance redox kinetics while excessive F terminations hinder charge transfer. in optoelectronics, termination composition governs carrier transport via energy level matching. However, to elevate this understanding from qualitative observations to rigorous materials design, precise quantitative descriptors are essential [149].

The work function and density of states (DOS) serve as these critical, measurable links. For instance, theoretical calculations (e.g., Khazaei et al. [127]) establish that while bare Ti_3C_2 exhibits a relatively low work function of ~3.2 eV, a fully oxygen-terminated surface ($Ti_3C_2O_2$) dramatically increases the Φ to ~6.0 eV due to strong surface dipole moments. Furthermore, highly electronegative –O groups shift the Fermi level deeper into the valence band, fundamentally altering the DOS. Experimentally, Schultz et al. [150] corroborated this by using XPS coupled with UPS, quantifying that the controlled desorption of –F and rearrangement of –O groups can precisely tune the experimental work function of $Ti_3C_2T_x$ across a range of 3.9–4.8 eV. Therefore, specific surface terminations act as rigorous modulators of intrinsic electronic parameters, governing device performance far beyond mere empirical surface decoration.

4 | Intercalation Chemistry in Intercalating Process

Tailoring the physicochemical properties of MXenes fundamentally relies on controlling their chemical structure through three primary avenues: (i) modulating synthesis parameters (e.g., temperature, time, and precursors) to dictate the initial composition; (ii) employing postsynthetic modifications to engineer surface functional groups; and (iii) utilizing intercalation chemistry to insert specific molecules or ions into the interlayer galleries. While the first two strategies govern the intrinsic lattice and surface terminations, intercalation provides a highly tunable mechanism to adjust interlayer spacing and modulate macroscopic electronic behaviors. The intercalation chemistry and surface chemistry of MXene are two concepts from different perspectives [16, 151]. Surface chemistry focuses on the chemical structure of the MXene surface (type, quantity, and position of groups), while intercalation chemistry focuses on the intercalants that function between the layers, the interlayer chemical reactions that take place, and the physical/chemical properties exhibited by the material based on these processes, with a distinct localization effect [152]. This section primarily introduces some of the advances in the study of MXene intercalation to deepen the understanding of intercalation and diffusion mechanisms for exploring new intercalation strategies to better control the intercalation chemistry.

4.1 | Various Intercalants

Intercalants are crucial to intercalation chemistry as the type of intercalants often dictates the reactants and reaction mechanisms in interlayer chemical reactions [153, 154]. So far, commonly developed intercalants are mainly divided into three categories [24]: molecular intercalants, cationic intercalants, and organic base intercalants.

4.1.1 | Molecular Intercalants

Common molecular intercalants include organic solvents like dimethyl sulfoxide (DMSO), [155] hydrazine (HM) [156], N, N-dimethylformamide (DMF) [157], and small molecules like water (H_2O) [158] and urea [159]. The first report of intercalation with organic solvents into 2D materials like Ti_3C_2, Ti_3CN, and TiNbC was in 2013 [160]. While specific intercalants generally yield characteristic interlayer spacings (Figure 6), these values represent empirical trends rather than absolute constants, as the final expansion heavily depends on the initial synthesis route and complex solvent interactions. Studies found that the intercalation of DMSO and urea led to an increase in the *c*-lattice parameter

16136829, 2026, 46, Downloaded from https://onlinelibrary.wiley.com/doi/10.1002/smll.74769 by Beihang University (Buaa), Wiley Online Library on [23/09/2026]. See the Terms and Conditions (https://onlinelibrary.wiley.com/terms-and-conditions) on Wiley Online Library for rules of use; OA articles are governed by the applicable Creative Commons License

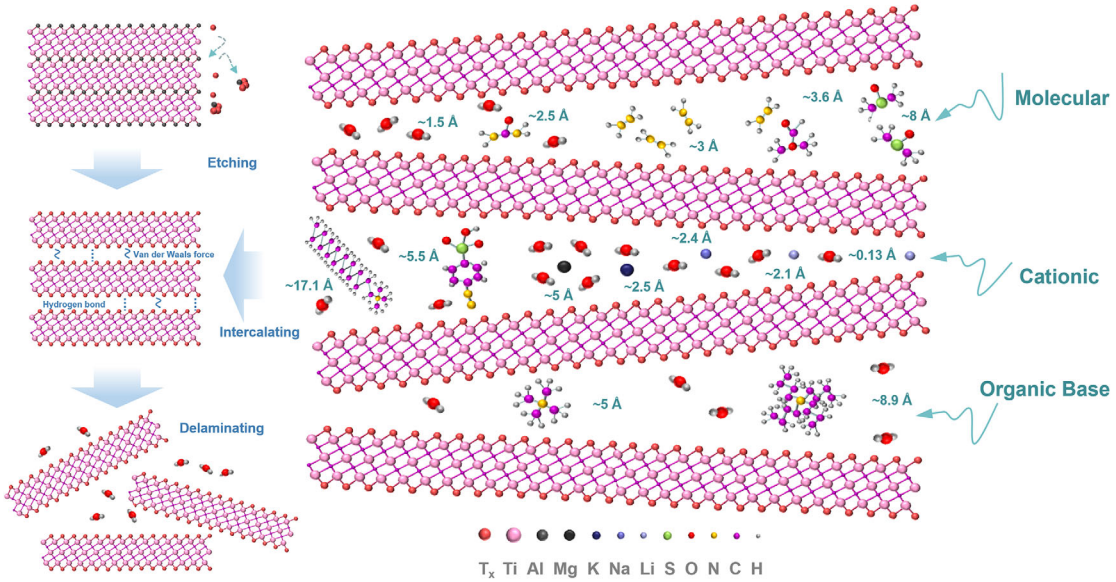

FIGURE 6 | Commonly used intercalants for MXene and their corresponding layer spacing.

(*c*-LP) of $Ti_3C_2T_x$ from 19.50 to 35.04 and 25.00 Å, respectively. The intercalation of HM and its co-intercalation with DMF led to an increase of the *c*-LP for $Ti_3C_2T_x$ from 19.50 to 25.48 and 26.80 Å. It's worth noting that DMF does not intercalate alone unless HM is present, which is similar to kaolinite [161]. Single or few-layer MXene can be obtained by ultrasonic treatment of the intercalated MXene, forming a stable colloidal solution. For MXene obtained from nonpure HF etching in a water environment, the intercalation of H_2O cannot be avoided. This is because water molecules and cations are often introduced between the layers during the etching process. Interlayer H_2O often combines with other cations to form a complex structure, which is difficult to remove through conventional drying. In fact, the interaction between only H_2O and MXene is very weak (this will be discussed later). According to structural estimation, single-layer water intercalation will change the *c*-LP by 2.5–3.0 Å [155]. At the same time, even if the same intercalant is used, different MXene preparation methods can cause significant changes in the intercalated *c*-LP. For example, in another study [162], the *c*-LP of $Ti_3C_2T_x$ prepared with NaF/HCl increased from 23.4 to 27.6 Å through DMSO, which may be due to the presence of Na^+. The process of molecular intercalation is a thermodynamic process sensitive to temperature. Raising the temperature often enhances intercalation ability. For example, Iakunkov et al. [155] found that the thickness of MXene immersed in DMSO changes with temperature, with the *c*-LP changing from 35 to 43 Å in the process of 362–370 K. This corresponds to the change from a single layer of DMSO to two layers of DMSO intercalated between the MXene layers. By heating to above 370 K and cooling to room temperature, a stable expanded two-layer MXene-DMSO solvated phase can be easily produced.

4.1.2 | Cationic Intercalants

Common cationic intercalants mainly include various inorganic cations, such as NH_4^+ [163], H^+ [164], Li^+ [163], Na^+ [163], K^+ [163], Sn^{4+} [165], Al^{3+} [166], Mn^{2+} [166], and Co^{2+} [167], as well as some organic cations like aryl diazonium salts [168] ($^+N_2$-phenyl-SO_3H) and alkyl trimethylammonium cations [165] ($[(CH_3)_3NR]^+$, where R represents CH_3, C_6H_{13}, $C_{10}H_{21}$, $C_{12}H_{25}$, $C_{16}H_{33}$). Small-radius metal cations (NH_4^+, Li^+, Na^+, K^+) can be directly intercalated, while larger ones like Sn^{4+} require cation exchange for intercalation. Studies indicate that not all salts behave similarly, and metal cation intercalation largely depends on the pH of the solution [163]. For high pH solutions such as KOH, NH_4OH, NaOH, and LiOH, the change in *c*-LP is significant. Conversely, solutions near neutrality (like Na_2SO_4, K_2SO_4, and $MgSO_4$) result in smaller changes in *c*-LP. When $Ti_3C_2T_x$ is immersed in acetic acid or sulfuric acid, there is almost no change in *c*-LP. Furthermore, the intercalation reaction is independent of anions, meaning anions do not intercalate themselves into the $Ti_3C_2T_x$ layers. The intercalation of small metal cations into $Ti_3C_2T_x$ generally results in a 4–5 Å change in the *c*-LP, which may include water complex because only cation intercalation cannot achieve such a large interlayer gap. For instance, when intercalation is carried out using n-butyllithium (n-BuLi) under a water-free environment [15], Li^+ intercalation only changes the *c*-LP from 22.16 to 22.42 Å. Metal cations with larger cationic radii bring about a slightly more considerable variation in *c*-LP, but this is not merely a simple spatial effect, and exceptions exist. For example, in the study of cation co-intercalation [166], the interlayer gap of Mn^{2+} intercalation is smaller than that of Co^{2+} intercalation. Metal cation intercalation significantly broadens the utility of MXenes in energy storage systems, particularly for batteries and hybrid metal-ion capacitors [158]. However, the limited interlayer expansion afforded by simple metal cations can restrict their application in fields requiring larger spatial confinement. For instance, synthesizing complex MXene-based composites [10, 29, 36, 169, 170] or conducting confined kinetic studies [171, 172] often requires substantially larger interlayer gaps. Specifically, utilizing the interlayer gallery as a templated nanoreactor to epitaxially grow 2D graphdiyne [171] necessitates precisely engineered and expanded spatial confinement that simple metal cations cannot provide. The organic cations

16136829, 2026, 46, Downloaded from https://onlinelibrary.wiley.com/doi/10.1002/smll.74769 by Beihang University (Buaa), Wiley Online Library on [23/09/2026]. See the Terms and Conditions (https://onlinelibrary.wiley.com/terms-and-conditions) on Wiley Online Library for rules of use; OA articles are governed by the applicable Creative Commons License

intercalation, compared with metal cations, often have a larger *c*-LP, for instance in alkyl trimethylammonium cations, when the carbon atom number in the alkyl chain is 16 (CTAB) [23, 165], a *c*-LP of 54.2 Å can be achieved. However, when the number of carbon atoms increases, under the same conditions, the interlayer distance of MXene decreases, which is understandable because larger alkyl chains often require higher activation energy. Elevated temperatures cause the interlayer distance to initially increase and subsequently decrease. This non-monotonic behavior occurs because higher thermal energy initially drives intercalation, but eventually leads to the detachment of alkyl chains. It is worth noting that there is no evidence of covalent bonding between the intercalated organic cationic groups and the surface [165]. This makes it convenient for the exchange with larger volume ions, such as Sn^{4+}. Phenyl diazonium salt is another common organic cation, adding diazonium salt solution to the MXene suspension will cause the electrons to inject from the MXene into the diazonium functional group, releasing N_2 and forming reactive phenyl radicals near the MXene, finally coupling the MXene surface with the phenyl radicals. Different from alkyl cations, due to the strong electron-attracting effect, this kind of intercalation often connects in the form of covalent bonds, and the resulting *c*-LP is 31.1 Å [173].

4.1.3 | Organic Base Intercalants

The common organic base intercalants are quaternary ammonium hydroxides, such as tetramethylammonium hydroxide [61] (TMAOH) and tetrabutylammonium hydroxide [174] (TBAOH), which could delaminate non-carbon titanium MXene. TMAOH intercalation is suitable for HF-etched $Ti_3C_2T_x$ [28], Ti_3CNT_x [28], and $Mo_4VC_4T_x$ [61], but it cannot spontaneously intercalate into non-carbon titanium MXene. On the contrary, TBAOH is often used for intercalation and delamination of various MXene (including Ti_3CNT_x [174]), but it is not suitable for $Ti_3C_2T_x$ [174]. After TBAOH treatment, the *c*-LP of V_2CT_x and Ti_3CNT_x increased from 19.9 to 38.72 Å, and 21.4 to 39.24 Å, respectively [174]. Considering the poor stability of MXene in high pH solutions [175] and the negative impact of large-volume quaternary ammonium ions on thin film conductivity [154], they still have limitations in some aspects, but this does not prevent their widespread use [176].

Currently, the developed intercalants are mostly limited to aqueous environments, and the presence of water makes the surface functional groups of MXene after intercalation complex. Compared with water between MXene layers, organics generally have lower boiling points and decomposition temperatures, and the residual substances after intercalation are easier to remove, which will have a smaller impact on the properties of MXene [167]. It is extremely important to develop anhydrous intercalants. However, there is not much research in this area at present [177, 178], and it deserves us to make more effort [15].

4.2 | Special Interlayer Water

The intercalation of water is an unavoidable issue in the interlayer reaction of the hydrate system [164, 172, 179]. It should be clear that the interlayer structure of only H_2O is weak [180]. Direct HF etching of the Ti_3AlC_2 MAX phase produces multilayered $Ti_3C_2T_x$ that resists spontaneous exfoliation in aqueous systems, with X-ray diffraction (XRD) confirming an absence of intercalated water [30], This structural observation presents an apparent paradox when juxtaposed with its macroscopic behavior: the clay-like $Ti_3C_2T_x$ exhibits pronounced hygroscopicity [57], and contact angle measurements confirm its strong intrinsic hydrophilicity (Figure 7a) [39]. Sharma et al. [109] conducted a more systematic study on the absorption of pure H_2O by calorimetry. $Ti_3C_2T_x$ was prepared by two methods (HF and LiF/HCl) and dried at 110 °C. As shown in Figure 7b, the water vapor adsorption isotherm showed that the amount of water absorbed under low pressure was greater for HF than for LiF/HCl prepared $Ti_3C_2T_x$, and the differential adsorption enthalpy of −28.7 kJ/mol indicated weak interaction between MXene and water. The weak interaction could also be due to water vapor not penetrating between layers, and only the adsorption on the outer surface was observed, possibly due to incomplete removal of moisture during drying. If it is due to incomplete water removal, then it is consistent with the report by Ghidiu et al. [57]. They found that when the relative humidity increased from 0% to 90%, the *c*-LP did not increase, as shown in Figure 7d. Only when the relative humidity exceeded 90% could they observe a jump in the *c*-LP. More extreme drying conditions (12 h under 200 °C vacuum) indicated that the adsorption measurement was again related to low enthalpy, and the water vapor adsorption isotherm of $Ti_3C_2T_x$ prepared by LiF/HCl showed the same results as the HF method [109]. Therefore, if strongly bound water is not removed during the drying process, the observed results may be consistent with those obtained by XRD [181], as shown in Figure 7c. Alternatively, changes in lattice parameters may be caused by the pillar of a small amount of water molecules, not by the continuous water layer around the intercalated cations, or by the presence of salt/ions after etching. TGA data (Figure 7e,f) suggests reaction mechanisms in agreement with these reported for Ca-montmorillonite [182]: as H_2O evolves from the structure, pillars of hydrated cations remain until the abrupt transition, at which point H_2O supporting the expanded structure is removed, leaving monolayer H_2O between the collapsed basal planes [183–185].

In any case, this does not contradict the observed facts. Although calorimetric measurements may indicate only limited direct interaction between pure water and the MXene surface, MXenes still show strong hygroscopicity and swelling [177–179]. This suggests that interlayer water is not uniform, but includes water more strongly bound to cations or surface groups, as well as more mobile water within the galleries [177, 178]. The relative amount and behavior of these water species depend on the interlayer spacing and the identity of the intercalated ions [187, 188]. Therefore, water should not be viewed only as a passive spacer, but also as an active participant in cation screening, the local dielectric environment, and charge-storage behavior [188]. This characteristic interaction with water also invites comparison with other anisotropic 2D materials. For instance, whereas water liquefaction on black phosphorus surfaces produces elliptical droplets due to its intrinsic crystalline anisotropy and direction-dependent binding energies [189], the dense coverage of hydrophilic functional groups on MXenes typically leads to a more uniform and complete wetting profile, which is crucial for maintaining stable interlayer hydration shells.

16136829, 2026, 46, Downloaded from https://onlinelibrary.wiley.com/doi/10.1002/smll.74769 by Beihang University (Buaa), Wiley Online Library on [23/09/2026]. See the Terms and Conditions (https://onlinelibrary.wiley.com/terms-and-conditions) on Wiley Online Library for rules of use; OA articles are governed by the applicable Creative Commons License

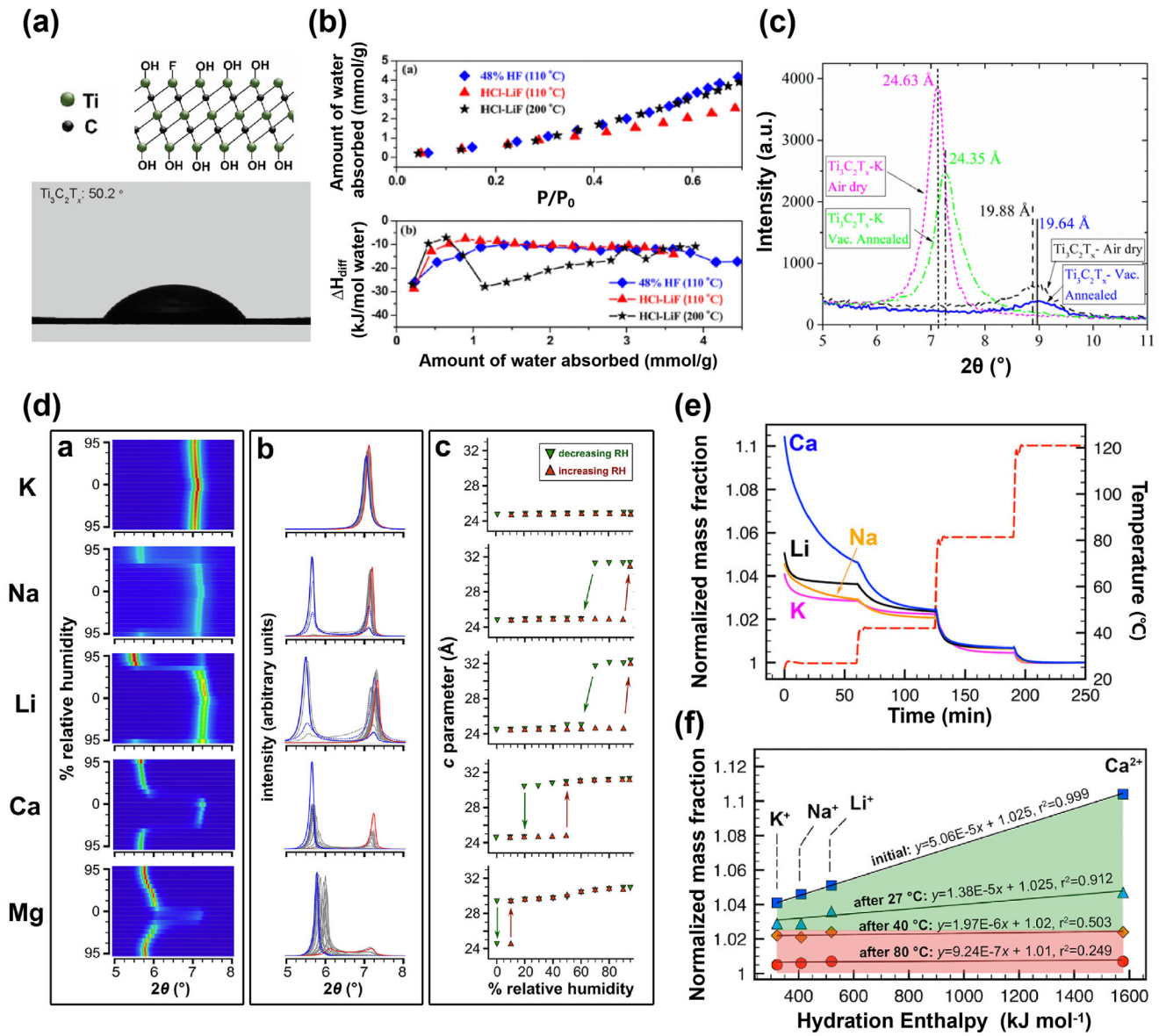

FIGURE 7 | (a) The contact angle measurement of MXene and its dispersity in water. Reproduced with permission [186]. Copyright 2019, American Chemical Society. (b) Water vapor adsorption isotherm MXenes and differential heat of adsorption as a function of the amount of water adsorbed. Reproduced with permission [109]. Copyright 2017, American Chemical Society. (c) XRD patterns of samples (with and without K^+) before and after vacuum annealing as specified in the figure. Reproduced with permission [181]. Copyright 2016, American Chemical Society. (d) Results of the 002 region of A-$Ti_3C_2T_x$ (with each intercalated cation A denoted at left). (e) Temperature during the TGA runs, showing the stepwise programming. (f) The same mass fraction data from e initially, and after equilibration steps. Reproduced with permission [57]. Copyright 2016, American Chemical Society.

4.3 | Intercalation Mechanism

Intercalation is a process of thermodynamic and dynamic coupling [187, 188, 190, 191], and is also related to the structural change of MXene. The opening of the gap between the layers requires overcoming van der Waals forces and hydrogen bonds. After opening, it is accompanied by the transfer of electronic and the formation of chemical bonds. Different types of intercalants diffuse into the interlayer gap to undergo intercalation or ion exchange [180]. In addition, the intercalants and the surface groups may also affect each other, leading to the change of chemical structure [192–194]. During this period, possible desolvation of the intercalant is also an important factor affecting the intercalation process [195, 196].

These chemical regulation techniques provide unlimited possibilities for the customized application of MXenes in many fields. Given the particular needs of strain sensors, intercalation chemistry is utilized to tune the interlayer structure and elasticity of MXenes, enabling them to withstand large deformations without losing electrical conductivity and achieve accurate measurement of strain [197, 198]. With regard to the specific demands of electromagnetic shielding films, chemical composition tuning optimizes the conductivity and film-forming

16136829, 2026, 46, Downloaded from https://onlinelibrary.wiley.com/doi/10.1002/smll.74769 by Beihang University (Buaa), Wiley Online Library on [23/09/2026]. See the Terms and Conditions (https://onlinelibrary.wiley.com/terms-and-conditions) on Wiley Online Library for rules of use; OA articles are governed by the applicable Creative Commons License

properties of MXenes, enhancing their electromagnetic shielding performance [199]. When it comes to the unique requirements of photodetectors, the optical properties of MXenes are tuned through chemical regulation to meet specific needs [200–202]. In the case of bio-inspired devices, where biocompatibility is crucial, the biocompatibility of MXenes is also adjusted through chemical means, expanding their application areas [203].

The premise of interlayer reaction in thermodynamics requires sufficient chemical driving force, i.e., electrostatic attraction or external driving forces, and the energy used for layer separation should be compensated by the energy of the interaction between the solvent and the intercalant [180]. Compared with the intercalation of only H_2O, the intercalation of cations is often easier due to the negative surface *zeta* potential of MXene [153, 204, 205]. Inevitably, environments that allow cations to exist freely mostly contain water, except for some anhydrous intercalation methods (terminal group exchange in molten salts, intercalation in organic ion solutions). This will lead to the need to value the interaction between water and cations during intercalating process. From a thermodynamic perspective, the interaction between cations and water is often represented by hydration enthalpy [206]:

$$\Delta H^{o}_{hyd} = -\frac{700z^2}{r + 0.85} kJ \cdot mol^{-1} \quad (4)$$

According to the formula, the absolute value of the hydration enthalpy is directly proportional to the square of the cationic charge *z*, and inversely proportional to the cationic radius *r*(Å). This also means that cations with smaller radius and bigger charge are more likely to complex with water, as shown in Figure 8a. For example, Ghidiu et al. [57] used in situ XRD with humidity control to study the hydration process of different cations (K^+, Na^+, Li^+, Mg^{2+}, and Ca^{2+}) intercalated into LiF/HCl MXene under various humidity levels, as shown in Figure 7d. They found that as the humidity increased, Li^+ to Mg^{2+}, there was little change in single-layer H_2O in the K^+ sample, and almost all Mg^{2+} samples were double-layer H_2O (at 0 RH, MXene is still assumed to contain single layers of H_2O molecules, because the *c*-LP is about 25Å, roughly equivalent to the thickness of one H_2O layer as prepared by HF [160]). It is easy to understand, the energy needed to intercalate $Ti_3C_2T_x$ layers could be provided through hydronium interaction with cations. Hydration enthalpy is an important descriptor of ion intercalation, but it cannot by itself fully explain intercalation behavior in MXenes. Although it reflects part of the thermodynamic driving force for ion insertion, the actual process is also strongly governed by kinetic factors, particularly interfacial desolvation and diffusion within the confined interlayer space. This is especially important for small and strongly hydrated multivalent ions such as Mg^{2+} and Al^{3+}, for which partial removal of the solvation shell may be required before entering the MXene galleries. In addition, the limited interlayer spacing can further hinder ion transport and increase the diffusion barrier after insertion. Therefore, understanding ion intercalation in MXenes requires considering not only hydration thermodynamics, but also the kinetic penalties associated with desolvation and transport in confined 2D channels. Quantitative mechanistic studies illustrate this delicate balance. First-principles calculations demonstrate that while the diffusion barrier for a naked Li^+ on a bare Ti_3C_2 surface is ultra-low (~0.07 eV), the presence of electronegative –F or –O terminations increases this barrier to ~0.15–0.30 eV due to enhanced electrostatic trapping. Furthermore, when multivalent ions (e.g., Mg^{2+} or Al^{3+}) enter highly confined interlayers (*d*-spacing < 10Å), the energy penalty to partially strip their strongly coordinated hydration shells can exceed 0.8 eV. This substantial kinetic barrier often restricts their intercalation despite favorable bulk thermodynamics. Explicitly quantifying these diffusion barriers and desolvation penalties mechanistically explains why macroscopic volumetric capacitances in MXene electrodes can vary so drastically—from below 300 to over 1500 $F \cdot cm^{-3}$—dictated by the exact match between the intercalant's hydration shell and the engineered interlayer spacing [126, 207, 208].

The interaction of molecules in the solvent with the MXene surface can be approached from physical parameters. It is usually considered that solvents with high surface tension, high boiling point and high dielectric constant interact more strongly with the MXene surface (but not necessarily), so we can consider the internal cohesive energy and solvent-related solubility parameters. The commonly used Hildebrand parameter δ [209]:

$$\delta = \sqrt{\frac{-U}{V_m}} \approx \sqrt{\frac{\Delta_{vap}H - RT}{V_m}} \quad (5)$$

where U is the internal energy of the solvent, and V_m is the molar volume. When the vapor pressure is below p°, the internal energy can be approximately calculated using the solvent evaporation enthalpy $\Delta_{vap}H$ and temperature T. Through experimental research, researchers can determine the solvent properties that match better with MXene. Maleski et al. [149] found that the absorbance at 800 nm of the solvent/$Ti_3C_2T_x$ system is related, as shown in Figure 8b, solvents such as DMF, DMSO with a δ of about 27 $MPa^{1/2}$ are good solvent systems. However, the dispersion concentration of $Ti_3C_2T_x$ in similar acetonitrile and methanol is very low (<0.1 mg mL^{-1}), which may be related to the consideration of the overall effect of the solvent, and the various forces are not divided in more detail (such as van der Waals forces and hydrogen bonds). The Hansen constant δ_T [210] takes into account the dispersion force (δ_D), the interaction produced by the permanent dipole (δ_P), and the hydrogen bond (δ_H):

$$\delta_T = \sqrt{{\delta_D}^2 + {\delta_P}^2 + {\delta_H}^2} \quad (6)$$

when the three parameters in the formula are all close, it can be considered that the surface properties of the dispersed phase and the solvent are relatively close, as shown in Figure 8c. Experiments have shown that good $Ti_3C_2T_x$ dispersions all have larger δ_P values, but the values of δ_H are dispersed. For intercalation, this indicates that dipole interactions are more significant on the $Ti_3C_2T_x$ surface. These parameters can to some extent predict the intercalation effect, and some have been confirmed by experiments [160]. However, we still need to consider the impact of other factors, such as dynamics and structure. For example, research has found that acetonitrile can also be intercalated [177], while it is difficult for DMF and H_2O to intercalate independently [30, 211].

16136829, 2026, 46, Downloaded from https://onlinelibrary.wiley.com/doi/10.1002/smll.74769 by Beihang University (Buaa), Wiley Online Library on [23/09/2026]. See the Terms and Conditions (https://onlinelibrary.wiley.com/terms-and-conditions) on Wiley Online Library for rules of use; OA articles are governed by the applicable Creative Commons License

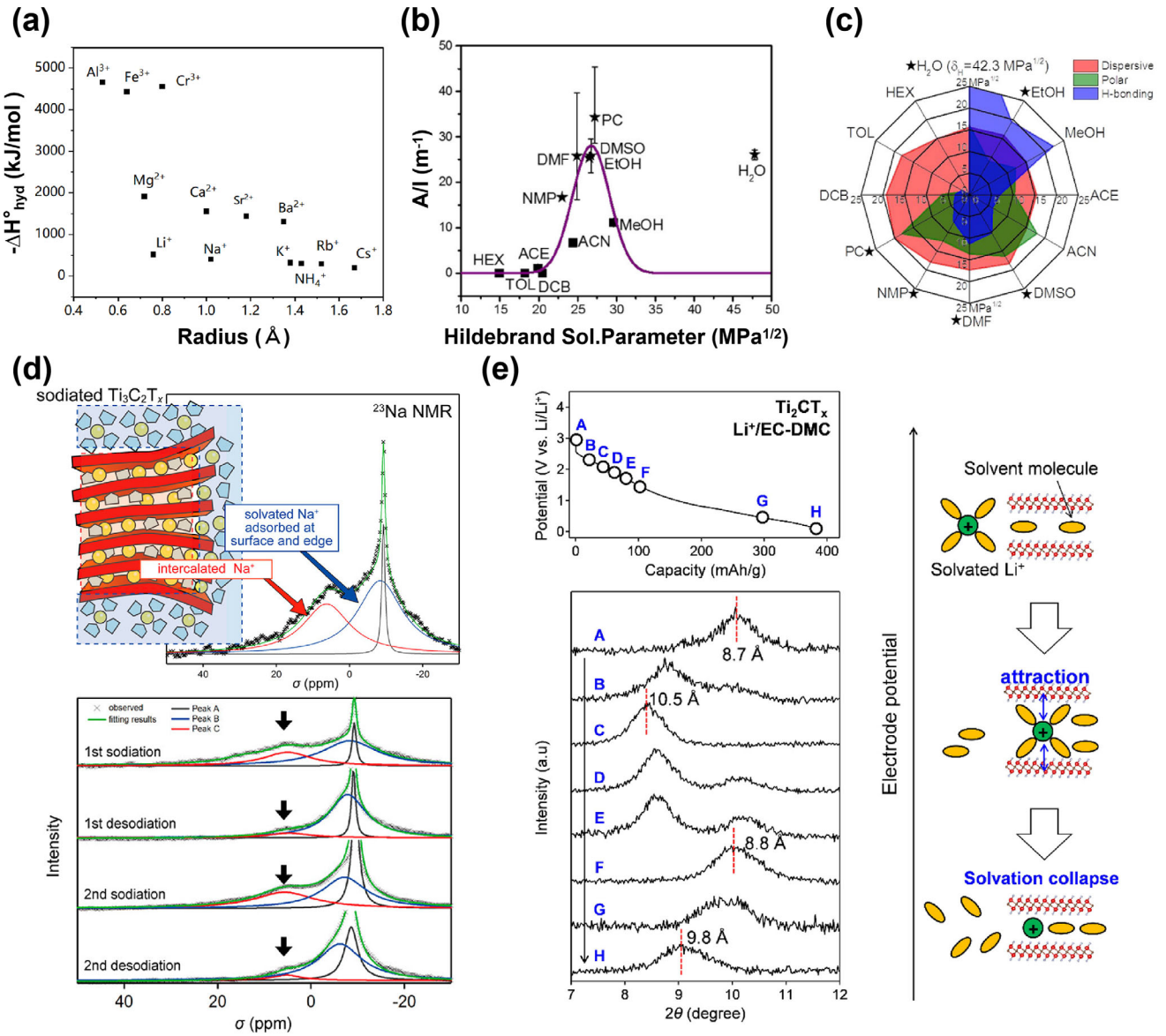

FIGURE 8 | (a) The relationship between cations radius and their hydration enthalpy. Reproduced with permission. (b) Hildebrand solubility parameters with respect to $Ti_3C_2T_x$/solvent absorbance per cell path length. (c) Hansen solubility parameters (δ_D, δ_P, and δ_H values) for each solvent. Reproduced with permission [149]. Copyright 2017, American Chemical Society. (d) NMR signals during the initial two cycles can be deconvoluted into three peaks (black, blue, and red lines). Reproduced with permission [196]. Copyright 2016, American Chemical Society. (e) Ex situ XRD results show a significant increase in *d*-spacing from 8.7 to 10.5 Å. Reproduced with permission [195]. Copyright 2018, American Chemical Society.

The study on the intercalation of cations in non-aqueous electrolytes is comprehensively investigated. Kajiyama et al. employed solid-state ^{23}Na magic angle spinning NMR and density functional theory calculations to reveal the reversible Na^+ intercalation/deintercalation in MXene $Ti_3C_2T_x$ in the interlayer space of nonaqueous Na^+ electrolytes [196]. NMR results (Figure 8d) demonstrate the amount of desolvated Na^+ (peak C) continuously increases or decreases, with normalizing the amount of adsorbed Na^+ (peak B), suggest the expansion of interlayer spacing in $Ti_3C_2T_x$ during the first sedation process, enabling the reversible intercalation/deintercalation of desolvated Na^+ as opposed to solvated Na^+. Furthermore, when Na^+ is intercalated along with solvent, the interlayer spacing remains almost unchanged upon de-sedation. This is attributed to the columnar effect of captured Na^+ and the expansion effect of solvent molecules permeating between $Ti_3C_2T_x$ layers, rather than the formation of double cation layers observed in V_2CT_x, as evidenced by the absence of large negative chemical shifts in NMR. Okubo et al. demonstrated the intercalation of solvated Li^+ into the MXene layers of ester-based organic electrolytes [195]. Ex situ XRD results show a significant increase in *d*-spacing from 8.7 to 10.5 Å (A–C), as shown in Figure 8e. Subsequently, the peak with large *d*-spacing disappears and a peak with a smaller *d*-spacing of 8.8 Å (C–F) appears upon further charging. This implies the collapsing of the solvation shell of interlayer cations during the charging process, which might be attributed to the coulombic attraction between Li^+ and MXene sheets, resulting in the transformation from intercalation capacitance to pseudocapacitance.

16136829, 2026, 46, Downloaded from https://onlinelibrary.wiley.com/doi/10.1002/smll.74769 by Beihang University (Buaa), Wiley Online Library on [23/09/2026]. See the Terms and Conditions (https://onlinelibrary.wiley.com/terms-and-conditions) on Wiley Online Library for rules of use; OA articles are governed by the applicable Creative Commons License

Therefore, we can summarize the intercalation mechanism of MXene as follows:

1. The intercalation process of cations in an aqueous environment is mainly controlled by the valence state and radius of cations, which is further summarized as the hydration enthalpy. Cations and H_2O form a water solvent shell between layers. At the same time, with the desolvation effect, the solvent shell collapses, and the cations orbitally couple with the MXene surface to form intercalated cations.
2. The intercalation process of organic molecules in non-aqueous environment is mainly controlled by molecular properties, which are further summarized as Hildebrand constant and Hansen constant. Properties closer to the MXene surface include stronger polarization, hydrogen bonding, and dispersion forces that encourage molecules to interact with the MXene surface to form intercalated molecules.

4.4 | Interactive Interlayer Diffusion

From a kinetic perspective, the interlayer reaction strongly depends on the diffusion of reactant molecules/cations, and this diffusion coefficient (D) can be described with a simple formula [212]:

$$D = D_0 \exp(-\Delta E/kT) \tag{7}$$

where D_0 is the diffusion constant, ΔE is the difference in diffusion barriers for molecules/cations in water, k is the Boltzmann constant, and T is the temperature. The magnitude of ΔE is related to a variety of factors, including the cation radius, interlayer gap, stress, and the complexation between cations and molecules. Voigt et al. [62] found that during the intercalating process, larger anions (Cl^-, Br^-) do not enter the interlayer space, but preferentially adsorb to the edges of the positively charged layers, keeping the interlayer space open, as shown in Figure 9a. This to a certain extent promotes diffusion process. Natu et al. [81] found that dehalogenation reactions can occur in alkaline systems, –OH can replace –F on $Ti_3C_2T_x$ surface, thereby reducing the interlayer binding force by reducing the strong hydrogen bonds of F to weaken the interlayer bonding force. In addition, they found that in an alkaline environment, cations (Na^+) may induce proton decoupling from –OH, producing –O terminations and water. The deprotonated terminations compensate with the cations, further reducing the interlayer force.

Sharma et al. [109] measured the exchange enthalpies for Li^+, Na^+, and K^+ in $Ti_3C_2T_x$ and showed that immersion of Li^+-intercalated $Ti_3C_2T_x$ in NaCl solution induces essentially complete the exchange from Li^+ to Na^+, whereas immersion in KCl solution only partial from Li^+ to K^+, with significant residual Li^+ remaining. In addition, it was measured that the exchange in KCl was exothermic, while the exchange in NaCl was endothermic. Theoretically, an exothermic reaction is more likely to proceed spontaneously, but the observed phenomenon contradicts this. This can be explained kinetically, that K^+ with a larger volume, may have greater resistance in the process of diffusion. Wang et al. [213] found that the cation diffusion in $Ti_3C_2T_x$ electrode material has a strong dependence on strain, according to the linear relationship $E = A_1\varepsilon + A_2$, the strain-related diffusion coefficient can be expressed as:

$$D = D_0 \exp(C_e \varepsilon) \tag{8}$$

$$C_e = -A_1/kT \tag{9}$$

where A_1 and A_2 are constants, C_e stands for the degree of coupling between strain and cation diffusion, determined by the dimensionless diffusion coefficient specified under the condition of $\varepsilon = \varepsilon_{max}$, ε is the strain from the strain field near defects such as dislocations, vacancies, and clusters of interstitial atoms [215]. Besides the microscopic stress (acting on the defects), the more macroscopic stress (acting on the whole layer) also greatly influences diffusion. For instance, stress in different directions can change the adsorption sites and diffusion path of cations [216] (biaxial stretching/compression increases/decreases the energy barrier, while uniaxial stress can adjust the diffusion path), as shown in Figure 9b [213]. There are many reasons of stress, such as mechanochemical treatment [213] and co-intercalation with different radii cations [166]. More importantly, the stress-diffusion coupling described in Equations (8) and (9) is also closely related to mechanical degradation during repeated cycling. Repeated intercalation and deintercalation, especially for large solvated ions, can cause repeated expansion and contraction of the interlayer space. Over time, this may lead to stress accumulation, mechanical fatigue, interlayer delamination, and even fragmentation of the electrode structure. In addition, the resistance of MXene stacks to such damage can depend on their surface chemistry. Different terminations and intercalants may influence interlayer interactions and therefore affect the mechanical stability of the stacked structure. For example, –O or –OH rich surfaces may strengthen interlayer interactions through hydrogen bonding, which could help relieve part of the cycling-induced strain. Therefore, the durability of MXene-based devices should be considered from both diffusion behavior and mechanical stability, rather than from ion transport alone.

Our discussion above mainly focuses on cation diffusion in water, correspondingly, the diffusion of cations also impacts the water. Osti et al. [181] used quasi-elastic neutron scattering (QENS) to study the dynamics of water in vacuum-annealed MXene samples, as shown in Figure 9c. They found that the diffusion coefficient of H_2O in multilayered $Ti_3C_2T_x$ without cation intercalation (1.19×10^{-9} cm^2 s^{-1}) is approximately half of the water, which is comparable to the reported values in pressurized water in vermiculite [217]. It is believed that this originates from the interlayer water between the stacked MXene. Besides, it was found that K^+ significantly slow down the diffusion of water, with a measured diffusion coefficient ($28.30 \pm 2.1 \times 10^{-12}$ m^2 s^{-1}) contrasting with that of $Ti_3C_2T_x$ without cation intercalation [218]. The experiment is consistent with molecular dynamics simulations (9.77×10^{-12} m^2 s^{-1}) in terms of magnitude (the difference may be due to the neglect of surface defects and other factors in the simulation). The further structure of cations and water was discovered using inelastic neutron scattering (INS), as shown in Figure 9d, and the results indicate that cation embedding greatly reduces the strength of hydrogen bonds acting on water [214]. Molecular dynamics models (Figure 9f) also show that the order

16136829, 2026, 46, Downloaded from https://onlinelibrary.wiley.com/doi/10.1002/smll.74769 by Beihang University (Buaa), Wiley Online Library on [23/09/2026]. See the Terms and Conditions (https://onlinelibrary.wiley.com/terms-and-conditions) on Wiley Online Library for rules of use; OA articles are governed by the applicable Creative Commons License

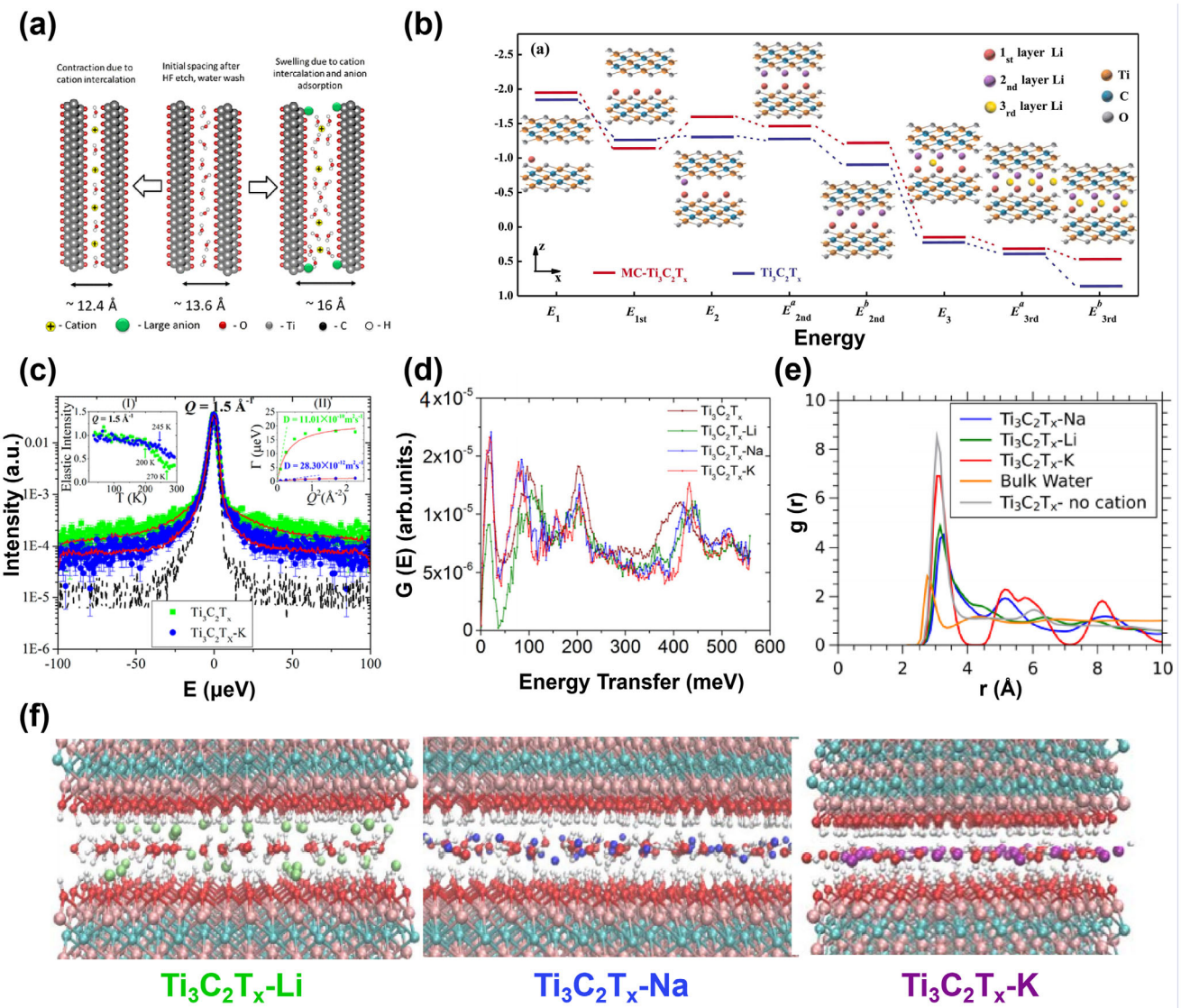

FIGURE 9 | (a) Schematic diagram of the effect of anions on $d_{c/2}$. Reproduced with permission [62]. Copyright 2018, American Chemical Society. Copyright 2017, Elsevier. (b) Geometric structures for Li adsorption on MC-$Ti_3C_2T_x$ and $Ti_3C_2T_x$ interlayers of side views and the related comparison of Li adsorption energy. Reproduced with permission [213]. Copyright 2017, Elsevier. (c) Representative QENS spectra of vacuum-annealed MXene samples. Reproduced with permission [181]. Copyright 2016, American Chemical Society. (d) GVDS of pristine and metal ions (Li^+, Na^+, and K^+) intercalated MXene measured at SEQUOIA. e Calculated RDF of water oxygen–oxygen (Ow–Ow) distances in MXene layers. (f) Snapshots from the ReaxFF molecular-dynamics simulations. Reproduced with permission [214]. Copyright 2017, American Physical Society.

of confined water increases with the size of the cations. Among them, Li^+ interfere least with water diffusion because it is closer to the MXene surface and further away from the water layer, making the system more disordered, while Na^+ and K^+ bind more with water, helping to increase the resistance to water movement and making the system more ordered. K^+ intercalated the most in water and cause the greatest interference. Notably, due to their small hydration radius, as shown in Figure 9e, Li^+ can enter the space between Ti–OH and water, which is different from Na^+ and K^+. This seems to explain the previously observed shrinkage related to Li^+ intercalating during electrochemical cycling, and the phenomenon [219] that there is almost no size change when K^+ is electrochemically intercalated from an aqueous electrolyte.

In sum, interlayer diffusion is an interactive process that includes the interaction between diffusing cations and water molecules or other cations, as well as the interaction between diffusing cations and the layer surface. The interaction between the cations and layers depends on the properties of the diffusing cations and the layer structures as well as the overall/microscopic stress. As for the interaction between the diffusion substances, especially regarding the interaction between H_2O and metal cations, metal cations with different radii produce different diffusion resistances due to their different degrees of binding to the layer surface. A smaller volume is conducive to making the diffusion system more orderly.

16136829, 2026, 46, Downloaded from https://onlinelibrary.wiley.com/doi/10.1002/smll.74769 by Beihang University (Buaa), Wiley Online Library on [23/09/2026]. See the Terms and Conditions (https://onlinelibrary.wiley.com/terms-and-conditions) on Wiley Online Library for rules of use; OA articles are governed by the applicable Creative Commons License

5 | Challenges and Perspectives

It is inevitable that despite our best efforts in this review to provide a clear understanding of MXene chemistry, we still cannot definitively provide a final conclusion for some of these confusions, including:

1. The precise influence and control of the synthesis process on the quantities of functional groups in MXene, especially the impact of precursors: Controlling the synthesis process is crucial for tailoring the number and type of functional groups on MXene, yet there remain uncertainties regarding how precursors behave in different synthesis conditions. Future research into precursor materials could allow scientists to predict and control how each precursor influences the formation of specific functional groups, such as –OH, –O, and –F, though the complexity of reaction pathways and potential side reactions introduces confusion. By fine-tuning factors like reaction time, temperature, and etching conditions, it may be possible to achieve consistent and predictable functionalization. However, achieving the desired consistency across various experimental setups might remain challenging, potentially limiting the level of customization possible for MXene in applications like electronics, energy, and catalysis.

2. The specific mechanisms and reaction processes involved in the conversion or reaction of functional groups in synthesized MXene: Understanding the specific reaction mechanisms that govern the transformation of functional groups in MXene opens new possibilities for material design, but there is still confusion about how certain external stimuli influence these reactions. Future research might uncover how different stimuli, such as heat, pressure, or chemical treatments, can selectively convert one functional group to another, though the selective nature of these processes could vary depending on the environment. For instance, converting –OH into –O, –F or other functional groups to achieve a desired chemical reactivity may become feasible, yet uncertainties surrounding competing reactions or incomplete conversions could complicate this process. A clearer understanding of these pathways will be essential for fully exploiting the potential of MXene in catalysis, energy storage, and sensing.

3. *The control of the position of functional groups in MXene to achieve customizable expansion*: Controlling the spatial distribution and enrichment of specific functional groups in targeted locations, such as at the edges or in the center of MXene layers, opens new possibilities for customizable material behavior. However, questions remain about the precise mechanisms behind functional group migration and enrichment at specific sites. By concentrating functional groups like –OH, –F, or –O at the edges, where coordination and bonding dynamics are more active, it may be possible to influence the interlayer spacing and interactions. While advances in synthesis techniques could allow researchers to achieve targeted enrichment, achieving precise control in all cases remains elusive. As such, the ability to consistently control expansion and other physical characteristics through these mechanisms might face challenges, especially when scaling up for industrial applications.

4. The precise control of intercalation processes in MXene, as well as the electron transfer and energy conversion processes between interlayer cations or molecules and the surface upon bonding: Achieving precise control over the intercalation of cations or molecules into MXene is crucial for optimizing its electronic and energy conversion properties. However, the complex interactions between interlayer cations and the MXene surface remain partially understood, leading to confusion about the most effective ways to manage electron transfer and energy conversion. While better control over these processes might allow MXene to reach unprecedented levels of efficiency in applications like supercapacitors, batteries, and sensors, uncertainties regarding the long-term stability and the exact nature of energy conversion mechanisms might limit the performance of materials. More research is needed to clarify these aspects and unlock full the potential of MXene.

5. *The accurate coupling relationship between the dynamics and thermodynamics of the interlayer diffusion process in MXene*: This becomes more complex when considering the influence of external stress, such as stretching or compressing MXene, which might alter the interlayer spacing and diffusion pathways. Understanding the coupling between dynamics and thermodynamics in the interlayer diffusion process of MXene is complicated by external factors, such as stress and multi-ion intercalation, which introduce confusion in predicting diffusion behavior. Stretching or compressing MXene might alter diffusion pathways, but how these mechanical changes interact with diffusion is not yet fully understood. The simultaneous intercalation of multiple ion species also complicates ion-exchange behavior, raising questions about the efficiency and stability of the diffusion process. In addition, the orientation control of long-chain ions intercalated between MXene layers is still poorly understood, leaving uncertainties about how their alignment affects conductivity and mechanical properties. While advances in modeling and experimentation may help clarify these factors, the complexity of these processes suggests that accurately predicting diffusion dynamics and thermodynamic coupling remains a significant challenge.

6. *The engineering trade-off between mass yield and precise termination uniformity during industrial scale-up*: While producing large quantities of MXene is now feasible, maintaining stringent batch-to-batch reproducibility of the surface chemistry across kilogram batches remains an open challenge. Future engineering efforts must focus on standardizing fluid dynamics and heat transfer within large reactors to eliminate localized gradients, ensuring that high-yield exfoliation does not compromise the precise atomic-level control of surface terminations.

These confusions arise partly from insufficient focus on MXene chemistry—with more emphasis on its applications. Another source of confusion stems from the challenges in characterizing MXene, especially their interlayer structures. Despite the development of synthetic strategies that yield MXene with uniform functional groups, making it easier to characterize and confirm their presence, there is still limited research on the use of new terminations for precise studies of MXene chemistry. During the 2020 International MXene Conference, a group

16136829, 2026, 46, Downloaded from https://onlinelibrary.wiley.com/doi/10.1002/smll.74769 by Beihang University (Buaa), Wiley Online Library on [23/09/2026]. See the Terms and Conditions (https://onlinelibrary.wiley.com/terms-and-conditions) on Wiley Online Library for rules of use; OA articles are governed by the applicable Creative Commons License

TABLE 2 | MXene synthesis strategies, surface terminations, typical applications, and the connections between them.

Synthesis method	Reaction medium and conditions	Surface terminations	Control strategy	Typical applications	Refs.
Direct HF etching	10–50 wt% HF aq., 15–50 °C, 0.5–24 h	–F, –OH, =O	Vary HF concentration, temperature, time	Supercapacitors, HER catalysis, sensing	[1, 30, 45, 48]
In situ HF	LiF + HCl (aq.), 30–50 C, 24–48 h	–Cl, –F, –OH, =O	Choice of fluoride salt; pH; washing protocol	Energy storage electrodes, electrochemical sensors	[31, 56, 58, 62]
Molten-salt (Lewis-acid) etching	$ZnCl_2$/NaCl/KCl molten salt, 400–600°C, N_2	Single halogen (–Cl, –Br, –S, –Se, –Te), =O	Lewis-acid type and ratio; post-wash	Photodetectors, EMI shielding materials	[5, 8, 15, 17, 68]
Alkali-assisted hydrothermal etching	NaOH (∼27.5 M), 270°C, hydrothermal	–OH, =O	NaOH concentration; temperature; time	Hydrophilic sensors, supercapacitors	[33, 60, 65]
Electrochemical etching	Aqueous NH_4OH (or other), applied potential	–OH, =O	Applied potential; electrolyte type	High-performance electrodes, water-splitting catalysis	[64, 69, 73]
Molten-salt-assisted electrochemical	Molten salt + electrochemical, ∼500°C	–Cl, –O, –S	Salt type; potential	Fluorine-free catalysts, functional coatings	[68, 69]
Bottom-up direct synthesis	CVD at 640–950 °C, $TiCl_4$ + CH_4/N_2 gas	–Cl	Precursor ratio; temperature; gas atmosphere	Vertical MXene sensors, flexible electronics	[9, 15, 91]

16136829, 2026, 46, Downloaded from https://onlinelibrary.wiley.com/doi/10.1002/smll.74769 by Beihang University (Buaa), Wiley Online Library on [23/09/2026]. See the Terms and Conditions (https://onlinelibrary.wiley.com/terms-and-conditions) on Wiley Online Library for rules of use; OA articles are governed by the applicable Creative Commons License

of renowned experts in the field, including conference chairs Huang and Gogotsi, highlighted the exploration and expansion of the chemical structure of MXene materials in over 30% of the challenges listed for the next decade, indicating a growing emphasis on MXene chemistry. We believe that the resolution of these confusions is only a matter of time, and future MXene research will undoubtedly be built on a base of precise MXene chemistry, requiring collective efforts from the research community.

6 | Conclusion

In this review, we summarized the synthetic strategies for MXenes and highlighted the latest discoveries and advancements in MXene chemistry, considering both surface and interlayer perspectives. These efforts aim to enhance our understanding of the precise chemistry of MXenes. Over the past decade, significant progress has been made in elucidating the chemical structure of MXenes, beginning with the initial discovery of $Ti_3C_2T_x$, the first identified MXene, where the T_x denoted the potential presence of mixed surface functional groups. This has since expanded into a broad and diverse family of MXenes, all of which are functionalized with similar surface groups. Today, there exists a range of customizable and scalable approaches for synthesizing and functionalizing MXenes, as well as diverse intercalation strategies. These advancements have facilitated their application in numerous fields, including electronics, energy storage, electromagnetic interference shielding, catalysis, and medicine. Such progress underscores the role of precise chemical tailoring in unlocking MXenes' full potential. Looking ahead, the future of MXene development appears highly promising, driven by ongoing innovations in chemistry and expanding applications.

To move MXene research beyond empirical optimization and toward truly rational design, the field needs a unified predictive framework linking synthesis conditions, surface terminations, intercalation behavior, and final properties. These factors should not be considered independently. Instead, future studies should work backward from the target function of the material. In practice, a specific application first sets the required macroscopic property, such as a tunable work function in catalysis or high pseudocapacitance in energy-storage systems. That property requirement then constrains the most favorable intercalation behavior, including reduced steric hindrance and lower desolvation barriers. The preferred intercalation process further determines the most suitable surface termination configuration, for instance, a uniform chloride termination or a mixed oxygen/hydroxyl surface. On this basis, the appropriate synthesis route can be selected accordingly, such as Lewis acid molten-salt treatment or conventional aqueous HF etching. If current empirical observations can be reorganized within such a framework, the correlations summarized in Table 2 may evolve from a descriptive summary into a practical design map for predicting synthesis conditions and guiding the preparation of MXenes with application-specific properties.

Precise chemistry of MXenes is anticipated to play a pivotal role in their future development, enabling enhanced control over their structural features, targeted functionalization, and expanded applications as shown in Table 2. Precise chemical synthesis is essential for tuning the physical properties of MXenes. By carefully controlling the synthesis process, it is possible to modulate their electronic, mechanical, and optical properties, thereby optimizing their performance across a range of applications, including electronics, sensors, and optoelectronics.

In addition, precise surface chemistry allows for the regulation of the composition and distribution of specific functional groups at designated sites. This capability is crucial for improving the environmental stability of MXenes, addressing challenges related to degradation, and ensuring the long-term viability of MXene-based technologies in various conditions. Moreover, leveraging precise interlayer chemistry has significant implications for expanding MXene applications, particularly in energy storage and catalysis. For instance, the intentional design of intrinsic properties can enhance the efficiency and capacity of energy storage devices, such as batteries and supercapacitors, while also improving catalytic performance.

Furthermore, the integration of MXenes with other nanoscale materials requires meticulous control over their intrinsic properties. This precision facilitates the development of multifunctional composite materials with exceptional performance, unlocking new opportunities for MXenes in cutting-edge technologies and broadening their impact across diverse fields.

Author Contributions

Zhifang Liu: conceptualization, writing – original draft, writing – review and editing. **Yipeng Cui:** writing – original draft. **Caofeng Pan:** conceptualization, writing – original draft, writing – review and editing, funding acquisition, project administration, supervision, resources. **Yilin Sun:** conceptualization, writing – original draft.

Acknowledgements

This work was funded by the National Natural Science Foundation of China (62304020, 52125205, 52532005, 52250398, 52192614, and 52203307), National Key Research and Development (R&D) Program from Ministry of Science and Technology of China (2024YFB3814100), Natural Science Foundation of Beijing Municipality (2222088 and L223006), and the Fundamental Research Funds for the Central Universities.

Conflicts of Interest

The authors declare no conflict of interest.

Data Availability Statement

Data sharing not applicable to this article as no datasets were generated or analyzed during the current study.

References

1. K. R. G. Lim, M. Shekhirev, B. C. Wyatt, B. Anasori, Y. Gogotsi, and Z. W. Seh, "Fundamentals of MXene Synthesis," *Nature Synthesis* 1, no. 8 (2022): 601–614, https://doi.org/10.1038/s44160-022-00104-6.

2. Y. Gogotsi and B. Anasori, "The Rise of MXenes," *ACS Nano* 13, no. 8 (2019): 8491–8494, https://doi.org/10.1021/acsnano.9b06394.

3. A. VahidMohammadi, J. Rosen, and Y. Gogotsi, "The World of Two-dimensional Carbides and Nitrides (MXenes)," *Science* 372, no. 6547 (2021): abf1581, https://doi.org/10.1126/science.abf1581.

16136829, 2026, 46, Downloaded from https://onlinelibrary.wiley.com/doi/10.1002/smll.74769 by Beihang University (Buaa), Wiley Online Library on [23/09/2026]. See the Terms and Conditions (https://onlinelibrary.wiley.com/terms-and-conditions) on Wiley Online Library for rules of use; OA articles are governed by the applicable Creative Commons License

4. Y. Gogotsi and Q. Huang, "MXenes: Two-Dimensional Building Blocks for Future Materials and Devices," *ACS Nano* 15, no. 4 (2021): 5775–5780, https://doi.org/10.1021/acsnano.1c03161.

5. H. Ding, Y. Li, M. Li, et al., "Chemical Scissor–mediated Structural Editing of Layered Transition Metal Carbides," *Science* 379, no. 6637 (2023): 1130–1135, https://doi.org/10.1126/science.add5901.

6. Y. Wei, P. Zhang, R. A. Soomro, Q. Zhu, and B. Xu, "Advances in the Synthesis of 2D MXenes," *Advanced Materials* 33, no. 39 (2021): 2103148, https://doi.org/10.1002/adma.202103148.

7. A. Thakur, J. Kim, B. C. Wyatt, Y. Gogotsi, and B. Anasori, "Composition–Structure–Property Relationships in MXenes," *Nature Reviews Materials* 11 (2026): 516–531, https://doi.org/10.1038/s41578-026-00911-9.

8. P. Huang and W.-Q. Han, "Recent Advances and Perspectives of Lewis Acidic Etching Route: An Emerging Preparation Strategy for MXenes," *Nano-Micro Lett* 15 (2023): 68, https://doi.org/10.1007/s40820-023-01039-z.

9. D. Wang, C. Zhou, A. S. Filatov, et al., "Direct Synthesis and Chemical Vapor Deposition of 2D Carbide and Nitride MXenes," *Science* 379, no. 6638 (2023): 1242–1247, https://doi.org/10.1126/science.add9204.

10. K. Sun, F. Wang, W. Yang, et al., "Flexible Conductive Polyimide Fiber/MXene Composite Film for Electromagnetic Interference Shielding and Joule Heating with Excellent Harsh Environment Tolerance," *ACS Applied Materials and Interfaces* 13 (2021): 50368–50380, https://doi.org/10.1021/acsami.1c15467.

11. H. Cheng, Y. Pan, W. Li, et al., "Facile Design of Multifunctional Melamine Foam with Ni-Anchored Reduced Graphene Oxide/MXene as Highly Efficient Microwave Absorber," *Nano Today* 52 (2023): 101958, https://doi.org/10.1016/j.nantod.2023.101958.

12. M. Naguib, M. W. Barsoum, and Y. Gogotsi, "Ten Years of Progress in the Synthesis and Development of MXenes," *Advanced Materials* 33, no. 39 (2021): 2103393, https://doi.org/10.1002/adma.202103393.

13. A. Lipatov, H. Lu, M. Alhabeb, et al., "Elastic Properties of 2D $Ti_3C_2T_X$ MXene Monolayers and Bilayers," *Science Advances* 4, no. 6 (2018): aat0491, https://doi.org/10.1126/sciadv.aat0491.

14. C. E. Shuck, A. Sarycheva, M. Anayee, et al., "Scalable Synthesis of $Ti_3C_2T_X$ MXene," *Advanced Engineering Materials* 22, no. 3 (2020): 1901241, https://doi.org/10.1002/adem.201901241.

15. V. Kamysbayev, A. S. Filatov, H. Hu, et al., "Covalent Surface Modifications and Superconductivity of Two-dimensional Metal Carbide MXenes," *Science* 369, no. 6506 (2020): 979–983, https://doi.org/10.1126/science.aba8311.

16. X. Li, Z. Huang, C. E. Shuck, G. Liang, Y. Gogotsi, and C. Zhi, "MXene Chemistry, Electrochemistry and Energy Storage Applications," *Nature Reviews Chemistry* 6, no. 6 (2022): 389–404, https://doi.org/10.1038/s41570-022-00384-8.

17. Y. Li, H. Shao, Z. Lin, et al., "A General Lewis Acidic Etching Route for Preparing MXenes with Enhanced Electrochemical Performance in Non-aqueous Electrolyte," *Nature Materials* 19 (2020): 894–899, https://doi.org/10.1038/s41563-020-0657-0.

18. T. Bashir, S. A. Ismail, J. Wang, W. Zhu, J. Zhao, and L. J. Gao, "MXene Terminating Groups O, –F or –OH, –F or O, –OH, –F, or O, –OH, –Cl?," *Journal of Energy Chemistry* 76 (2023): 90–104, https://doi.org/10.1016/j.jechem.2022.08.032.

19. A. Iqbal, T. Hassan, S. M. M. Naqvi, Y. Gogotsi, and C. M. Koo, "MXenes for Multispectral Electromagnetic Shielding," *Nature Reviews Electrical Engineering* 1 (2024): 180–198, https://doi.org/10.1038/s44287-024-00024-x.

20. H. Wu, J. Pang, S. Liang, et al., "MXene Materials Based Printed Flexible Devices for Healthcare, Biomedical and Energy Storage Applications," *Materials Today* 45 (2021): 99–131, https://doi.org/10.1016/j.mattod.2020.10.025.

21. J. L. Hart, K. Hantanasirisakul, A. C. Lang, et al., "Engineering MXenes for Thermal and Photothermal Catalysis," *Chemical Reviews* 126 (2026): 3664–3729, https://doi.org/10.1021/acs.chemrev.5c00705.

22. Y. Jiang, C. Zhao, Z. Song, et al., "MXene-Triggered 3D Printing of Gradient-Modulus Iontronic Pressure Sensors for Adaptive Robotic Grasping," *Advanced Functional Materials* 36, no. 24 (2026): 22891, https://doi.org/10.1002/adfm.202522891.

23. K. Liang, R. A. Matsumoto, W. Zhao, et al., "Engineering the Interlayer Spacing by Pre-Intercalation for High Performance Supercapacitor MXene Electrodes in Room Temperature Ionic Liquid," *Advanced Functional Materials* 31, no. 33 (2021): 2104007, https://doi.org/10.1002/adfm.202104007.

24. J. Zou, J. Wu, Y. Wang, et al., "Correction: Additive-Mediated Intercalation and Surface Modification of MXenes," *Chemical Society Reviews* 51, no. 8 (2022): 2972–2990, https://doi.org/10.1039/D2CS90024F.

25. N. Shpigel, M. D. Levi, S. Sigalov, T. S. Mathis, Y. Gogotsi, and D. Aurbach, "Direct Assessment of Nanoconfined Water in 2D Ti_3C_2 Electrode Interspaces by a Surface Acoustic Technique," *Journal of the American Chemical Society* 140, no. 28 (2018): 8910–8917, https://doi.org/10.1021/jacs.8b04862.

26. M. Paillet, R. Parret, J. L. Sauvajol, and P. Colomban, "Graphene and Related 2D Materials: An Overview of the Raman Studies," *Journal of Raman Spectroscopy* 49, no. 1 (2018): 8–12, https://doi.org/10.1002/jrs.5295.

27. V. Natu and M. W. Barsoum, "MXene Surface Terminations: A Perspective," *The Journal of Physical Chemistry C* 127, no. 41 (2023): 20197–20206, https://doi.org/10.1021/acs.jpcc.3c04324.

28. K. Hantanasirisakul, M. Alhabeb, A. Lipatov, et al., "Effects of Synthesis and Processing on Optoelectronic Properties of Titanium Carbonitride MXene," *Chemistry of Materials* 31, no. 8 (2019): 2941–2951, https://doi.org/10.1021/acs.chemmater.9b00401.

29. S. K. Nemani, B. Zhang, B. C. Wyatt, et al., "High-Entropy 2D Carbide MXenes: $TiVNbMoC_3$ and $TiVCrMoC_3$," *ACS Nano* 15, no. 8 (2021): 12815–12825, https://doi.org/10.1021/acsnano.1c02775.

30. M. Naguib, M. Kurtoglu, V. Presser, et al., "Two-Dimensional Nanocrystals Produced by Exfoliation of Ti_3AlC_2," *Advanced Materials* 23, no. 37 (2011): 4248–4253, https://doi.org/10.1002/adma.201102306.

31. M. Ghidiu, M. R. Lukatskaya, M. Q. Zhao, Y. Gogotsi, and M. W. Barsoum, "Conductive Two-dimensional Titanium Carbide 'Clay' With High Volumetric Capacitance," *Nature* 516, no. 7529 (2014): 78–81, https://doi.org/10.1038/nature13970.

32. T. Li, L. Yao, Q. Liu, et al., "Fluorine-Free Synthesis of High-Purity $Ti_3C_2T_X$ (T=OH, O) via Alkali Treatment," *Angewandte Chemie International Edition* 57, no. 21 (2018): 6115–6119, https://doi.org/10.1002/anie.201800887.

33. S. Yang, P. P. Zhang, F. X. Wang, et al., "Fluoride-Free Synthesis of Two-Dimensional Titanium Carbide (MXene) Using a Binary Aqueous System," *Angewandte Chemie International Edition* 57, no. 47 (2018): 15491–15495, https://doi.org/10.1002/anie.201809662.

34. M. Hu, H. Zhang, T. Hu, B. Fan, X. Wang, and Z. Li, "Emerging 2D MXenes for Supercapacitors: Status, Challenges and Prospects," *Chemical Society Reviews* 49, no. 18 (2020): 6666–6693, https://doi.org/10.1039/D0CS00175A.

35. H. Riazi, G. Taghizadeh, and M. Soroush, "MXene-Based Nanocomposite Sensors," *ACS Omega* 6, no. 17 (2021): 11103–11112, https://doi.org/10.1021/acsomega.0c05828.

36. Y. Yang, K. Li, Y. Wang, Z. Wu, T. P. Russell, and S. Shi, "MXene-Based Porous Monoliths," *Nanomaterials* 12, no. 21 (2022): 3792, https://doi.org/10.3390/nano12213792.

37. U. Amara, I. Hussain, M. Ahmad, K. Mahmood, and K. Zhang, "2D MXene-Based Biosensing: A Review," *Small* 19, no. 2 (2023): 2205249, https://doi.org/10.1002/smll.202205249.

16136829, 2026, 46, Downloaded from https://onlinelibrary.wiley.com/doi/10.1002/smll.74769 by Beihang University (Buaa), Wiley Online Library on [23/09/2026]. See the Terms and Conditions (https://onlinelibrary.wiley.com/terms-and-conditions) on Wiley Online Library for rules of use; OA articles are governed by the applicable Creative Commons License

38. X. Sang, Y. Xie, M. W. Lin, et al., "Atomic Defects in Monolayer Titanium Carbide ($Ti_3C_2T_x$) MXene," *ACS Nano* 10, no. 10 (2016): 9193–9200, https://doi.org/10.1021/acsnano.6b05240.

39. M. Naguib, O. Mashtalir, J. Carle, et al., "Two-Dimensional Transition Metal Carbides," *ACS Nano* 6, no. 2 (2012): 1322–1331, https://doi.org/10.1021/nn204153h.

40. B. Anasori, Y. Xie, M. Beidaghi, et al., "Two-Dimensional, Ordered, Double Transition Metals Carbides (MXenes)," *ACS Nano* 9, no. 10 (2015): 9507–9516, https://doi.org/10.1021/acsnano.5b03591.

41. M. Alhabeb, K. Maleski, T. S. Mathis, et al., "Selective Etching of Silicon from Ti_3SiC_2 (MAX) to Obtain 2D Titanium Carbide (MXene)," *Angewandte Chemie International Edition* 57, no. 19 (2018): 5444–5448, https://doi.org/10.1002/anie.201802232.

42. C. Shen, L. Wang, A. Zhou, et al., "Synthesis and Electrochemical Properties of Two-Dimensional RGO/$Ti_3C_2T_x$ Nanocomposites," *Nanomaterials* 8, no. 2 (2018): 80, https://doi.org/10.3390/nano8020080.

43. Y. J. Kim, S. J. Kim, D. Seo, et al., "Etching Mechanism of Monoatomic Aluminum Layers during MXene Synthesis," *Chemistry of Materials* 33, no. 16 (2021): 6346–6355, https://doi.org/10.1021/acs.chemmater.1c01263.

44. Y. Kim, A. Gkountaras, O. Chaix-Pluchery, et al., "Elementary Processes Governing V_2AlC Chemical Etching in HF," *RSC Advances* 10, no. 42 (2020): 25266–25274, https://doi.org/10.1039/d0ra00842g.

45. Z. Li, L. Wang, D. Sun, et al., "Synthesis and Thermal Stability of Two-dimensional Carbide MXene Ti_3C_2," *Materials Science and Engineering: B* 191 (2015): 33–40, https://doi.org/10.1016/j.mseb.2014.10.009.

46. Y. Jiang, D. Baimanov, S. Jin, et al., "In Situ Turning Defects of Exfoliated Ti_3C_2 MXene into Fenton-Like Catalytic Active Sites," *Proceedings of the National Academy of Sciences* 120, no. 1 (2023): 2210211120, https://doi.org/10.1073/pnas.2210211120.

47. D. Zhao, Z. Chen, W. Yang, et al., "MXene (Ti_3C_2) Vacancy-Confined Single-Atom Catalyst for Efficient Functionalization of CO_2," *Journal of the American Chemical Society* 141, no. 9 (2019): 4086–4093, https://doi.org/10.1021/jacs.8b13579.

48. S. Hu, S. Li, W. Xu, J. Zhang, Y. Zhou, and Z. Cheng, "Rapid Preparation, Thermal Stability and Electromagnetic Interference Shielding Properties of Two-dimensional Ti_3C_2 MXene," *Ceramics International* 45, no. 16 (2019): 19902–19909, https://doi.org/10.1016/j.ceramint.2019.06.246.

49. B. C. Wyatt, M. G. Boebinger, Z. D. Hood, et al., "Alkali Cation Stabilization of Defects in 2D MXenes at Ambient and Elevated Temperatures," *Nature Communications* 15, no. 1 (2024): 6353, https://doi.org/10.1038/s41467-024-50713-2.

50. R. Ibragimova, P. Rinke, and H. P. Komsa, "Native Vacancy Defects in MXenes at Etching Conditions," *Chemistry of Materials* 34, no. 7 (2022): 2896–2906, https://doi.org/10.1021/acs.chemmater.1c03179.

51. I. Persson, A. el Ghazaly, Q. Tao, et al., "Tailoring Structure, Composition, and Energy Storage Properties of MXenes from Selective Etching of In-Plane, Chemically Ordered MAX Phases," *Small* 14, no. 17 (2018): 1703676, https://doi.org/10.1002/smll.201703676.

52. T. Zhang, L. Chang, X. Zhang, et al., "Simultaneously Tuning Interlayer Spacing and Termination of MXenes by Lewis-Basic Halides," *Nature Communications* 13 (2022): 6731, https://doi.org/10.1038/s41467-022-34569-y.

53. R. E. Ustad, S. S. Kundale, K. A. Rokade, et al., "Recent Progress in Energy, Environment, and Electronic Applications of MXene Nanomaterials," *Nanoscale* 15, no. 23 (2023): 9891–9926, https://doi.org/10.1039/d2nr06162g.

54. M. Anayee, N. Kurra, M. Alhabeb, et al., "Role of acid mixtures etching on the surface chemistry and sodium ion storage in $Ti3C2T_x$ MXene," *Chemical Communications* 56, no. 45 (2020): 6090–6093, https://doi.org/10.1039/d0cc01042a.

55. M. Wu, B. Wang, Q. Hu, L. Wang, and A. Zhou, "The Synthesis Process and Thermal Stability of V_2C MXene," *Materials* 11, no. 11 (2018): 2112, https://doi.org/10.3390/ma11112112.

56. F. Liu, A. Zhou, J. Chen, et al., "Preparation of Ti_3C_2 and Ti_2C MXenes by Fluoride Salts Etching and Methane Adsorptive Properties," *Applied Surface Science* 416 (2017): 781–789, https://doi.org/10.1016/j.apsusc.2017.04.239.

57. M. Ghidiu, J. Halim, S. Kota, D. Bish, Y. Gogotsi, and M. W. Barsoum, "Ion-Exchange and Cation Solvation Reactions in Ti_3C_2 MXene," *Chemistry of Materials* 28, no. 10 (2016): 3507–3514, https://doi.org/10.1021/acs.chemmater.6b01275.

58. M. Benchakar, L. Loupias, C. Garnero, et al., "One MAX Phase, Different MXenes: A Guideline to Understand the Crucial Role of Etching Conditions on $Ti_3C_2T_x$ Surface Chemistry," *Applied Surface Science* 530 (2020): 147209, https://doi.org/10.1016/j.apsusc.2020.147209.

59. M. Guo, W. C. Geng, C. B. Liu, J. Y. Gu, Z. Z. Zhang, and Y. H. Tang, "Ultrahigh Areal Capacitance of Flexible MXene Electrodes: Electrostatic and Steric Effects of Terminations," *Chemistry of Materials* 32, no. 19 (2020): 8257–8265, https://doi.org/10.1021/acs.chemmater.0c02026.

60. X. Zou, H. Liu, H. Xu, et al., "A Simple Approach to Synthesis Cr_2CT_x MXene for Efficient Hydrogen Evolution Reaction," *Materials Today Energy* 20 (2021): 100668, https://doi.org/10.1016/j.mtener.2021.100668.

61. P. Liu, R. Pan, B. Li, Z. Su, B. Lin, and M. Tong, "Mild and Efficient Method for the In Situ Preparation of High-Quality MXene Materials Enabled by Hexafluoro Complex Anion Contained Salts Etching," *Advanced Functional Materials* 34, no. 2 (2024): 2308532, https://doi.org/10.1002/adfm.202308532.

62. C. A. Voigt, M. Ghidiu, V. Natu, and M. W. Barsoum, "Anion Adsorption, $Ti_3C_2T_Z$ MXene Multilayers, and Their Effect on Claylike Swelling," *The Journal of Physical Chemistry C* 122, no. 40 (2018): 23172–23179, https://doi.org/10.1021/acs.jpcc.8b07447.

63. A. Lipatov, M. Alhabeb, M. R. Lukatskaya, A. Boson, Y. Gogotsi, and A. Sinitskii, "Effect of Synthesis on Quality, Electronic Properties and Environmental Stability of Individual Monolayer Ti_3C_2 MXene Flakes," *Advanced Electronic Materials* 2, no. 12 (2016): 1600255, https://doi.org/10.1002/aelm.201600255.

64. M. Jeon, B. M. Jun, S. Kim, et al., "A Review on MXene-Based Nanomaterials as Adsorbents in Aqueous Solution," *Chemosphere* 261 (2020): 127781, https://doi.org/10.1016/j.chemosphere.2020.127781.

65. N. Zhang, Y. Hong, S. Yazdanparast, and M. A. Zaeem, "Superior Structural, Elastic and Electronic Properties of 2D Titanium Nitride MXenes over Carbide MXenes: A Comprehensive First Principles Study," *2D Materials* 5 (2018): 1–22, https://doi.org/10.48550/arXiv.1802.06648.

66. M. Naguib, V. N. Mochalin, M. W. Barsoum, and Y. Gogotsi, "25th Anniversary Article: MXenes: A New Family of Two-Dimensional Materials," *Advanced Materials* 26, no. 7 (2014): 992–1005, https://doi.org/10.1002/adma.201304138.

67. P. Urbankowski, B. Anasori, T. Makaryan, et al., "Synthesis of Two-dimensional Titanium Nitride Ti_4N_3 (MXene)," *Nanoscale* 8, no. 22 (2016): 11385–11391, https://doi.org/10.1039/C6NR02253G.

68. C. Xie, L. Xu, J. Peng, et al., "Halogenated Ti_3C_2 MXenes Prepared by Microwave Molten Salt for Hg^0 Photo-Oxidation," *Advanced Functional Materials* 33, no. 14 (2023): 2213782, https://doi.org/10.1002/adfm.202213782.

69. M. Shen, W. Jiang, K. Liang, et al., "One-Pot Green Process to Synthesize MXene with Controllable Surface Terminations Using Molten Salts," *Angewandte Chemie International Edition* 60, no. 52 (2021): 27013–27018, https://doi.org/10.1002/anie.202110640.

70. L. Liu, M. Orbay, S. Luo, et al., "Exfoliation and Delamination of $Ti3C2T_x$ MXene Prepared via Molten Salt Etching Route," *ACS Nano* 16, no. 1 (2021): 111–118, https://doi.org/10.1021/acsnano.1c08498.

71. Y. Bai, C. Liu, T. Chen, et al., "MXene-Copper/Cobalt Hybrids via Lewis Acidic Molten Salts Etching for High Performance Symmetric Supercapacitors," *Angewandte Chemie International Edition* 60, no. 48 (2021): 25318–25322, https://doi.org/10.1002/anie.202112381.

16136829, 2026, 46, Downloaded from https://onlinelibrary.wiley.com/doi/10.1002/smll.74769 by Beihang University (Buaa), Wiley Online Library on [23/09/2026]. See the Terms and Conditions (https://onlinelibrary.wiley.com/terms-and-conditions) on Wiley Online Library for rules of use; OA articles are governed by the applicable Creative Commons License

72. K. Arole, J. W. Blivin, S. Saha, et al., "Water-Dispersible $Ti_3C_2T_z$ MXene Nanosheets by Molten Salt Etching," *Iscience* 24, no. 12 (2021): 103403, https://doi.org/10.1016/j.isci.2021.103403.

73. S. Y. Pang, Y. T. Wong, S. Yuan, et al., "Universal Strategy for HF-Free Facile and Rapid Synthesis of Two-dimensional MXenes as Multifunctional Energy Materials," *Journal of the American Chemical Society* 141, no. 24 (2019): 9610–9616, https://doi.org/10.1021/jacs.9b02578.

74. G. Zou, J. Guo, X. Liu, et al., "Hydrogenated Core–Shell MAX@$K_2Ti_8O_{17}$ Pseudocapacitance with Ultrafast Sodium Storage and Long-Term Cycling," *Advanced Energy Materials* 7, no. 18 (2017): 1700700, https://doi.org/10.1002/aenm.201700700.

75. S. Gokul Eswaran, M. Rashad, K. Santhana, A. Kumar, and A. F. EL-Mahdy, "A Comprehensive Review of MXene-Based Emerging Materials for Energy Storage Applications and Future Perspectives," *Chemistry—An Asian Journal* 20 (2025): 202401181, https://doi.org/10.1002/asia.202401181.

76. W. Bao, H. Shen, G. Zeng, et al., "Engineering the Next Generation of MXenes: Challenges and Strategies for Scalable Production and Enhanced Performance," *Nanoscale* 17 (2025): 6204–6265, https://doi.org/10.1039/D4NR04560B.

77. M. Alhabeb, K. Maleski, B. Anasori, et al., "Guidelines for Synthesis and Processing of Two-Dimensional Titanium Carbide ($Ti_3C_2T_x$ MXene)," *Chemistry of Materials* 29 (2017): 7633–7644, https://doi.org/10.1021/acs.chemmater.7b02847.

78. Y. Xu, X. Shi, Y. Zhang, et al., "Epitaxial Nucleation and Lateral Growth of High-Crystalline Black Phosphorus Films on Silicon," *Nature Communications* 11, no. 1 (2020): 1330, https://doi.org/10.1038/s41467-020-14902-z.

79. J. Song, H. Chen, Y. Sun, and Z. Liu, "Layered MXene Films via Self-Assembly," *Small* 20, no. 51 (2024): 2406855, https://doi.org/10.1002/smll.202406855.

80. X. D. Xu, Y. L. Zhang, H. Y. Sun, et al., "Progress and Perspective: MXene and MXene-Based Nanomaterials for High-Performance Energy Storage Devices," *Advanced Electronic Materials* 7, no. 7 (2021): 2000967, https://doi.org/10.1002/aelm.202000967.

81. V. Natu, R. Pai, O. Wilson, et al., "Effect of Base/Nucleophile Treatment on Interlayer Ion Intercalation, Surface Terminations, and Osmotic Swelling of $Ti_3C_2T_Z$ MXene Multilayers," *Chemistry of Materials* 34, no. 2 (2022): 678–693, https://doi.org/10.1021/acs.chemmater.1c03390.

82. K. Arole, J. W. Blivin, A. M. Bruce, et al., "Exfoliation, Delamination, and Oxidation Stability of Molten Salt Etched Nb_2CT_Z MXene Nanosheets," *Chemical Communications* 58, no. 73 (2022): 10202–10205, https://doi.org/10.1039/d2cc02237k.

83. M. Malaki, A. Maleki, and R. S. Varma, "MXenes and Ultrasonication," *Journal of Materials Chemistry A* 7, no. 18 (2019): 10843–10857, https://doi.org/10.1039/C9TA01850F.

84. D. R. Baer and I. S. Gilmore, "Responding to the Growing Issue of Research Reproducibility," *Journal of Vacuum Science & Technology, A: Vacuum, Surfaces, and Films* 36, no. 6 (2018): 068502, https://doi.org/10.1116/1.5049141.

85. Q. Fan, M. Chen, L. Li, et al., "Gaseous Molecules-mediated Electrochemical Exfoliation of Halogenated MXenes and Its Boosting in Wear-Resisting Tribovoltaic Devices," *Nature Communications* 16, no. 1 (2025): 5051, https://doi.org/10.1038/s41467-025-60303-5.

86. V. Natu, J. L. Hart, M. Sokol, H. Chiang, M. L. Taheri, and M. W. Barsoum, "Edge Capping of 2D-MXene Sheets with Polyanionic Salts to Mitigate Oxidation in Aqueous Colloidal Suspensions," *Angewandte Chemie International Edition* 58, no. 36 (2019): 12655–12660, https://doi.org/10.1002/anie.201906138.

87. M. A. Hope, A. C. Forse, K. J. Griffith, et al., "NMR Reveals the Surface Functionalisation of Ti_3C_2 MXene," *Physical Chemistry Chemical Physics* 18, no. 7 (2016): 5099–5102, https://doi.org/10.1039/C6CP00330C.

88. S. Kajiyama, L. Szabova, H. Iinuma, et al., "Enhanced Li-Ion Accessibility in MXene Titanium Carbide by Steric Chloride Termination," *Advanced Energy Materials* 7, no. 9 (2017): 1601873, https://doi.org/10.1002/aenm.201601873.

89. Y. Li, H. Shao, Z. Lin, et al., "Element Replacement Approach by Reaction with Lewis Acidic Molten Salts to Synthesize Nanolaminated MAX Phases and MXenes," *Journal of the American Chemical Society* 141 (2019): 4730–4737, https://doi.org/10.1021/jacs.9b00574.

90. C. Zhou, D. Wang, F. Lagunas, et al., "Hybrid Organic–Inorganic Two-dimensional Metal Carbide MXenes with Amido- and Imido-Terminated Surfaces," *Nature Chemistry* 15, no. 12 (2023): 1722–1729, https://doi.org/10.1038/s41557-023-01288-w.

91. Y. Guo, S. Wu, Z. Liu, Z. Du, and S. Yang, "Topological Transformation of MXenes to Non-Van Der Waals Artificial Solids with Well-Defined Structure," *Advanced Materials* 37, no. 40 (2025): 2507705, https://doi.org/10.1002/adma.202507705.

92. L. Vicarelli, S. J. Heerema, C. Dekker, and H. W. Zandbergen, "Controlling Defects in Graphene for Optimizing the Electrical Properties of Graphene Nanodevices," *ACS Nano* 9, no. 4 (2015): 3428–3435, https://doi.org/10.1021/acsnano.5b01762.

93. M. Amani, D. H. Lien, D. Kiriya, et al., "Near-Unity Photoluminescence Quantum Yield in MoS_2," *Science* 350, no. 6264 (2015): 1065–1068, https://doi.org/10.1126/science.aad2114.

94. W. Zhou, X. Zou, S. Najmaei, et al., "Intrinsic Structural Defects in Monolayer Molybdenum Disulfide," *Nano Letters* 13, no. 6 (2013): 2615–2622, https://doi.org/10.1021/nl4007479.

95. A. Saha, N. Shpigel, N. Leifer, et al., "Enhancing the Energy Storage Capabilities of $Ti_3C_2T_X$ MXene Electrodes by Atomic Surface Reduction," *Advanced Functional Materials* 31, no. 52 (2021): 2106294, https://doi.org/10.1002/adfm.202106294.

96. A. Brückner, "In Situ Electron Paramagnetic Resonance: A Unique Tool for Analyzing Structure–Reactivity Relationships in Heterogeneous Catalysis," *Chemical Society Reviews* 39, no. 12 (2010): 4673, https://doi.org/10.1039/B919541F.

97. H. Zhou, Z. Chen, E. Kountoupi, et al., "Two-Dimensional Molybdenum Carbide 2D-Mo_2C as a Superior Catalyst for CO_2 Hydrogenation," *Nature Communications* 12, no. 1 (2021): 5510, https://doi.org/10.1038/s41467-021-25784-0.

98. X. Hui, D. Zhao, P. Wang, et al., "Oxide Nanoclusters on Ti_3C_2 MXenes to Deactivate Defects for Enhanced Lithium Ion Storage Performance," *Small* 18, no. 5 (2022): 2104439, https://doi.org/10.1002/smll.202104439.

99. Z. Hu, C. Geng, L. Wang, W. Lv, and Q.-H. Yang, "Revisiting the Roles of Carbon in the Catalysis of Lithium–Sulfur Batteries," *Advanced Energy Sustainability Research* 5 (2023): 2300148, https://doi.org/10.1002/aesr.202300148.

100. Y. Fang, Z. Liu, J. Han, et al., "High-Performance Electrocatalytic Conversion of N_2 to NH_3 Using Oxygen-Vacancy-Rich TiO_2 in Situ Grown on $Ti_3C_2T_X$ MXene," *Advanced Energy Materials* 9, no. 16 (2019): 1803406, https://doi.org/10.1002/aenm.201803406.

101. Y. Zhou, Y. Chai, X. Li, et al., "Defect-Rich TiO_2 in Situ Evolved from MXene for the Enhanced Oxidative Dehydrogenation of Ethane to Ethylene," *ACS Catalysis* 11, no. 24 (2021): 15223–15233, https://doi.org/10.1021/acscatal.1c04409.

102. B. X. Chen, Z. X. Lu, S. Y. Feng, Z. H. Zhou, and C. H. Lu, "Redox-Active Nitroxide Radicals Grafted onto MXene: Boosting Energy Storage via Improved Charge Transfer and Surface Capacitance," *ACS Energy Letters* 8, no. 2 (2023): 1096–1106, https://doi.org/10.1021/acsenergylett.2c02595.

103. J. K. El-Demellawi, A. E. Mansour, A. M. El-Zohry, et al., "Tuning the Work Function of $Ti_3C_2T_x$ MXene by Molecular Doping Without Changing Its Surface Functional Groups," *ACS Materials Letters* 4, no. 12 (2022): 2480–2490, https://doi.org/10.1021/acsmaterialslett.2c00796.

16136829, 2026, 46, Downloaded from https://onlinelibrary.wiley.com/doi/10.1002/smll.74769 by Beihang University (Buaa), Wiley Online Library on [23/09/2026]. See the Terms and Conditions (https://onlinelibrary.wiley.com/terms-and-conditions) on Wiley Online Library for rules of use; OA articles are governed by the applicable Creative Commons License

104. T. Hassan, D. Lee, S. M. Naqvi, et al., "Quantitative Defect–Property Correlations in $Ti_3C_2T_x$ MXenes via Precursor-Controlled Defect Engineering," *Nano-Micro Letters* 18 (2026): 264, https://doi.org/10.1007/s40820-026-02106-x.

105. J. Halim, K. M. Cook, M. Naguib, et al., "X-ray Photoelectron Spectroscopy of Select Multi-layered Transition Metal Carbides (MXenes)," *Applied Surface Science* 362 (2016): 406–417, https://doi.org/10.1016/j.apsusc.2015.11.089.

106. D. R. Baer, K. Artyushkova, C. R. Brundle, et al., "Practical Guides for X-ray Photoelectron Spectroscopy: First Steps in Planning, Conducting, and Reporting XPS Measurements," *Journal of Vacuum Science & Technology, A: Vacuum, Surfaces, and Films* 37, no. 3 (2019): 031401, https://doi.org/10.1116/1.5065501.

107. D. R. Baer, K. Artyushkova, H. Cohen, et al., "XPS Guide: Charge Neutralization and Binding Energy Referencing for Insulating Samples," *Journal of Vacuum Science & Technology, A: Vacuum, Surfaces, and Films* 38, no. 3 (2020): 031204, https://doi.org/10.1116/6.0000057.

108. M. Magnuson, J. Halim, and L. Å. Näslund, "Chemical Bonding in Carbide MXene Nanosheets," *Journal of Electron Spectroscopy and Related Phenomena* 224 (2018): 27–32, https://doi.org/10.1016/j.elspec.2017.09.006.

109. G. Sharma, E. Muthuswamy, M. Naguib, Y. Gogotsi, A. Navrotsky, and D. Wu, "Calorimetric Study of Alkali Metal Ion (K^+ , Na^+ , Li^+) Exchange in a Clay-Like MXene," *The Journal of Physical Chemistry C* 121, no. 28 (2017): 15145–15153, https://doi.org/10.1021/acs.jpcc.7b02419.

110. B. Anasori and Y. Gogotsi, "2D Metal Carbides and Nitrides (MXenes) for Energy Storage," *Nature Reviews Materials* 2 (2017): 16098, https://doi.org/10.1038/natrevmats.2016.98.

111. K. J. Harris, M. Bugnet, M. Naguib, M. W. Barsoum, and G. R. Goward, "Direct Measurement of Surface Termination Groups and Their Connectivity in the 2D MXene V_2CT_X Using NMR Spectroscopy," *The Journal of Physical Chemistry C* 119, no. 24 (2015): 13713–13720, https://doi.org/10.1021/acs.jpcc.5b03038.

112. M. R. Chierotti and R. Gobetto, "Solid-State NMR Studies on Supramolecular Chemistry," *Supramolecular Chemistry: From Molecules to Nanomaterials* 2 (2012): 331–347, https://doi.org/10.1002/9780470661345.smc026.

113. I. Persson, L. Å. Näslund, J. Halim, et al., "On the Organization and Thermal Behavior of Functional Groups on Ti3C2 MXene Surfaces in Vacuum," *2D Materials* 5, no. 1 (2017): 015002, https://doi.org/10.1088/2053-1583/aa89cd.

114. P. P. Michalowski, M. Anayee, T. S. Mathis, et al., "Oxycarbide MXenes and MAX Phases Identification Using Monoatomic Layer-by-Layer Analysis with Ultralow-Energy Secondary-Ion Mass Spectrometry," *Nature Nanotechnology* 17, no. 11 (2022): 1192–1197, https://doi.org/10.1038/s41565-022-01214-0.

115. W. W. Sun, H. W. Wang, L. Vlcek, et al., "Multiscale and Multimodal Characterization of 2D Titanium Carbonitride MXene," *Advanced Materials Interfaces* 7, no. 11 (2020): 1902207, https://doi.org/10.1002/admi.201902207.

116. A. Sugahara, Y. Ando, S. Kajiyama, et al., "Negative Dielectric Constant of Water Confined in Nanosheets," *Nature Communications* 10, no. 1 (2019): 850, https://doi.org/10.1038/s41467-019-08789-8.

117. T. Kobayashi, Y. Sun, K. Prenger, D.-E. Jiang, M. Naguib, and M. Pruski, "Nature of Terminating Hydroxyl Groups and Intercalating Water in $Ti_3C_2T_X$ MXenes: A Study by ^1H Solid-State NMR and DFT Calculations," *The Journal of Physical Chemistry C* 124, no. 25 (2020): 13649–13655, https://doi.org/10.1021/acs.jpcc.0c04744.

118. F. Brette, D. Kourati, M. Paris, et al., "Assessing the Surface Chemistry of 2D Transition Metal Carbides (MXenes): A Combined Experimental/Theoretical ^{13}C Solid State NMR Approach," *Journal of the American Chemical Society* 145, no. 7 (2023): 4003–4014, https://doi.org/10.1021/jacs.2c11290.

119. G. Lu, S. L. Bernasek, and J. Schwartz, "Oxidation of a Polycrystalline Titanium Surface by Oxygen and Water," *Surface Science* 458, no. 1-3 (2000): 80–90, https://doi.org/10.1016/S0039-6028(00)00420-9.

120. M. Shekhirev, C. E. Shuck, A. Sarycheva, and Y. Gogotsi, "Characterization of MXenes at Every Step, from Their Precursors to Single Flakes and Assembled Films," *Progress in Materials Science* 120 (2021): 100757, https://doi.org/10.1016/j.pmatsci.2020.100757.

121. Y. Xie, Y. Dall'Agnese, M. Naguib, et al., "Prediction and Characterization of MXene Nanosheet Anodes for Non-Lithium-Ion Batteries," *ACS Nano* 8, no. 9 (2014): 9606–9615, https://doi.org/10.1021/nn503921j.

122. X. Wang, S. Kajiyama, H. Iinuma, et al., "Pseudocapacitance of MXene Nanosheets for High-Power Sodium-Ion Hybrid Capacitors," *Nature Communications* 6, no. 1 (2015): 6544, https://doi.org/10.1038/ncomms7544.

123. M. Naguib, R. A. Adams, Y. Zhao, et al., "Electrochemical Performance of MXenes as K-ion Battery Anodes," *Chemical Communications* 53, no. 51 (2017): 6883–6886, https://doi.org/10.1039/c7cc02026k.

124. M. Lounasvuori, Y. Sun, T. S. Mathis, et al., "Vibrational Signature of Hydrated Protons Confined in MXene Interlayers," *Nature Communications* 14, no. 1 (2023): 1322, https://doi.org/10.1038/s41467-023-36842-0.

125. J. Halim, S. Kota, M. R. Lukatskaya, et al., "Synthesis and Characterization of 2D Molybdenum Carbide (MXene)," *Advanced Functional Materials* 26, no. 18 (2016): 3118–3127, https://doi.org/10.1002/adfm.201505328.

126. Q. Tang, Z. Zhou, and P. Shen, "Are MXenes Promising Anode Materials for Li Ion Batteries? Computational Studies on Electronic Properties and Li Storage Capability of Ti_3C_2 and $Ti_3C_2X_2$ (X = F, OH) Monolayer," *Journal of the American Chemical Society* 134, no. 40 (2012): 16909–16916, https://doi.org/10.1021/ja308463r.

127. M. Khazaei, M. Arai, T. Sasaki, et al., "Novel Electronic and Magnetic Properties of Two-Dimensional Transition Metal Carbides and Nitrides," *Advanced Functional Materials* 23, no. 17 (2013): 2185–2192, https://doi.org/10.1002/adfm.201202502.

128. A. Enyashin and A. Ivanovskii, "Two-dimensional Titanium Carbonitrides and Their Hydroxylated Derivatives: Structural, Electronic Properties and Stability of MXenes $Ti_3C_{2-x}N_x(OH)_2$ from DFTB Calculations," *Journal of Solid State Chemistry* 207 (2013): 42–48, https://doi.org/10.1016/j.jssc.2013.09.010.

129. A. Michael and M. Kiran, "Predicted Surface Composition and Thermodynamic Stability of MXenes in Solution" *Journal of Physical Chemistry C* 120 (2016): 3550–3556, https://doi.org/10.1021/acs.jpcc.5b11887.

130. J. Lu, I. Persson, H. Lind, et al., "$Ti_{n+1}C_n$ MXenes with Fully Saturated and Thermally Stable Cl Terminations," *Nanoscale Advances* 1, no. 9 (2019): 3680–3685, https://doi.org/10.1039/c9na00324j.

131. J. Kim, L. J. Cote, F. Kim, W. Yuan, K. R. Shull, and J. Huang, "Graphene Oxide Sheets at Interfaces," *Journal of the American Chemical Society* 132, no. 23 (2010): 8180–8186, https://doi.org/10.1021/ja102777p.

132. V. Natu, M. Sokol, L. Verger, and M. W. Barsoum, "Effect of Edge Charges on Stability and Aggregation of $Ti_3C_2T_Z$ MXene Colloidal Suspensions," *The Journal of Physical Chemistry C* 122, no. 48 (2018): 27745–27753, https://doi.org/10.1021/acs.jpcc.8b08860.

133. S. Kumar, S. M. Zain Mehdi, M. Taunk, et al., "Synergistic Effects of Polymer Integration on the Properties, Stability, and Applications of MXenes," *Journal of Materials Chemistry A* 13, no. 16 (2025): 11050–11113, https://doi.org/10.1039/d4ta08094g.

134. W. Lawrence, "Theory of Ion Exchange and Development of Charge in Kaolinite-Water Systems," *Journal of the American Ceramic Society* 41, no. 4 (1958): 136–140, https://doi.org/10.1111/j.1151-2916.1958.tb13527.x.

135. R. H. Ras, Y. Umemura, C. T. Johnston, A. Yamagishi, and R. A. Schoonheydt, "Ultrathin Hybrid Films of Clay Minerals," *Physical*

16136829, 2026, 46, Downloaded from https://onlinelibrary.wiley.com/doi/10.1002/smll.74769 by Beihang University (Buaa), Wiley Online Library on [23/09/2026]. See the Terms and Conditions (https://onlinelibrary.wiley.com/terms-and-conditions) on Wiley Online Library for rules of use; OA articles are governed by the applicable Creative Commons License

Chemistry Chemical Physics 9, no. 8 (2007): 918–932, https://doi.org/10.1039/B610698F.

136. F. Bergaya and G. Lagaly, "Chapter 1 General Introduction: Clays, Clay Minerals, and Clay Science," *Developments in Clay Science* 1 (2006): 1–18, https://doi.org/10.1016/S1572-4352(05)01001-9.

137. A. Ferris and W. Jepson, "The Exchange Capacities of Kaolinite and the Preparation of Homoionic Clays," *Journal of Colloid and Interface Science* 51, no. 2 (1975): 245–259, https://doi.org/10.1016/0021-9797(75)90110-1.

138. P. Lian, Y. Dong, Z. S. Wu, et al., "Alkalized Ti_3C_2 MXene Nanoribbons with Expanded Interlayer Spacing for High-Capacity Sodium and Potassium Ion Batteries," *Nano Energy* 40 (2017): 1–8, https://doi.org/10.1016/j.nanoen.2017.08.002.

139. Y. Dall'Agnese, M. R. Lukatskaya, K. M. Cook, P. L. Taberna, Y. Gogotsi, and P. Simon, "High Capacitance of Surface-Modified 2D Titanium Carbide in Acidic Electrolyte," *Electrochemistry Communications* 48 (2014): 118–122, https://doi.org/10.1016/j.elecom.2014.09.002.

140. E. J. W. Verwey, "Theory of the Stability of Lyophobic Colloids," *The Journal of Physical and Colloid Chemistry* 51, no. 3 (1947): 631–636, https://doi.org/10.1021/j150453a001.

141. X. Wang, H. Zhang, L. Dong, et al., "Self-Powered High-Resolution and Pressure-Sensitive Triboelectric Sensor Matrix for Real-Time Tactile Mapping," *Advanced Materials* 28, no. 15 (2016): 2896–2903, https://doi.org/10.1002/adma.201503407.

142. H. Liu, Q. Li, Y. Bu, et al., "Stretchable Conductive Nonwoven Fabrics with Self-cleaning Capability for Tunable Wearable Strain Sensor," *Nano Energy* 66 (2019): 104143, https://doi.org/10.1016/j.nanoen.2019.104143.

143. G. Cheng, Z. Xuan, S. Tian, Z. Tang, G. Ding, and X. Wan, "$Ti_3C_2T_x$ MXene Modification Using Silicane or Quaternary Ammonium Salt via Covalent Bonding or Interaction for High-performance Composites," *Polymer Composites* 44, no. 12 (2023): 8378–8388, https://doi.org/10.1002/pc.27704.

144. P. Cai, L. Ding, Z. Chen, et al., "Tetrabutylammonium Bromide Functionalized Ti_3C_2 T_X MXene as Versatile Cathode Buffer Layer for Efficient and Stable Inverted Perovskite Solar Cells," *Advanced Functional Materials* 33, no. 30 (2023): 2300113, https://doi.org/10.1002/adfm.202300113.

145. R. Wu, P. Jia, L. Song, J. Li, B. Wang, and Y. Hu, "Construction of MXene-Mediated Inorganic-Organic Quaternary Ammonium Salt-Hybrid Coating for Fire Safety and Multi-mode Synergistic Antibacterial of Cotton Fabric," *International Journal of Biological Macromolecules* 264 (2024): 130157, https://doi.org/10.1016/j.ijbiomac.2024.130157.

146. S. Song, F. Yin, Y. Fu, et al., "Simultaneous Regulation of Li-ion Intercalation and Oxygen Termination Decoration on $Ti_3C_2T_x$ MXene Toward Enhanced Oxygen Electrocatalysis for Li-O_2 Batteries," *Chemical Engineering Journal* 451 (2023): 138818, https://doi.org/10.1016/j.cej.2022.138818.

147. H. Li, X. Wang, H. Li, et al., "Capacitance Improvements of V_4C_3T by NH_3 Annealing," *Journal of Alloys and Compounds* 784 (2019): 923–930, https://doi.org/10.1016/j.jallcom.2019.01.111.

148. K. Zhang, M. Di, L. Fu, Y. Deng, Y. Du, and N. Tang, "Enhancing the Magnetism of 2D Carbide MXene $Ti_3C_2T_x$ by H_2 Annealing," *Carbon* 157 (2020): 90–96, https://doi.org/10.1016/j.carbon.2019.10.016.

149. L. Tian, F. Xu, G. Sastre, A. Primo, J. Yu, and H. Garcia, "Engineering MXene Surfaces and Heterostructure Interfaces for Efficient Heterogeneous Catalysis," *Chemical Society Reviews* 55, no. 7 (2026): 4244–4302, https://doi.org/10.1039/d5cs00376h.

150. T. Schultz, N. C. Frey, K. Hantanasirisakul, et al., "Surface Termination Dependent Work Function and Electronic Properties of $Ti_3C_2T_X$ MXene," *Chemistry of Materials* 31, no. 17 (2019): 6590–6597, https://doi.org/10.1021/acs.chemmater.9b02060.

151. K. J. Griffith, M. A. Hope, P. J. Reeves, M. Anayee, Y. Gogotsi, and C. P. Grey, "Bulk and Surface Chemistry of the Niobium MAX and MXene Phases from Multinuclear Solid-State NMR Spectroscopy," *Journal of the American Chemical Society* 142, no. 44 (2020): 18924–18935, https://doi.org/10.1021/jacs.0c09044.

152. S. Yazdanparast, S. Soltanmohammad, A. Fash-White, G. J. Tucker, and G. L. Brennecka, "Synthesis and Surface Chemistry of 2D TiVC Solid-Solution MXenes," *ACS Applied Materials & Interfaces* 12, no. 17 (2020): 20129–20137, https://doi.org/10.1021/acsami.0c03181.

153. B. M. Jun, C. M. Park, J. Heo, and Y. Yoon, "Adsorption of Ba^{2+} and Sr^{2+} on $Ti_3C_2T_x$ MXene in Model Fracking Wastewater," *Journal of Environmental Management* 256 (2020): 109940, https://doi.org/10.1016/j.jenvman.2019.109940.

154. J. L. Hart, K. Hantanasirisakul, A. C. Lang, et al., "Control of MXenes' Electronic Properties through Termination and Intercalation," *Nature Communications* 10, no. 1 (2019): 522, https://doi.org/10.1038/s41467-018-08169-8.

155. A. Iakunkov, A. Nordenstrom, N. Boulanger, C. Hennig, I. Baburin, and A. V. Talyzin, "Temperature-Dependent Swelling Transitions in MXene $Ti_3C_2T_x$," *Nanoscale* 14, no. 30 (2022): 10940–10949, https://doi.org/10.1039/d2nr03075f.

156. S. Shen, T. Ke, K. Rajavel, K. Yang, and D. Lin, "Dispersibility and Photochemical Stability of Delaminated MXene Flakes in Water," *Small* 16, no. 36 (2020): 2002433, https://doi.org/10.1002/smll.202002433.

157. Q. Zhang, H. Lai, R. Fan, P. Ji, X. Fu, and H. Li, "High Concentration of $Ti_3C_2T_x$ MXene in Organic Solvent," *ACS Nano* 15, no. 3 (2021): 5249–5262, https://doi.org/10.1021/acsnano.0c10671.

158. Y. Wang, M. Liu, Z. Wang, et al., "Interlayer Environment Engineered MXene: Pre-intercalated Zn^{2+} Ions as Intercalants Renders the Modulated Li Storage," *Journal of Energy Chemistry* 68 (2022): 306–313, https://doi.org/10.1016/j.jechem.2021.11.019.

159. C. Liang, Z. Yen, T. Salim, and Y. M. Lam, "Elucidation of the Synergistic Effects of 3d Metal (M = Cu, Co, and Ni) Dopants and Terminations (T = –O– and –OH) of Ti3C2T_x MXenes for Urea Adsorption Ability via DFT Calculations and Experiments," *Physical Chemistry Chemical Physics* 25, no. 46 (2023): 31874–31883, https://doi.org/10.1039/D3CP03263A.

160. O. Mashtalir, M. Naguib, V. N. Mochalin, et al., "Intercalation and Delamination of Layered Carbides and Carbonitrides," *Nature Communications* 4, no. 1 (2013): 1716, https://doi.org/10.1038/ncomms2664.

161. R. L. Ledoux and J. L. White, "Infrared Studies of Hydrogen Bonding Interaction between Kaolinite Surfaces and Intercalated Potassium Acetate, Hydrazine, Formamide, and Urea," *Journal of Colloid and Interface Science* 21, no. 2 (1966): 127–152, https://doi.org/10.1016/0095-8522(66)90029-8.

162. B. X. Wang, A. G. Zhou, F. F. Liu, J. L. Cao, L. B. Wang, and Q. K. Hu, "Carbon Dioxide Adsorption of Two-dimensional Carbide MXenes," *Journal of Advanced Ceramics* 7, no. 3 (2018): 237–245, https://doi.org/10.1007/s40145-018-0275-3.

163. M. R. Lukatskaya, O. Mashtalir, C. E. Ren, et al., "Cation Intercalation and High Volumetric Capacitance of Two-Dimensional Titanium Carbide," *Science* 341, no. 6153 (2013): 1502–1505, https://doi.org/10.1126/science.1241488.

164. Y. Sun, C. Zhan, P. R. C. Kent, M. Naguib, Y. Gogotsi, and D. E. Jiang, "Proton Redox and Transport in MXene-Confined Water," *ACS Applied Materials & Interfaces* 12, no. 1 (2020): 763–770, https://doi.org/10.1021/acsami.9b18139.

165. J. Luo, W. Zhang, H. Yuan, et al., "Pillared Structure Design of MXene with Ultralarge Interlayer Spacing for High-Performance Lithium-Ion Capacitors," *ACS Nano* 11, no. 3 (2017): 2459–2469, https://doi.org/10.1021/acsnano.6b07668.

166. Z. Wang, Y. Wang, Q. Gu, et al., "Multi-ion Intercalated $Ti_3C_2T_x$ MXene and the Mutual Modulation within Interlayer," *Particuology* 72 (2023): 10–16, https://doi.org/10.1016/j.partic.2022.02.006.

16136829, 2026, 46, Downloaded from https://onlinelibrary.wiley.com/doi/10.1002/smll.74769 by Beihang University (Buaa), Wiley Online Library on [23/09/2026]. See the Terms and Conditions (https://onlinelibrary.wiley.com/terms-and-conditions) on Wiley Online Library for rules of use; OA articles are governed by the applicable Creative Commons License

167. D. Qu, Y. Jian, L. Guo, et al., "An Organic Solvent-Assisted Intercalation and Collection (OAIC) for $Ti_3C_2T_x$ MXene with Controllable Sizes and Improved Yield," *Nano-Micro Letters* 13, no. 1 (2021): 188, https://doi.org/10.1007/s40820-021-00705-4.

168. P. Zhang, L. Wang, Z. Huang, et al., "Aryl Diazonium-Assisted Amidoximation of MXene for Boosting Water Stability and Uranyl Sequestration via Electrochemical Sorption," *ACS Applied Materials & Interfaces* 12, no. 13 (2020): 15579–15587, https://doi.org/10.1021/acsami.0c00861.

169. J. Wang, H. Ma, Y. Liu, Z. Xie, and Z. Fan, "MXene-Based Humidity-Responsive Actuators: Preparation and Properties," *ChemPlusChem* 86, no. 3 (2021): 406–417, https://doi.org/10.1002/cplu.202000828.

170. N. H. Solangi, N. M. Mubarak, R. R. Karri, S. A. Mazari, S. K. Kailasa, and A. Alfantazi, "Applications of Advanced MXene-Based Composite Membranes for Sustainable Water Desalination," *Chemosphere* 314 (2023): 137643, https://doi.org/10.1016/j.chemosphere.2022.137643.

171. S. Chen, S. F. Tan, H. Singh, L. Liu, M. Etienne, and P. S. Lee, "Functionalized MXene Films with Substantially Improved Low-Voltage Actuation," *Advanced Materials* 36 (2023): 2307045, https://doi.org/10.1002/adma.202307045.

172. Y. Zhu, S. Zheng, P. Lu, et al., "Kinetic Regulation of MXene with Water-in-LiCl Electrolyte for High-Voltage Micro-supercapacitors," *National Science Review* 9, no. 7 (2022): nwac024, https://doi.org/10.1093/nsr/nwac024.

173. H. Wang, J. Zhang, Y. Wu, et al., "Surface Modified MXene Ti_3C_2 Multilayers by Aryl Diazonium Salts Leading to Large-Scale Delamination," *Applied Surface Science* 384 (2016): 287–293, https://doi.org/10.1016/j.apsusc.2016.05.060.

174. M. Naguib, R. R. Unocic, B. L. Armstrong, and J. Nanda, "Large-Scale Delamination of Multi-layers Transition Metal Carbides and Carbonitrides 'MXenes'," *Dalton Transactions* 44, no. 20 (2015): 9353–9358, https://doi.org/10.1039/c5dt01247c.

175. X. Zhao, A. Vashisth, J. W. Blivin, et al., "pH, Nanosheet Concentration, and Antioxidant Affect the Oxidation of $Ti3C_2T_X$ and Ti_2CT_X MXene Dispersions," *Advanced Materials Interfaces* 7, no. 20 (2020): 2000845, https://doi.org/10.1002/admi.202000845.

176. X. Liu, W. Zhang, X. Zhang, et al., "Transparent Ultrahigh-Molecular-Weight Polyethylene/MXene Films with Efficient UV-Absorption for Thermal Management," *Nature Communications* 15, no. 1 (2024): 3076, https://doi.org/10.1038/s41467-024-47432-z.

177. V. Natu, R. Pai, M. Sokol, M. Carey, V. Kalra, and M. W. Barsoum, "2D $Ti_3C_2T_z$ MXene Synthesized by Water-Free Etching of Ti_3AlC_2 in Polar Organic Solvents," *Chemistry* 6, no. 3 (2020): 616–630, https://doi.org/10.1016/j.chempr.2020.01.019.

178. T. Oh, S. Lee, H. Kim, T. Y. Ko, S. J. Kim, and C. M. Koo, "Fast and High-Yield Anhydrous Synthesis of $Ti_3C_2T_x$ MXene with High Electrical Conductivity and Exceptional Mechanical Strength," *Small* 18, no. 46 (2022): 2203767, https://doi.org/10.1002/smll.202203767.

179. H. Wang, Y. Wu, X. Yuan, et al., "Clay-Inspired MXene-Based Electrochemical Devices and Photo-Electrocatalyst: State-of-the-Art Progresses and Challenges," *Advanced Materials* 30, no. 12 (2018): 1704561, https://doi.org/10.1002/adma.201704561.

180. H. Chen, H. Ma, and C. Li, "Host–Guest Intercalation Chemistry in MXenes and Its Implications for Practical Applications," *ACS Nano* 15, no. 10 (2021): 15502–15537, https://doi.org/10.1021/acsnano.1c04423.

181. N. C. Osti, M. Naguib, A. Ostadhossein, et al., "Effect of Metal Ion Intercalation on the Structure of MXene and Water Dynamics on Its Internal Surfaces," *ACS Applied Materials & Interfaces* 8, no. 14 (2016): 8859–8863, https://doi.org/10.1021/acsami.6b01490.

182. F. Salles, I. Beurroies, O. Bildstein, et al., "A Calorimetric Study of Mesoscopic Swelling and Hydration Sequence in Solid Na-montmorillonite," *Applied Clay Science* 39, no. 3-4 (2008): 186–201, https://doi.org/10.1016/j.clay.2007.06.001.

183. M. L. Martins, T. S. Mathis, X. Wang, L. L. Daemen, Y. Gogotsi, and E. Mamontov, "Water Dynamics in Pristine and Porous $Ti_3C_2T_x$ MXene as Probed by Quasielastic Neutron Scattering," *Physical Review Materials* 6, no. 3 (2022): 034001, https://doi.org/10.1103/PhysRevMaterials.6.034001.

184. Y.-H. Tong, L.-H. Luo, R. Jia, R. Han, S.-J. Xu, and Z. L. Xu, "Whether Membranes Developed for Organic Solvent Nanofiltration (OSN) Tend to be Hydrophilic or Hydrophobic? — A Review," *Heliyon* 10, no. 2 (2024): e24330, https://doi.org/10.1016/j.heliyon.2024.e24330.

185. M. Lounasvuori, T. Zhang, Y. Gogotsi, and T. Petit, "Tuning the Microenvironment of Water Confined in $Ti_3C_2T_x$ MXene by Cation Intercalation," *The Journal of Physical Chemistry C* 128, no. 7 (2024): 2803–2813, https://doi.org/10.1021/acs.jpcc.4c00247.

186. D. Kim, T. Y. Ko, H. Kim, G. H. Lee, S. Cho, and C. M. Koo, "Nonpolar Organic Dispersion of 2D $Ti3C2T_x$ MXene Flakes via Simultaneous Interfacial Chemical Grafting and Phase Transfer Method," *ACS Nano* 13, no. 12 (2019): 13818–13828, https://doi.org/10.1021/acsnano.9b04088.

187. Y. Soma and M. Soma, "Multi-ion Intercalated $Ti_3C_2T_x$ MXene and the Mutual Modulation within Interlayer," *Environmental Health Perspectives* 83 (1989): 205–214, https://doi.org/10.1289/ehp.8983205.

188. K. Zhang, L. Chen, D. Geng, J. Lu, and J. Wu, "Thermal Stability Mechanism via Energy Absorption by Chemical Bonds Bending and Stretching in Free Space and the Interlayer Reaction of Layered Molecular Structure Explosives," *Physical Chemistry Chemical Physics* 22, no. 23 (2020): 13248–13260, https://doi.org/10.1039/d0cp01470b.

189. J. Zhao, J. Zhu, R. Cao, et al., "Liquefaction of Water on the Surface of Anisotropic Two-dimensional Atomic Layered Black Phosphorus," *Nature Communications* 10, no. 1 (2019): 4062, https://doi.org/10.1038/s41467-019-11937-9.

190. M. S. J. M. B. Dresselhaus, "Intercalation in Layered Materials," *MRS Bulletin* 12 (1987): 24–28, https://doi.org/10.1557/S0883769400068093.

191. R. Majee, S. Parvin, Q. Arif Islam, et al., "The Perfect Imperfections in Electrocatalysts," *The Chemical Record* 22, no. 9 (2022): 202200070, https://doi.org/10.1002/tcr.202200070.

192. J. Guerrero-Sanchez, D. M. Munoz-Pizza, M. G. Moreno-Armenta, and N. Takeuchi, "Atomic-Scale Understanding of the Na and Cl Trapping on the $Mo_{1.33}C(OH)_2$-MXene Atomic-Scale Understanding of the Na and Cl Trapping on the $Mo_{1.33}C(OH)_2$-MXene," *Scientific Reports* 12, no. 1 (2022): 8340, https://doi.org/10.1038/s41598-022-12177-6.

193. S. Wan, X. Li, Y. Chen, et al., "Ultrastrong MXene Films via the Synergy of Intercalating Small Flakes and Interfacial Bridging," *Nature Communications* 13, no. 1 (2022): 7340, https://doi.org/10.1038/s41467-022-35226-0.

194. J. Yang, S. Zhu, and H. Zhang, "Polycation-Intercalated MXene Membrane with Enhanced Permselective and Anti-Microbial Properties," *Nanomaterials* 13, no. 21 (2023): 2885, https://doi.org/10.3390/nano13212885.

195. M. Okubo, A. Sugahara, S. Kajiyama, and A. Yamada, "MXene as a Charge Storage Host," *Accounts of Chemical Research* 51, no. 3 (2018): 591–599, https://doi.org/10.1021/acs.accounts.7b00481.

196. S. Kajiyama, L. Szabova, K. Sodeyama, et al., "Sodium-Ion Intercalation Mechanism in MXene Nanosheets," *ACS Nano* 10, no. 3 (2016): 3334–3341, https://doi.org/10.1021/acsnano.5b06958.

197. C. Chen, S. Zhao, C. Pan, et al., "A Method for Quantitatively Separating the Piezoelectric Component from the As-received 'Piezoelectric' Signal," *Nature Communications* 13, no. 1 (2022): 1391, https://doi.org/10.1038/s41467-022-29087-w.

198. W. Yang, H. Liu, H. Du, et al., "Robust and Superelastic Spider Web-like Polyimide Fiber-Based Conductive Composite Aerogel for Extreme Temperature-Tolerant Linear Pressure Sensor," *Sci China Mater* 66, no. 7 (2023): 2829–2842, https://doi.org/10.1007/s40843-022-2418-1.

199. R. Zhu, Z. Li, G. Deng, et al., "Anisotropic Magnetic Liquid Metal Film for Wearable Wireless Electromagnetic Sensing and Smart Electro-

16136829, 2026, 46, Downloaded from https://onlinelibrary.wiley.com/doi/10.1002/smll.74769 by Beihang University (Buaa), Wiley Online Library on [23/09/2026]. See the Terms and Conditions (https://onlinelibrary.wiley.com/terms-and-conditions) on Wiley Online Library for rules of use; OA articles are governed by the applicable Creative Commons License

magnetic Interference Shielding," *Nano Energy* 92 (2022): 106700, https://doi.org/10.1016/j.nanoen.2021.106700.

200. Y. Peng, J. Lu, X. Wang, et al., "Self-powered High-Performance Flexible GaN/ZnO Heterostructure UV Photodetectors with Piezo-phototronic Effect Enhanced Photoresponse," *Nano Energy* 94 (2022): 106945, https://doi.org/10.1016/j.nanoen.2022.106945.

201. S. T. Han, L. Hu, X. Wang, et al., "Black Phosphorus Quantum Dots with Tunable Memory Properties and Multilevel Resistive Switching Characteristics," *Advancement of Science* 4, no. 8 (2017): 1600435, https://doi.org/10.1002/advs.201600435.

202. J. Meng, Q. Li, J. Huang, C. Pan, and Z. Li, "Self-powered Photodetector for Ultralow Power Density UV Sensing," *Nano Today* 43 (2022): 101399, https://doi.org/10.1016/j.nantod.2022.101399.

203. M. Qi, R. Yang, Z. Wang, et al., "Bioinspired Self-healing Soft Electronics," *Advanced Functional Materials* 33, no. 17 (2023): 2214479, https://doi.org/10.1002/adfm.202214479.

204. P. E. Lokhande, A. Pakdel, H. M. Pathan, et al., "Prospects of MXenes in Energy Storage Applications," *Chemosphere* 297 (2022): 134225, https://doi.org/10.1016/j.chemosphere.2022.134225.

205. M. Manciu, F. S. Manciu, and E. Ruckenstein, "On the Surface Tension and Zeta Potential of Electrolyte Solutions," *Advances in Colloid and Interface Science* 244 (2017): 90–99, https://doi.org/10.1016/j.cis.2016.06.006.

206. D. W. Smith, "Ionic Hydration Enthalpies," *Journal of Chemical Education* 54, no. 9 (1977): 540, https://doi.org/10.1021/ed054p540.

207. M. R. Lukatskaya, S. Kota, Z. Lin, et al., "Ultra-high-rate Pseudocapacitive Energy Storage in Two-dimensional Transition Metal Carbides," *Nature Energy* 2 (2017): 17105, https://doi.org/10.1038/nenergy.2017.105.

208. Z. W. Seh, K. D. Fredrickson, B. Anasori, et al., "Two-Dimensional Molybdenum Carbide (MXene) as an Efficient Electrocatalyst for Hydrogen Evolution," *ACS Energy Lett* 1, no. 3 (2016): 589–594, https://doi.org/10.1021/acsenergylett.6b00247.

209. A. F. Barton, *CRC Handbook of Solubility Parameters and Other Cohesion Parameters* (Routledge, 2017), https://doi.org/10.1201/9781315140575.

210. C. M. Hansen, *Hansen Solubility Parameters: A User's Handbook* (CRC Press, 2007), https://doi.org/10.1201/9781420006834.

211. O. Mashtalir, M. R. Lukatskaya, A. I. Kolesnikov, et al., "The Effect of Hydrazine Intercalation on the Structure and Capacitance of 2D Titanium Carbide (MXene)," *Nanoscale* 8, no. 17 (2016): 9128–9133, https://doi.org/10.1039/c6nr01462c.

212. F. Hao, D. N. Fang, and X. Chen, "The Coupling of Strain and Lithium Diffusion: A Theoretical Model Based on First-Principles Calculations," *Journal of The Electrochemical Society* 162, no. 12 (2015): A2266–A2270, https://doi.org/10.1149/2.0341512jes.

213. J. Wang, Y. J. Hu, B. F. Yang, X. Wang, J. W. Qin, and M. H. Cao, "Mechanochemistry-Induced Biaxial Compressive Strain Engineering in MXenes for Boosting Lithium Storage Kinetics," *Nano Energy* 87 (2021): 106053, https://doi.org/10.1016/j.nanoen.2021.106053.

214. N. C. Osti, M. Naguib, K. Ganeshan, et al., *Physical Review Materials* 1, no. 6 (2017): 065406, https://doi.org/10.1103/PhysRevMaterials.1.065406.

215. J. S. Koehler, "Diffusion of Lattice Defects in a Stress Field," *Physical Review* 181, no. 3 (1969): 1015–1019, https://doi.org/10.1103/PhysRev.181.1015.

216. J. Wen, Q. Fu, W. Wu, H. Gao, X. Zhang, and B. Wang, "Understanding the Different Diffusion Mechanisms of Hydrated Protons and Potassium Ions in Titanium Carbide MXene," *ACS Applied Materials & Interfaces* 11, no. 7 (2019): 7087–7095, https://doi.org/10.1021/acsami.8b21117.

217. J. Swenson, R. Bergman, and W. S. Howells, "Quasielastic Neutron Scattering of Two-dimensional Water in a Vermiculite Clay," *The Journal of Chemical Physics* 113, no. 7 (2000): 2873–2879, https://doi.org/10.1063/1.1305870.

218. N. Malikova, A. Cadene, V. Marry, E. Dubois, and P. Turq, "Diffusion of Water in Clays on the Microscopic Scale: Modeling and Experiment," *The Journal of Physical Chemistry B* 110, no. 7 (2006): 3206–3214, https://doi.org/10.1021/jp056954z.

219. J. Come, J. M. Black, M. R. Lukatskaya, et al., "Controlling the Actuation Properties of MXene Paper Electrodes Upon Cation Intercalation," *Nano Energy* 17 (2015): 27–35, https://doi.org/10.1016/j.nanoen.2015.07.028.

16136829, 2026, 46, Downloaded from https://onlinelibrary.wiley.com/doi/10.1002/smll.74769 by Beihang University (Buaa), Wiley Online Library on [23/09/2026]. See the Terms and Conditions (https://onlinelibrary.wiley.com/terms-and-conditions) on Wiley Online Library for rules of use; OA articles are governed by the applicable Creative Commons License